



<https://theses.gla.ac.uk/>

Theses Digitisation:

<https://www.gla.ac.uk/myglasgow/research/enlighten/theses/digitisation/>

This is a digitised version of the original print thesis.

Copyright and moral rights for this work are retained by the author

A copy can be downloaded for personal non-commercial research or study,
without prior permission or charge

This work cannot be reproduced or quoted extensively from without first
obtaining permission in writing from the author

The content must not be changed in any way or sold commercially in any
format or medium without the formal permission of the author

When referring to this work, full bibliographic details including the author,
title, awarding institution and date of the thesis must be given

Enlighten: Theses

<https://theses.gla.ac.uk/>
research-enlighten@glasgow.ac.uk

ENERGY TRANSPORT IN RADIALLY ACCRETING WHITE DWARF STARS

by

Alan McLure Thompson

Thesis
submitted to the
University of Glasgow
for the Degree of
Ph.D.

Department of Astronomy
University of Glasgow
Glasgow, G12 8QW.

October 1986

ProQuest Number: 10991890

All rights reserved

INFORMATION TO ALL USERS

The quality of this reproduction is dependent upon the quality of the copy submitted.

In the unlikely event that the author did not send a complete manuscript and there are missing pages, these will be noted. Also, if material had to be removed, a note will indicate the deletion.



ProQuest 10991890

Published by ProQuest LLC (2018). Copyright of the Dissertation is held by the Author.

All rights reserved.

This work is protected against unauthorized copying under Title 17, United States Code
Microform Edition © ProQuest LLC.

ProQuest LLC.
789 East Eisenhower Parkway
P.O. Box 1346
Ann Arbor, MI 48106 – 1346

**To the memory of the Glasgow University Department of
Astronomy.**

ACKNOWLEDGEMENTS

The research presented in this Thesis could not have been performed without the assistance of a great many people. In particular I would like to thank University of Glasgow for its financial support and its Department of Astronomy for the use of its facilities. In addition, I would like to thank my supervisor, Professor J.C. Brown, for his help and guidance and Drs. T.V. Cawthorne, J Kuijpers, I.J.D. Craig, R.W.P. McWhirter, H.P. Summers, I.W. Walker, A.L. MacKinnon, Mr A.J.C McDonald and Professor P.A. Sweet for their assistance with varying aspects of the research presented here. Finally, I would like to thank the many other colleagues, family and friends, too numerous to name, for their support and encouragement over the last three years.

SUMMARY

AM Herculis stars form a subclass of cataclysmic variables, the defining characteristic of which is that they possess a high degree of polarisation at optical frequencies. Physically they have two notable features. Firstly, the white dwarf star has a sufficiently high magnetic field ($B \sim 10^3 - 10^4$ Tesla) to prevent the formation of an accretion disk. The accreting matter is instead funnelled along magnetic field lines onto its magnetic poles where it forms an accretion column. Secondly, the soft X-ray emission from the white dwarf, usually attributed to the photospheric reprocessing of energy emitted in a shock in the accretion column, exceeds the total directly visible radiation from the shock by a factor $\sim 2 - 6$ (Heise et al, 1986), producing the so called 'Soft X-ray Puzzle'. In this Thesis we examine some of the non-thermal energy transport processes which may be present in a white dwarf accretion column and determine whether these could in any way contribute to a resolution of this paradox.

The first two Chapters of this Thesis constitute a review of the observations and proposed models for white dwarf accretion columns. In Chapter 1 we review the observations of white dwarf accretion columns and examine the constraints that these place on accretion column models. In Chapter 2, in addition to reviewing the previous models of radial accretion onto white dwarfs, we examine in detail the 'Non-Local Electron Transport Model' proposed by Frank et al (1983) and Frank and King (1984). We demonstrate that, due to a misinterpretation of

the standard Coulomb collisional timescales by Frank and King, this model is not self consistent.

Chapters 3 to 5 represent the bulk of the original work in this Thesis. In Chapters 3 and 4 we examine in detail the bombardment model of white dwarf accretion columns proposed by Kuijpers and Pringle (1982). In Chapter 3 we show that in Kuijpers and Pringle's original treatment, in which the energy of the accreting material is deposited uniformly into a static atmosphere which then radiates the energy away as optically thin bremsstrahlung/line radiation, they too used an incorrect Coulomb collisional timescale. We repeat Kuijpers and Pringle's calculation using the correct timescale and show that the mean temperature obtained is reduced from $\sim 10^7$ to $\sim 10^5$ K, close to the observed soft X-ray temperature of AM Her. We also show, however, that when the energy loss of the accreting matter is balanced locally against bremsstrahlung/line losses no solution can be found and conclude that a bombardment solution of this type cannot exist. We extend this local energy balance calculation to include the effect of diffusive thermal conduction and show that, although self consistent accretion column structures can be found, they only exist for accretion rates very much less than those inferred for radially accreting white dwarfs.

In Chapter 4 we extend the calculations of Chapter 3 to include the effect of cyclotron radiation. We show that accreted energy fluxes $\sim 10^{14} \text{ W m}^{-2}$ (typical of AM Her. stars) can be radiated in the form of optically thick cyclotron radiation from a uniform temperature layer of thickness equal to the Coulomb

collisional stopping length of the accreting matter at a temperature $\sim 10^8$ K, slightly less than the shock temperature. We conclude, therefore, that a cyclotron cooled bombardment solution for a white dwarf accretion column may exist. We extend this calculation to derive a simple piecewise uniform temperature structure for such an accretion column, incorporating the effect of thermal conduction.

In Chapter 5 we examine two of the non thermal emission mechanisms that might be present in white dwarf accretion columns:- non thermal Lyman- α emission and non thermal inverse bremsstrahlung emission. We show that although non thermal L_α emission could, in principle, yield information about the structure of the accretion column, and inverse bremsstrahlung could, in principle, contribute to the soft X-ray flux, neither would be sufficiently large to be detectable.

Finally, in Chapter 6 we recapitulate the conclusions reached in the previous Chapters and suggest some possible extensions to the work presented in this Thesis.

CONTENTS

	Page
ACKNOWLEDGEMENTS	
SUMMARY	
<u>CHAPTER 1</u> - REVIEW OF THE OBSERVATIONS OF WHITE DWARF ACCRETION COLUMNS	
1.1 Introduction	1
1.2 Observations of the Optical Continuum	4
1.3 The Soft and Hard X-ray Observations	8
1.4 'Low' State Observations	12
1.5 Summary	13
<u>CHAPTER 2</u> - REVIEW OF THE THEORY OF WHITE DWARF ACCRETION COLUMNS	
2.1 Introduction	22
2.2 Steady Nuclear Burning Models	24
2.3 Shock Models of White Dwarf Accretion Columns	27
2.4 The Suprathermal Conduction Treatment	33
2.5 The Bombardment Model	37
<u>CHAPTER 3</u> - OPTICALLY THIN BOMBARDMENT MODELS	
3.1 Introduction	41
3.2 Coulomb Collisional Timescales	43
3.3 Global Argument	44
3.4 The Spatial Structure of a Bombarded Column	48
3.5 The Spatial Structure of the Bombarded Column Including Thermal Conduction	53
3.6 The Validity of the Radiative Loss Curve	61
3.7 Conclusions	64

	Page
<u>CHAPTER 4 - CYCLOTRON COOLED BOMBARDMENT MODELS</u>	
4.1 Introduction	75
4.2 The Cyclotron Opactity due to Mildly Relativistic Electrons	76
4.3 The Collisional Stopping Length of Accreting Protons	80
4.4 The Estimation of Cyclotron Losses	83
4.5 The Temperature Structure of a Cyclotron Cooled Accretion Column	85
4.6 Comparison with Observations	101
4.7 Conclusions and Discussion	104
<u>CHAPTER 5 - NON THERMAL EMISSION PROCESSES</u>	
5.1 Introduction	113
5.2 Non Thermal Lyman- α Emission	115
5.3 Non Thermal Inverse Bremsstrahlung Emission	123
5.4 Conclusions	127
<u>CHAPTER 6 - CONCLUSIONS AND FUTURE WORK</u>	135
<u>APPENDIX A - COULOMB COLLISIONAL TIMESCALES</u>	142
<u>APPENDIX B - COLLISIONAL BROADENING OF CYCLOTON LINES</u>	147
<u>REFERENCES</u>	155

CHAPTER 1

REVIEW OF THE OBSERVATIONS OF WHITE DWARF ACCRETION COLUMNS

SECTION 1.1 INTRODUCTION

AM Herculis stars form an interesting subclass of cataclysmic variables (CVs), the main characteristic of which is that they possess a sufficiently strong magnetic field to prevent the formation of the accretion disc normally associated with CVs. The generally accepted model for these objects, illustrated in Figure 1.1, is that described in Stockman et al (1977) in which matter from a low mass, dM 4-5, red dwarf (Liebert et al, 1978; Young and Schneider, 1979; Williams et al, 1979; Szkody and Capps, 1980; Young et al, 1981; Allen and Cherepashchuck, 1982) which is overflowing its Roche lobe flows from the secondary to the primary through the inner Lagrange (L1) point. The accreting matter accelerates towards the primary, a $1M_{\odot}$ white dwarf (Williams et al 1979; Touhy et al, 1978), where it attaches itself to magnetic field lines and flows onto the white dwarf's magnetic poles. (For a more detailed description of the accretion flow see Liebert and Stockman 1985).

As matter flows onto the surface of the white dwarf it passes through a deceleration region in which the the energy of the inflowing material is thermalised. (This region is often described as a shock and we shall, therefore, adopt this terminology within this Chapter). The heated material then loses

its energy radiatively as it cools and settles onto the surface of the white dwarf star. It is this part of the accretion column, between the onset of thermalisation and the white dwarf's photosphere, with which this Thesis is mainly concerned.

Clearly, any attempt to model the structure of the accretion column, even though the model may represent an interesting mathematical problem, must ultimately be tested against the observations. It is with this in mind that, in this Chapter, we review the observational characteristics which determine the parameters that can realistically be chosen for an accretion column model, and the features that the model must attempt to explain.

Before we proceed to look at these characteristics in detail, several broad properties should be emphasized. Firstly, since AM Her. objects lack an accretion disc reservoir, any changes in the rate of mass flow from the secondary to the primary result in a rapid change in the system's luminosity. Consequently, AM Her. stars exhibit high and low states. Low states last for typically a few months and during this period the optical brightness is usually reduced by 3-5 magnitudes from its maximum value. In this Thesis, like most previous authors (e.g. Lamb and Masters, 1979; Frank et al, 1983), we will concern ourselves with the high state, when the object is accreting.

The second point that should be noted is that the spectrum of an AM Her. object, particularly during the low state, consists not only of radiation from the accretion column itself, but also exhibits features originating further out in the

accretion flow and in the secondary star. For example, it was observations of strong HeII lines, which are produced in the accretion flow well away from the white dwarf, that led Bond and Tifft (1974) to suggest that AM Her. was a CV like object, and it was infra-red observations of the secondary star (Liebert et al, 1978; Young and Schneider, 1979; Szkody and Capps, 1980; Young et al, 1981; and Allen and Cherepushchuck, 1982) that identified it as a low mass main sequence red dwarf.

In this Chapter we shall concentrate only on the features which are believed to originate in the accretion column: the polarised optical continuum (Section 1.2); and the soft and hard X-ray fluxes (Section 1.3). In addition, in Section 1.4 we will review the observations made during the low states which yield information about the region of the system close to the white dwarf. In Section 1.5 we summarise the constraints on simple accretion column models and the features that they are trying to explain.

Finally, it should be noted that the strong magnetic field of the primary has the effect of locking the white dwarf's rotation period to the system's orbital period so that the system co-rotates. The result of this is that all the spectral features are modulated with the orbital frequency (see Figures 1.2, 1.3 and 1.5). Indeed it was the 3.09 hour periodicity of both the polarisation (Tapia, 1977) and the soft X-ray flux (Hearn and Richardson, 1977) which confirmed AM Her. as being the optical counterpart of the X-ray source 3U 1809+50.

SECTION 1.2 OBSERVATIONS OF THE OPTICAL CONTINUUM

AM Herculis stars possess one unique characteristic which separates them from all other classes of cataclysmic variables, a high degree of polarisation in the near infra-red, optical, and ultra-violet part of the spectrum. First observed by Tapia (1977), the polarised optical radiation is attributed to a thermal cyclotron source situated in the accretion column close to the 'shock' region (e.g. Lamb and Masters, 1979; Chanmugam and Dulk, 1981; Meggitt and Wickramasinghe, 1982).

Figure 1.2 (Chanmugam and Dulk, 1982) shows an example of the smoothed visual light curves and the variations of polarisation with phase of three AM Her. stars. The illustrations above the light curves show the estimated position of the accretion column on the star's disc, assuming a radial geometry for the column.

These curves have several main characteristics of note. Firstly, there is one feature which is common to all three of these stars - the linear polarisation pulse. This feature is used to define the magnetic phase of the star (phase zero being defined as the phase of maximum linear polarisation), and can be attributed to the observer viewing the cyclotron source at the maximum angle of inclination (θ) relative to the magnetic field. In the case of AM Her. and VV Pup., which both eclipse the column, this corresponds to the eclipse ingress. Surprisingly, neither of these stars exhibit a linear polarisation pulse at egress and in fact only one radially accreting white dwarf, CW 1103+254 (Figure 1.3, Stockman et al, 1983), shows a linear

pulse at egress. As yet no satisfactory explanation for this has been proffered.

The second point to note is that the polarisation observations of VV Pup. have divided AM Her. stars into two sub-classes, the one and two polar accreters. As we can see in Figure 1.2b, the primary pole of VV Pup. is eclipsed for roughly 60% of its period (between phases 0.1 and 0.7). During epochs when it is actively accreting matter (i.e. VV Pup. is in its high state) the polarisation remains while the accretion column is eclipsed. This has generally been interpreted as being due to a second, less active, magnetic pole which only accretes material when there is a great deal of matter around (e.g. Liebert and Stockman, 1979; Liebert et al, 1978). This interpretation also has the advantage of providing a ready explanation for the dip in the optical brightness, which occurs immediately after eclipse ingress (Liebert et al, 1978), as a slight offsetting of the line of the pole from the white dwarf diameter would allow both poles to be out of view for a short time. Further evidence of this type of two pole geometry has been provided by the recent EXOSAT observation observations of AM Her., made by Heise et al (1986), which are discussed in Section 1.3.

The third striking feature of Figure 1.2 is the rapid ingress and egress of VV Pup. from eclipse ($\sim 2\%$ of the period) which indicates that the primary pole must cover only a small fraction ($f \sim 10^{-4}$) of the total surface area of the star (Liebert et al, 1978). The smoother variations in the light curves of the other two objects, particularly that of AM Her.,

which also eclipses, tends to suggest that they may have a larger area of accretion.

In addition to these three characteristics, there is one other feature not illustrated in Figure 1.2 which should be mentioned - the optical light curve also shows rapid 'twinkling' which has generally been neglected in the modelling of accretion columns.

Finally, it is worth mentioning that, because the optical radiation is predominantly from an optically thick cyclotron source (e.g. Chanmugam and Dulk, 1981), the anisotropy of the cyclotron emissivity means that the maximum optical flux does not necessarily correspond to the maximum in the apparent surface area. The effect of this is most clearly seen in the light curve of AM Her., where the X-ray maximum, which co-incides with a maximum in the projected surface area, also coincides with a minimum in the optical light curve. In fact the maximum in the optical intensity occurs at an angle between the observers line of sight and the magnetic field $\sim 45^\circ$ (see Chapter 4)

Further evidence that the optical component of the spectrum of AM Her. stars is dominated by cyclotron radiation can be obtained from the observation of the optical spectrum of VV Pup. (Figure 1.4), made by Visvinath and Wicramasinghe (1979) during an active accreting period, which clearly show the existence of cyclotron emission lines. These observations are unique to VV Pup. and it has therefore been suggested that in other AM Her. stars the harmonics are so wide that they smear into a polarised continuum.

So what do these observations tell us about the accretion columns of magnetic white dwarf stars? Originally the polarisation was attributed to an optically thin, first harmonic, cyclotron line (e.g. Tapia, 1977) and early estimates of the magnetic fields from the optical data yielded a value of $B \sim 10^4$ Tesla. More recently, however, 'successful' attempts have been made to fit both the polarisation light-curve of AM Her. (Chanmugam and Dulk, 1981; Barrett and Chanmugam, 1984), and the cyclotron lines of VV Pup. (Wickramasinghe and Meggitt, 1982; Barrett and Chanmugam, 1985) using a marginally optically thick cyclotron source, i.e. the source has an optical depth $\tau \approx 1$ at optical frequencies.

Table 1.1 shows the best fit values for the magnetic field B , plasma parameter $\Lambda = \frac{\omega_p^2 l}{\omega c}$ (where ω_p is the plasma frequency, l is the length of the emitting region, and c is the speed of light), the column density $N = nl$ (where n is the electron number density in the white dwarf atmosphere) which corresponds to the above Λ , and the temperature T obtained by the above authors for the accretion column. All three sets of results agree on one of the parameters $B \approx 3 \cdot 10^3$ Tesla. The fits to the polarisation light curves and the cyclotron lines, on the other hand, do not give consistent values for the temperature or the column depth of the emitting region. However, the results from the observations of VV Puppis, which because of the relative simplicity of fitting a model to three cyclotron lines are probably more reliable, do agree well with theory. Firstly, the temperature, $T \sim 10^8$ K (10KeV), is consistent with the expected temperature of 'shock' region which is the likely

source of the cyclotron radiation (Lamb and Masters, 1979). Secondly, the value for the column density of the cyclotron emitting region is of the same order as the expected thickness of the 'shock' region (Thompson and Cawthorne, 1986). This is perhaps to be expected since Meggitt and Wickramasinghe (1984) have shown that the marginally optically thick assumption, used by Wickramasinghe and Meggitt (1982) and Barrett and Chanmugam (1985), is not necessary if a steep temperature gradient, such as occurs in the 'shock' region, is present. In addition to these two factors, Barrett and Chanmugam (1985) have estimated the fraction of VV Puppis's surface area (f) covered by the cyclotron source to be $\sim 6 \cdot 10^{-5}$. This result is consistent with the value determined by Liebert et al (1978) from the light-curve.

SECTION 1.3 THE SOFT AND HARD X-RAY OBSERVATIONS

Probably one of the clearest examples of the typical X-ray spectrum of a radially accreting white dwarf is that obtained by Rothschild et al (1981) using HEAO-1 (Figure 1.5), which clearly demonstrates the two component nature of the spectrum. The 'hard' X-ray component ($h\nu \gtrsim 1\text{KeV}$) is generally attributed to an optically thin bremsstrahlung source (e.g. Rothschild et al, 1981), while the 'soft' X-ray component ($h\nu \lesssim 1\text{KeV}$) is usually interpreted as a black-body continuum (Tuohy et al, 1978).

The hard X-ray component can be fitted fairly simply and fairly well by a bremsstrahlung source with a temperature

$T \approx 1-3 \cdot 10^8 \text{ K}$ ($kT \approx 10 - 30 \text{ KeV}$) and a column density $N_{\text{H}} \approx 2.4 \cdot 10^{26} \text{ m}^{-2}$ lying above a photosphere with an albedo of 0.2 (Rothschild et al, 1981). In addition, the hard X-ray luminosity can be estimated as $\sim 3 \cdot 10^{25} \text{ W}$, assuming a distance of 100 parsecs for AM Her. (Dahn, 1980, referenced in Schmidt, 1981).

Fitting the soft X-ray spectrum to a black-body spectrum does, however, represent a somewhat more difficult problem. The observed soft X-ray spectrum represents the Wein tail of a black-body spectrum, the peak of which lies between 100\AA and 1000\AA , a region which is currently unobservable. The best fits to this spectrum produce a temperature $T \approx 1-5 \cdot 10^5 \text{ K}$ (10-40eV) and a luminosity $L_{\text{bb}} \approx 10^{27} \text{ W}$. More recently, Heise et al (1986) (c.f. Heise, 1982) have fitted observations made with the Einstein satellite to a black-body with a temperature $T \approx 5.3 \cdot 10^5$ (46eV) and a luminosity $L_{\text{bb}} \approx 6.3 \cdot 10^{25} \text{ W}$. Heise et al (1986) also fitted the soft X-ray spectrum to the spectrum emitted by an atmosphere in radiative equilibrium. This yields an effective temperature $T \approx 2-2.4 \cdot 10^5 \text{ K}$, which is lower and a luminosity $L \approx 2 \cdot 10^{26} \text{ W}$ (which corresponds to a fractional emitting area $f \approx 10^{-3}$) which is larger than that obtained for a black-body fit.

It has been argued by theorists that the soft X-ray component is due to the reprocessing of the cyclotron and hard X-ray radiation, which is produced in the region behind a standing shock wave in the infalling material (Lamb and Masters, 1977; King and Lasota, 1979). Consequently, the 'black-body', soft X-ray luminosity would not be expected to exceed the total cyclotron and bremsstrahlung luminosities of the source (i.e.

$L_{bb} \lesssim L_{cyc} + L_{HX}$). Raymond et al (1979) and Fabbiano et al (1981) have, however, argued that the emitted energy at optical and hard X-ray wavelengths is 1.5 orders of magnitude smaller than the soft X-ray luminosity, and the observed soft X-ray flux cannot, therefore, be explained as reprocessed cyclotron and bremsstrahlung emission. This discrepancy is the so called 'Soft X-ray Puzzle'.

Three possible solutions to this paradox have been suggested.

1) Fabbiano et al (1981) have suggested that the soft X-ray flux could be enhanced by steady nuclear burning at the base of the column, along the lines of Weast et al (1979). Papaloizou et al (1982), on the other hand, have pointed out that, unless the accreting matter is carbon, nitrogen, and oxygen deficient ($X_{CNO} \sim 10^{-8}$), the dominant fusion process would be the CNO cycle, the temperature dependence of which results in an instability which prevents steady nuclear burning from taking place (c.f. Section 2.2).

2) Frank and King (1984) have proposed a model involving energy transport by suprathermal, shock electrons. They suggest that these could allow more than 50% of the energy of the accreting matter to reach the photosphere. Thompson et al (1986) have, however, pointed out an error in Frank and King's treatment which may prevent this model from working. Their analysis is elaborated more fully in Section 2.4.

3) Patterson et al (1984) have recalculated the energy emitted in the form of reprocessed, cyclotron and hard X-ray radiation and suggest that the soft X-ray radiation is

consistent with the reprocessing argument of Lamb and Masters (1979) (Table 1.2). The question of whether or not the soft X-ray puzzle still exists does, however, depend fairly crucially on the interpretation of the origin of the UV flux between 1000 - 2000Å. Raymond et al (1979), Fabbiano et al (1981), and Heise et al (1986) have found this to be consistent with the Rayleigh-Jeans tail of the 'black-body' distribution. Patterson et al (1984), on the other hand, have included this in the 'primary' radiation from the 'shock' region. If this latter interpretation is correct then the soft X-ray puzzle has truly disappeared. If, however, the interpretation of Raymond et al, Fabbiano et al, and Heise et al is correct then the soft X-ray puzzle still exists, although the results of Heise et al (1986) do indicate that the soft X-ray excess may not be as great as originally suggested by Fabbiano et al (1981). Heise et al have estimated that the soft X-ray luminosity is only 2-6 times the combined cyclotron and bremsstrahlung luminosities.

The picture of the X-ray source has been further complicated by the recent EXOSAT observations of the X-ray light curves of AM Her. (Heise et al, 1985). Previous observations, by Touhy et al (1978) and Swank et al (1977) had indicated that the soft and hard X-ray light curves of AM Her. were in phase (Figure 1.6a). The results of Heise et al (1985), on the other hand, indicate that the reverse is true and that they are in fact in antiphase (Figure 1.6b). This change in the light curve has been attributed by Heise et al (1985) to the precession of AM Her. This precession results from the rotation of the white

dwarf being slightly out of synchronisation with the orbital motion (Campbell, 1983; King and Williams, 1985) and this has allowed AM Her. to start accreting onto both poles, as in the case of VV Puppis.

SECTION 1.4 'LOW' STATE OBSERVATIONS

As we said in the introduction, because of the absence of an accretion disc reservoir, changes in the accretion rate can rapidly result in changes in the luminosity of radially accreting white dwarfs. During these 'low' states additional information about the system can be gained from the changes in the spectrum and the appearance of features which are not visible during the 'high' state (when the white dwarf is actively accreting). For example, it was during such 'low' states that Liebert et al (1979) and Young and Schneider (1980) detected the infra-red and optical emission from the secondary stars in AM Her. and VV Pup., identifying them as low mass M4-5 main sequence red dwarfs.

During these low periods two features have been observed which yield information about the the accretion column. Firstly, Schmidt et al (1981) and Liebert et al (1982) have identified Zeeman hydrogen absorption features, in the spectrum of VV Pup. and AN UMa. resectively, which are consistent with a surface magnetic field for the primary $\sim 1-2 \cdot 10^3$ Tesla, in agreement with the estimates of Meggitt and Wickramasinghe (1982) and Barrett and Chanmugam (1984), made from cyclotron emission lines.

Secondly, during 'low' states the optical polarisation increases (Liebert et al, 1982). This indicates that either the cyclotron emitting region, or the 'shock' itself (c.f. Meggitt and Wickramasinghe, 1984) is reduced in length during these periods.

SECTION 1.5 SUMMARY

In this Chapter we have reviewed some of the observations of radially accreting, magnetic, white dwarf stars and the constraints that these place on models of white dwarf accretion columns. In this Section we briefly summarize these and outline the characteristics that white dwarf accretion column models should explain.

White dwarf accretion columns produce, basically, three types of continuum radiation: optical cyclotron radiation; hard X-ray bremsstrahlung radiation; and reprocessed soft X-ray radiation.

The cyclotron radiation is believed to originate in an optically thick source, consisting of a thermal plasma at a temperature $T \sim 10^8$ K, with a length (in column density) $N \sim 10^{25} - 10^{26} \text{ m}^{-2}$, situated in a magnetic field $B \sim 10^3 - 10^4$ Tesla (probably $\sim 3 \cdot 10^3$ Tesla, Wickramasinghe and Meggitt, 1982; Barrett and Chanmugam, 1984). In addition, it has an estimated luminosity $L_{\text{cyc}} \sim 6 \cdot 10^{25} \text{ W}$ (Fabbianno et al, 1981). The fact that the optical polarisation increases as the accretion rate decreases (Liebert et al, 1982) means that the spatial structure of the cyclotron emitting region must, to some extent, depend on

the accretion rate.

The hard X-ray source is due to an optically thin bremsstrahlung source with a temperature $\sim 2 \cdot 10^8 \text{K}$ and a luminosity $L_{\text{HX}} \sim 3 \cdot 10^{25} \text{W}$ (Rothschild et al, 1981). The similarities between the temperature of the source of optical and hard X-ray radiation and the shock temperature have led most authors (e.g. Lamb and Masters, 1979) to assume that these sources are co-incident and due to an adiabatic shock wave in the white dwarfs atmosphere.

Finally, the soft X-ray source has been attributed to radiation from the optical and hard X-ray sources being reprocessed in the white dwarf's photosphere. The most recent determinations of the temperature and luminosity of the soft X-ray source (Heise et al, 1986, c.f. Heise, 1982), using an atmosphere in local thermodynamic equilibrium, produce a value for the effective temperature $T \sim 2 \cdot 10^5 \text{K}$ and a luminosity $L_{\text{SX}} \sim 2 \cdot 10^{26} \text{W}$. This is in excess of the power emitted directly to the observer, by the cyclotron/bremsstrahlung source, by a factor ~ 2 , creating the so called 'Soft X-ray Puzzle'. If this radiation is to be produced by reprocessing, the emission from the column must be anisotropic so that more energy is emitted towards the star's photosphere than away from it. This is phenomenon which any accretion column model must ultimately explain.

Finally, the observations of these three components of the spectrum of AM Her. determine the three principal 'input' parameters which form the boundary conditions used when comparing models of accretion columns with observations.

- 1) The accretion rate $\dot{M}_* \sim 10^{13} \text{Kgs}^{-1}$.
- 2) The magnetic field $B \sim 10^3 - 10^4 \text{T}$ (probably $\sim 3 \cdot 10^3 \text{T}$).
- 3) The accretion must take place over a fraction of the white dwarf's surface area $f \sim 10^{-2} - 10^{-4}$.

Table 1.1: Best fit values for the properties of the cyclotron sources in AM Her. and VV Pup.

	B(T)	Λ	N (m^{-2})	T(K)
* Barrett and Chanmugam (1984)	$2.7 \cdot 10^3$	10^8	$4.5 \cdot 10^{27}$	$2.3 \cdot 10^6$
** Barrett and Chanmugam (1985)	$3.15 \cdot 10^3$	10^6	$5.2 \cdot 10^{25}$	10^8
** Wickramasinghe and Meggitt (1982)	$3.18 \cdot 10^3$	10^5	$5.3 \cdot 10^{24}$	$1.2 \cdot 10^8$

*) Fit to the polarisation light curve of AM Her.

***) Fit to the cyclotron lines of VV Pup.

Table 1.2: Observed orbit averaged continuum luminosities of AM Her. stars in their high state.

Source	AM Her.*	AM Her.**	VV Pup.**
L_{SX}	} $2 \cdot 10^{27}$	$4.8 \cdot 10^{25}$	$1.8 \cdot 10^{24}$
L_{UV}		$1.8 \cdot 10^{25}$	$9.6 \cdot 10^{23}$
L_{opt}	$6 \cdot 10^{25}$	$5.4 \cdot 10^{24}$	$4.0 \cdot 10^{23}$
L_{HX} (2-6Kev)	$7.5 \cdot 10^{24}$	$5.8 \cdot 10^{24}$	$1.4 \cdot 10^{23}$
L_{HX} (2-60Kev)		$3.6 \cdot 10^{25}$	$>3.6 \cdot 10^{23}$

*) Luminosities determined by Fabbiano et al (1981)

***) Luminosities determined by Patterson et al (1984) (converted from the values of observed flux, assuming a source distance of 100 pc.)

(All luminosities are measured in Watts.)

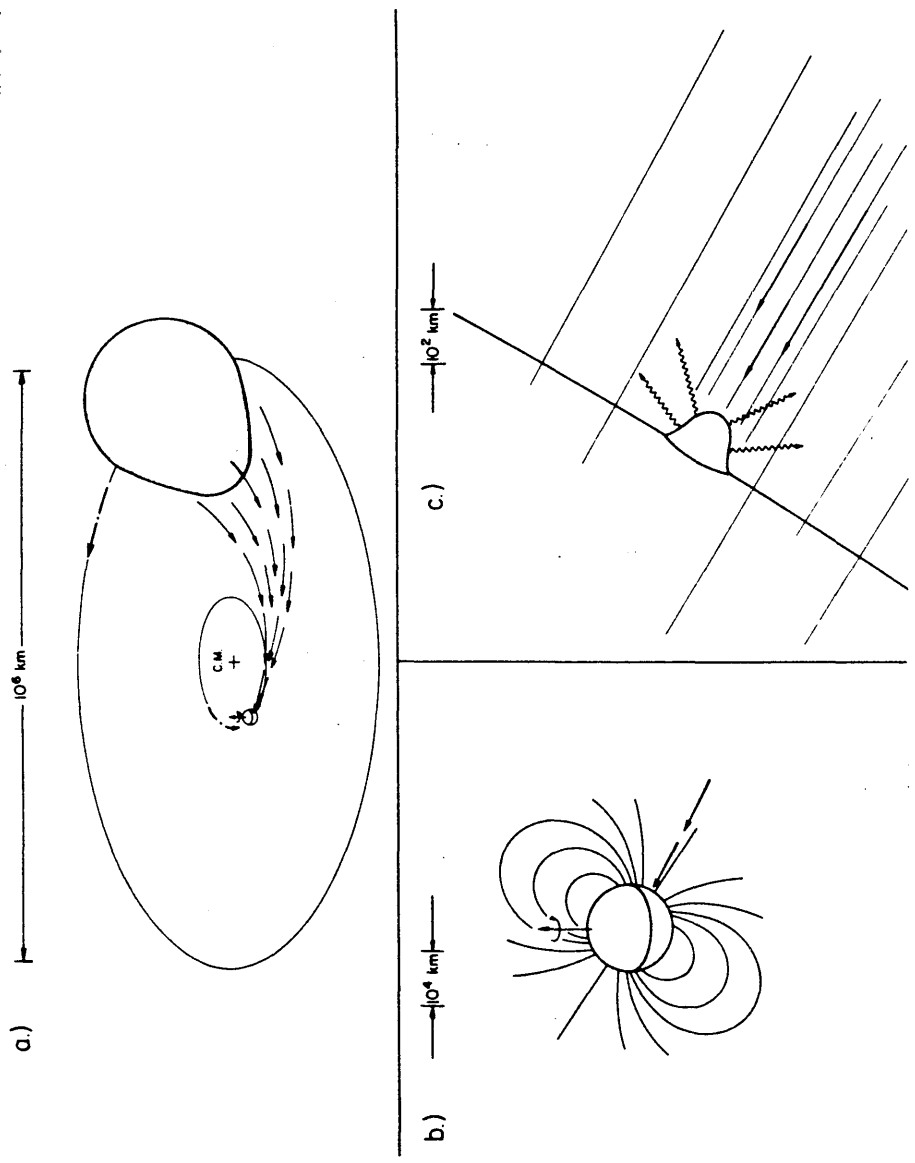


Figure 1.1: Shows three physical scales of AM. Her stars each differing by two orders of magnitude. Matter flows from a main sequence red dwarf towards the primary where it attaches itself to magnetic field lines and is channelled onto a small area around the magnetic pole (Liebert et al, 1978).

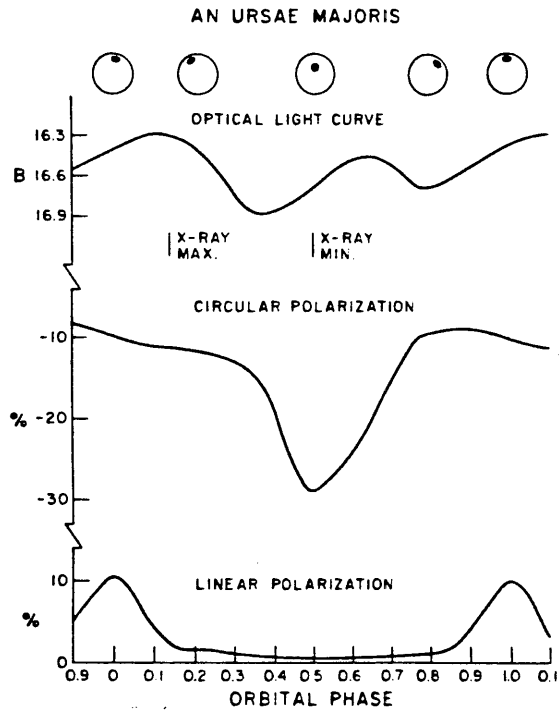
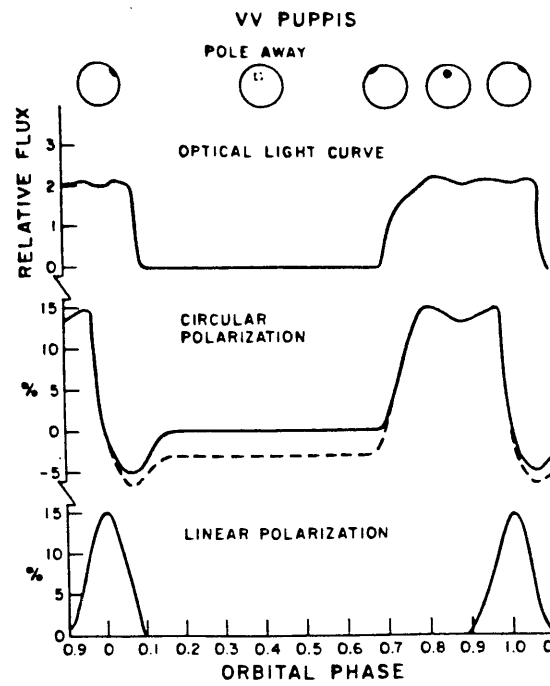
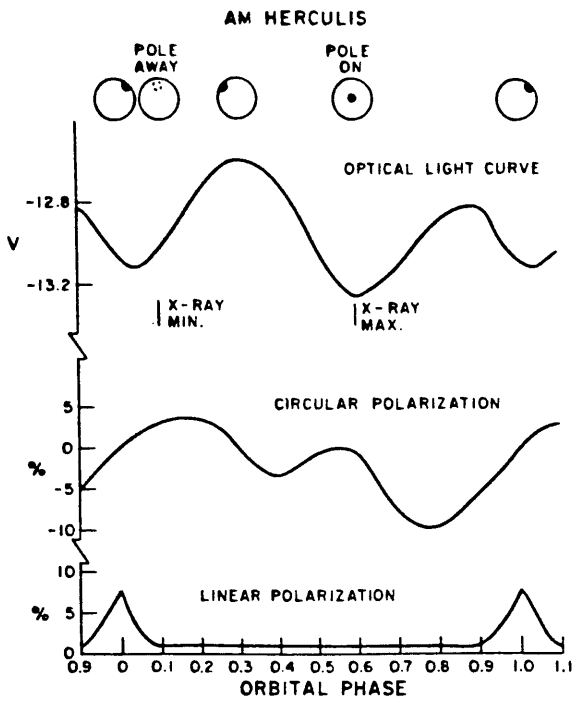


Figure 1.2: The smoothed optical and polarisation light curves for three AM Her. stars. The illustrations above each diagram show the position of the accretion column on the star's disc, assuming a radial geometry for the column. (Chanmugam and Dulk, 1980).

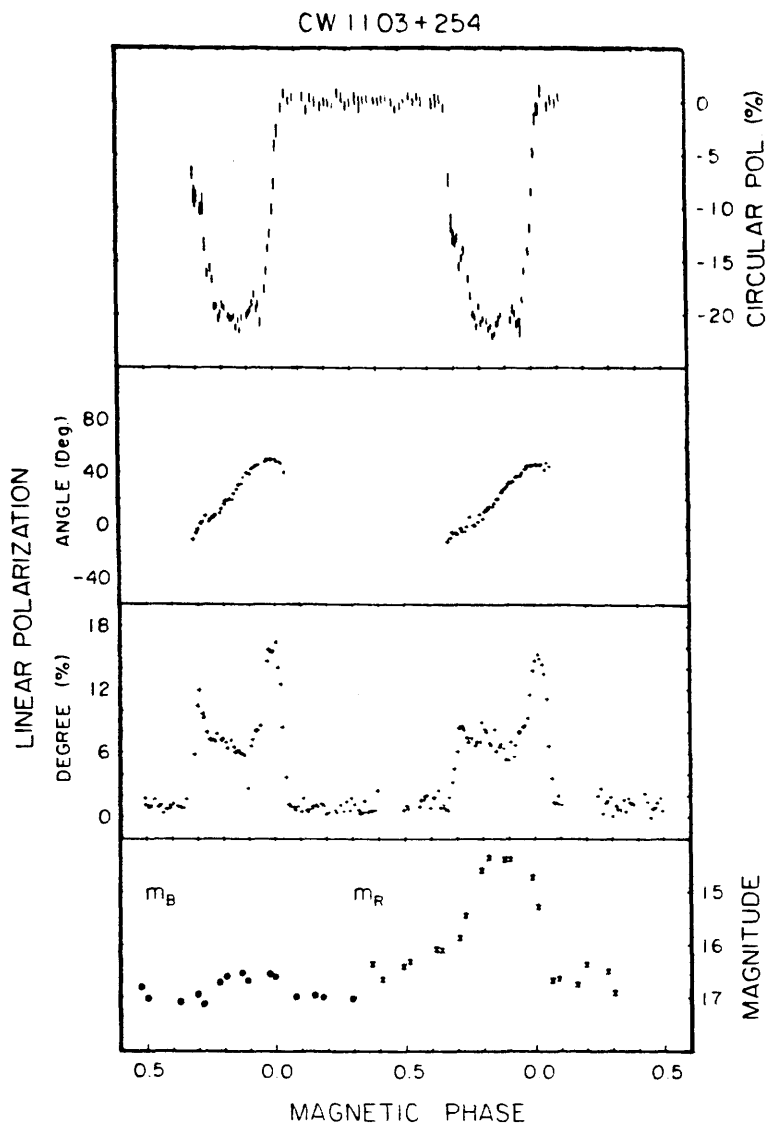


Figure 1.3: The polarimetric and photometric variations of the AM Her. star CW 1103+254 (Stockman *et al*, 1983) showing the twin linear polarisation pulses unique to this object (second from bottom panel).

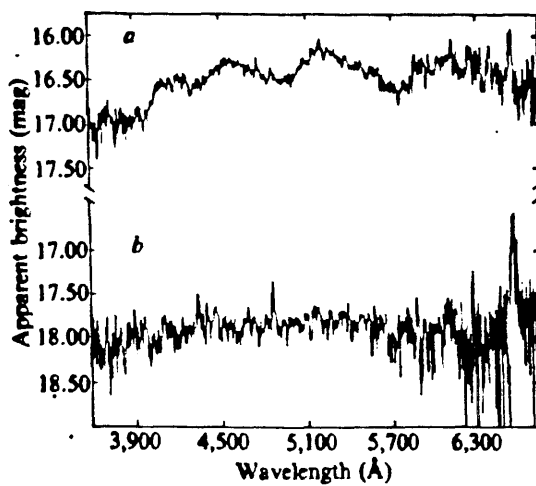


Figure 1.4: The spectrum of VV Puppis showing 3 cyclotron absorption lines (Visvinath and Wickramasinghe, 1979).

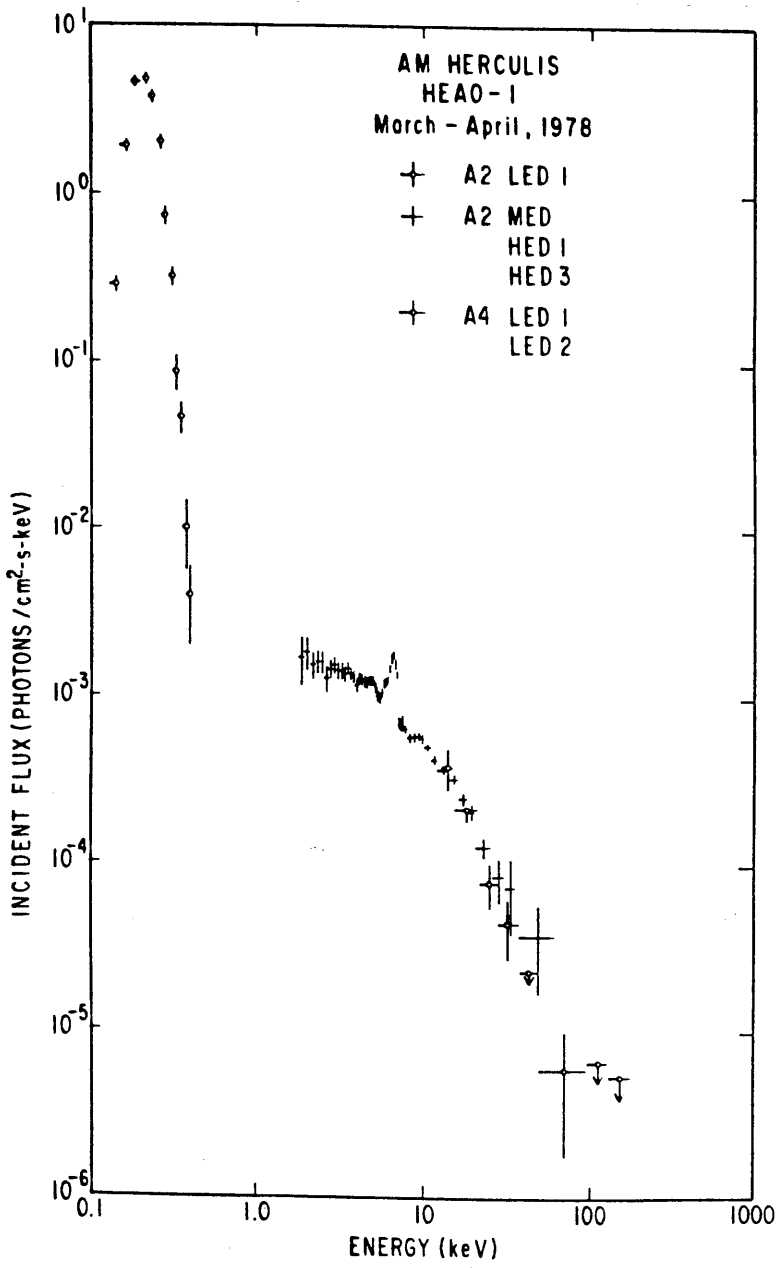


Figure 1.5: The spectrum of AM Her. above 100eV (Rothschild et al, 1981).

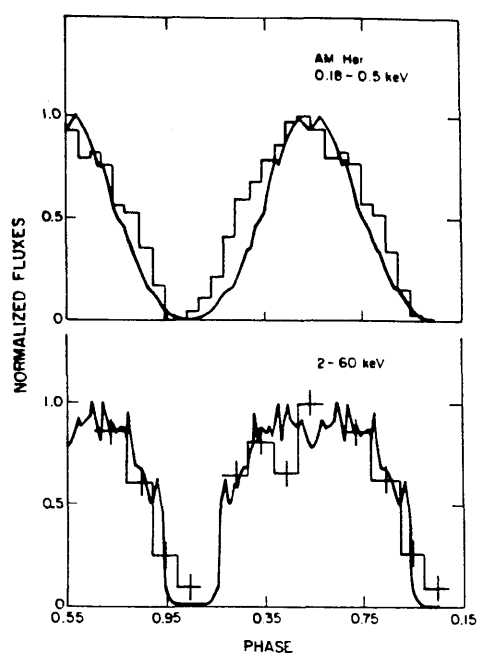


Figure 1.6a: Soft and Hard X-ray light curve of AM Her. (Immamura, 1984)

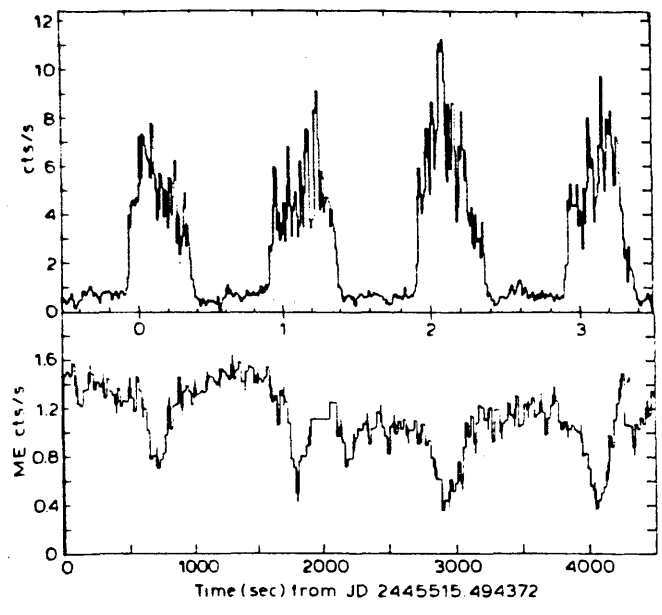


Figure 1.6b: Soft and Hard X-ray light curves of AM Her. (Heise et al, 1985)

CHAPTER 2

REVIEW OF THE THEORY OF WHITE DWARF ACCRETION COLUMNS

SECTION 2.1 INTRODUCTION

Theoretical models of accretion columns can be split into several classes and subclasses. Figure 2.1 shows a 'family tree' for various types of theory and lists the principal references for each. In this Chapter we review these models and, where appropriate, compare the predicted spectral properties with the observations described in Chapter 1.

The primary classification of accretion column models that can be made is into those driven by nuclear burning and those in which the only method of energy generation is the thermalisation of the bulk kinetic energy of the infalling material. The first of these classes, the nuclear burning treatment, is discussed in Section 2.2. The accretion driven models can, on the other hand, be subdivided into three categories: Shock models; bombardment models; and the non-uniform accretion model.

The shock models and bombardment models represent two limiting cases in which matter is being accreted uniformly. In both cases, the accreting matter is envisaged as falling at a constant rate and with a uniform flux onto a fraction of the white dwarf's surface area. This infalling matter passes through a region in which its kinetic energy is thermalised. It is then cooled by a combination of radiative and energy transport

processes. Throughout most of the accretion column the length scales over which the bulk properties of the accreting matter change are very long compared to the mean free paths of the individual particles in the fluid. The structure of these parts of the accretion column can, therefore, be represented by a set of fluid equations. Within the thermalisation (shock) region, however, the temperature and density of the infalling material changes on a length scale equal to the mean free path of the accreting protons. The structure of this region of the column therefore requires a kinetic treatment. In the case of the shock models, it is assumed that there is no energy loss within the region of thermalisation. Consequently, there is no need to calculate, in detail, the structure of the thermalisation region. It can instead be represented by a discontinuity in the in the fluid motion (i.e. as an adiabatic shock). In the bombardment approach, on the other hand, the assumption is made that all (or at least a large fraction) of the accreted energy is lost in the thermalisation region, and a determination of its detailed structure is, therefore, necessary. In these circumstances, this region of the column can be approximated by a static atmosphere being struck by a beam of suprathermal protons, similar to the treatment of solar flares (Brown, 1972, 1973; Emslie, 1978; Brown and Craig, 1984).

In Section 2.3 we briefly discuss three of the shock models: the bremsstrahlung; conduction; and cyclotron cooled models. The remaining shock model, the suprathermal conduction model, is discussed at greater length in Section 2.4. In Section 2.5 we discuss the previous work on bombardment models.

Finally, the non-uniform accretion model was proposed by Kuijpers and Pringle (1982). They suggested that as matter enters the white dwarf's magnetosphere it cools (Elsner and Lamb, 1977; Arons and Lea, 1976), resulting in the production of density inhomogeneities which are preserved during the infall. If these blobs (inhomogeneities) are sufficiently dense, they can penetrate to the depth at which $P \sim P_{\text{RAM}}$ (the ram pressure of the accreting material). At such a depth the atmosphere may be optically thick and, consequently, most of the energy carried by the blob will be radiated at the black body temperature.

Recent calculations by Cawthorne (1986, private communication) suggest that the density inhomogeneities, produced by the process described above, may not be sufficient to allow the resulting blobs to penetrate to the photosphere. These conclusions are, however, very tentative and we will, therefore, not discuss this model further.

SECTION 2.2 STEADY NUCLEAR BURNING MODELS

Isolated white dwarf stars consist, primarily, of a degenerate core and a non-degenerate envelope which are made up, principally, of helium and carbon. If, however, the white dwarf is accreting material from a companion star it may also develop a hydrogen rich outer layer. Such an envelope will gradually increase in size until the pressure and the temperature inside it become large enough to allow nuclear burning to take place, typically when the envelope mass $M_{\text{env}} > 10^{-4} M_{\odot}$ (Truran et al,

1977). For sufficiently large abundances of carbon and nitrogen, the dominant nuclear burning process will be the CNO cycle. The temperature sensitivity of this mechanism does, however, mean that in these circumstances, this process is unstable with the consequence that an outburst occurs (Starrfield et al, 1981). If, on the other hand, the dominant nuclear burning process is the p-p chain, which is less sensitive to temperature, the nuclear burning process is stable and steady burning can occur within the envelope (Starrfield et al, 1981).

The essence of the nuclear burning model is that the accreting matter is funnelled onto the poles of the white dwarf by the magnetic field. As it approaches the surface, it passes through an adiabatic shock. It then cools and settles onto the surface of the white dwarf forming a hydrogen rich 'puddle' which is confined by the magnetic field. This 'puddle' gradually builds up until it is sufficiently massive for the base to start to burn by means of the p-p chain. An equilibrium is then set up by replacing the burnt hydrogen with more, freshly accreted, matter. Starrfield et al, assuming a carbon-nitrogen abundance $X_{\text{CN}} = 0$, calculated that steady nuclear burning would produce ~ 20 times more energy than is produced by the gravitational infall of the accreted matter.

This model has one very attractive feature. The nuclear burning takes place in a region which is optically thick to electron scattering. The majority of the energy produced by the accreting matter is, therefore, released below the photosphere. The steady nuclear burning approach, consequently, provides a ready explanation for the large soft X-ray flux observed from

white dwarf accretion columns.

Weast et al (1979) examined the effect of steady nuclear burning at the base of an accretion column on its emitted spectrum. They showed that energy loss from the shock heated region would be dominated by inverse Compton cooling. This results in a softening of the predicted hard X-ray spectrum and, consequently, the observed hard X-ray temperature would be expected to be below the shock temperature. Again this is in agreement with observations.

One question does, however, remain to be answered. Is the abundance of carbon and nitrogen in this envelope likely to be sufficiently small to allow steady nuclear burning to take place? The answer, for realistic accretion rates ($\dot{M}_* \sim 10^{13} \text{Kgs}^{-1}$) and normal solar carbon and nitrogen abundances ($X_{\text{CN}} \sim 10^{-2}$), is no (Starrfield et al, 1981; Papaloizou et al, 1982). For these parameters, nuclear burning would take place via the CNO cycle and the process would be unstable. Starrfield et al (1981) suggested that the abundance of heavy elements in the envelope might be depleted by gravitational diffusion, thus stabilising the process. Papaloizou et al, however, determined that for steady nuclear burning to occur a carbon-nitrogen abundance $X_{\text{CN}} \sim 10^{-7} - 10^{-9}$ would be required, a depletion factor of five orders of magnitude. To do this by gravitational diffusion would require a diffusion time-scale $\leq 10^{-5} M_{\text{env}} / \dot{M}_*$ the timescale on which the envelope is replenished, i.e. the diffusion timescale must be $\leq 10^2$ years. Papaloizou et al (1982) calculated that the gravitational diffusion timescale, for carbon and nitrogen, to be $\sim 10^7$ years. They, therefore,

concluded that gravitational diffusion could not deplete the carbon and nitrogen abundances significantly and, consequently, steady nuclear burning could not take place.

SECTION 2.3 SHOCK MODELS OF WHITE DWARF ACCRETION COLUMNS.

Shock models of accretion columns represent one extreme of a complete range of possible models which have as their primary source of energy the thermalisation of the bulk kinetic energy of the accreting material. In this Section we discuss three of the four types of shock models shown in Figure 2.1 the bremsstrahlung; conduction/bremsstrahlung; and cyclotron cooled models. We shall discuss the fourth model shown in Figure 2.1: the suprathreshold conduction approach, in Section 2.4.

The essence of the shock treatment is that matter, channelled by the magnetic field, falls radially onto a fraction of the white dwarf's surface area around the magnetic pole. The accreting matter is initially cool so that as it approaches the surface of the star it is moving highly supersonically. A strong standing shock wave can, therefore, form (Sakashita, 1968; Hoshi, 1973; Aizu, 1973).

At this point it is useful to distinguish between the one fluid and the two fluid approach. As the ions (protons) and electrons enter the shock, the ions, which carry most of the energy, have their kinetic energy thermalised, i.e. it is the ions that are heated first in the shock. The ions then transfer their energy, more slowly, to the electrons. If the timescale

for the accreted matter to cool $t_{\text{cool}} < t_{\text{ei}}$ the electron-ion equilibration timescale then the electrons will, for most of the length of the column, be cooler than the ions and it is necessary to treat the electrons and ions as two separate but electrostatically coupled fluids. If, on the other hand, $t_{\text{ei}} < t_{\text{cool}}$ the two fluids will achieve equal temperatures sufficiently rapidly to allow the accreted matter to be treated as one single fluid. The models described in this Section are of this one fluid type.

As the accreted matter passes through the shock its density increases and its velocity decreases by a factor of 4. In addition, the inflowing material is increased to the shock temperature.

$$T_s = \frac{3}{16} \frac{GM_* m_p \mu}{k R} = 3.7 \cdot 10^8 M_1 R_7^{-1} \text{ K} \quad (2.1)$$

where $M_* = M_1 M_\odot$ is the white dwarf mass, $R_* = R_7 \cdot 10^7 \text{ m}$ is the stars radius and μ is the mean molecular mass. The shock heated matter then cools by some combination of energy transport processes (e.g thermal conduction) and radiative processes (e.g. cyclotron or bremsstrahlung radiation). Where the three shock models we discuss here differ is in the type of radiative and energy transport processes which are reckoned to be important.

2.3.1 Bremsstrahlung cooled models.

Sagashita (1968), Hoshi (1973), Aizu (1973) and Fabian et al (1976) considered the case in which the shock heated material simply cools by thermal bremsstrahlung as it settles

onto the stellar surface. The calculations of Sagashita (1968), Hoshi (1973), and Aizu (1973), which predate the discovery of AM Her., were primarily aimed at demonstrating that white dwarfs were potential X-ray sources. They consequently considered the effect of uniform spherical accretion onto a non-magnetic white dwarf. Fabian et al (1976) extended these calculations to include a magnetic white dwarf in which accretion may take place over a fraction of the total surface area. Fabian et al also demonstrated that the cooling timescale in this type of model is very much greater than the electron-ion equilibration timescale, confirming the validity of the one fluid approach.

In the absence of any other energy emission or transport process, all the accreted energy will be radiated, initially, in the form of hard X-rays with a characteristic temperature of $\sim 4 \times 10^7$ K. Consequently, the bremsstrahlung model predicts a soft X-ray (reprocessed) 'black-body' component with a luminosity $L_{\text{bb}} \leq 0.5 L_{\text{tot}}$ (where L_{tot} = the total luminosity of the source), and a hard X-ray (bremsstrahlung) component with a luminosity $L_{\text{HX}} \geq 0.5 L_{\text{tot}}$.

Clearly, these predictions, made before the discovery of AM Her., cannot explain its observed spectrum. This treatment has, however, inspired at least three modified versions of the shock model.

2.3.2 Bremsstrahlung/conduction cooled models.

Fabian et al (1986) noted the possibility that a self-consistent accretion column model might exist in which a

standing shock wave is set up close to the white dwarf surface, and in which the dominant post shock cooling mechanism is the diffusive thermal conduction of the energy below the photosphere. This has the obvious attraction, in terms of explaining the soft X-ray puzzle, that the energy conducted into the photosphere would be emitted at the black-body temperature, thus enhancing the total soft X-ray flux.

Kuijpers and Pringle (1982) demonstrated the limitations of conduction cooled shock models. By consideration of the mean free paths and thermal energies of shock heated particles, they showed that the total energy flux across the shock front could not, even by free convection, be carried into a region with a temperature $T < 10^{-2} T_s$ (about 10 times the photospheric temperature of a radially accreting white dwarf). They concluded, therefore, that thermal conduction was insufficient to transport any significant fraction of the total accreted energy flux, from a shock with temperature $\sim 4 \cdot 10^8$ K down to a photosphere with a temperature $\sim 10^5$ K.

The same conclusion was reached from a more detailed calculation of the temperature structure of the accretion column, carried out by Frank et al (1983), in which shock heated material is cooled by both thermal conduction and bremsstrahlung radiation. They showed that two types of conduction solution exist: one in which the conductive flux saturates as the temperature decreases monotonically to zero, and a second in which the conductive flux always remains small and the temperature reaches a minimum. Which of these solutions, then, is appropriate to a white dwarf accretion column? One unique

solution can be chosen from these solutions by imposing the boundary condition, at the base of the column, that the column must match onto an atmosphere. To do this the conductive flux must vanish at some temperature, so that only solutions of the second type can be appropriate. Consequently, no energy can be conducted into the photosphere.

The inclusion of conduction does, however, modify the temperature structure of the accretion column in two ways: the height of the shock above the photosphere and the temperature immediately behind the shock are both reduced. The first of these is as a result of conduction transporting energy to a point in the column where it can be radiated more efficiently. The second result is a direct consequence of some of the energy flux being conducted rather than advected away from behind the shock. This model is, however, in terms of observational predictions, somewhat similar, to the bremsstrahlung cooled models described above.

2.3.3 Cyclotron cooled models.

In addition to pointing out that a magnetised white dwarf would accrete matter radially onto its magnetic poles, Fabian et al (1976) noted that any shock formed in the inflowing material would cool both by cyclotron radiation and bremsstrahlung radiation. Masters et al (1979) noted that the matter heated in the shock wave is mildly relativistic ($T \sim 10^8 - 10^9 \text{K}$) and that, as a result, the cooling material would be optically thick up to some frequency $\omega^* > \omega_c$ (typically $(\omega^*/\omega_c) \sim 10-100$; where ω_c is

the cyclotron frequency). They therefore estimated that the cyclotron luminosity could be approximated by

$$L_{\text{cyc}} \approx AkT_s \omega^*{}^3 / (12 \pi^2 c^2) \quad (2.2)$$

where A is the surface area of the shock and where ω^* must be determined in some way from a knowledge of the length of the accretion column.

Clearly, for a sufficiently strong magnetic field, cyclotron radiation will be the dominant radiative process in the accretion column. Lamb and Masters (1979) calculated the range of luminosity/fractional accreting area (L/f) and magnetic field (B) for which cyclotron radiation is the dominant cooling mechanism (Figure 2.2). They also showed that the cyclotron cooled model could be split into three regimes.

I) For the cyclotron cooling timescale $t_{\text{cyc}} > t_{\text{ei}}$ a one fluid approach can be used.

II) For $t_{\text{ei}} < t_{\text{cyc}} < t_{\text{ii}}$ the ion-ion energy exchange timescale the electron temperature never reaches the shock temperature and a two fluid treatment is necessary.

III) For $t_{\text{cyc}} < t_{\text{ii}}$ the accreted ions do not have time to form a Maxwellian distribution and a fluid dynamical, 'shock', model is no longer appropriate. A kinetic treatment, of the type described in Chapter 4, must be used instead,

The cyclotron cooled shock treatment predicts a three component spectrum (Figure 2.3) of the type observed in AM Her. type stars. This consists of an optical Rayleigh-Jeans tail, a hard X-ray bremsstrahlung component, and a soft X-ray component

produced by the reprocessing, in the photosphere, of the first two spectral components. Although this model does account, at least qualitatively, for the spectral features observed from white dwarf accretion columns, it does not produce an obvious solution to the soft X-ray puzzle as it does not explain how the reprocessed photospheric radiative flux can exceed the flux from the shock region.

SECTION 2.4 THE SUPRATHERMAL CONDUCTION TREATMENT.

The suprathemal conduction approach to the problem of the soft X-ray puzzle was proposed by Frank et al (1983) and Frank and King (1984) as a response to the failure of the (diffusive) thermal conduction model, described in the previous Section, to explain the soft X-ray puzzle. Frank et al (1983) and Frank and King (1984) argued that the high velocity electrons which populate the exponential tail of the Maxwellian distribution produced in the shock will have sufficiently long mean free path to allow them to traverse the gap between the hot 'shock' region and the cool photosphere, where they deposit their energy by means of Coulomb collisions. They proposed, therefore, that steady state solutions to the accretion column structures could be found in which the ion shock (two fluid approximation) lies close to the white dwarf surface and the dominant cooling process is the 'leaking' of these high velocity electrons into the photosphere.

This is essentially the same method of energy transport

that is observed in the solar transition region and should, as in that case, be treated by solving the Fokker-Planck equation (Shoub, 1983). Frank and King, however, employed a somewhat simpler treatment. They assumed that any electron with a velocity component directed towards the photosphere $v_z > v_{\min}$, the minimum velocity necessary to reach the photosphere, could deposit a fraction ϵ of its initial energy into the photosphere. They then incorporated this as an extra energy loss term into the standard fluid equations and derived the temperature structure and soft X-ray ratio ($L_{\text{bb}}/L_{\text{brems}}$) in terms of the two parameters ϵ and $\theta_{\min} = \left(\frac{2m_e v_{\min}^2}{2kT_s} \right)$. The predicted soft X-ray ratios are shown in Table (2.1) and, as can be clearly seen, this model does indeed predict a large soft X-ray excess. This is to be expected, since, mathematically, the effect of the 'leak factor' is to make energy vanish from the shock region and re-appear in the photosphere.

Frank and King (1984) have, however, misinterpreted the standard Coulomb collisional timescales derived in Spitzer (1962). As we shall show, they have as a result overestimated the mean free paths of the high energy electrons, thus raising doubts about the whole basis of this model (c.f. Thompson et al, 1986).

The timescales of interest are those in which suprathermal electrons give up most of their energy to a target plasma. The relevant results can be readily derived from Spitzer's (1962) treatment (c.f. Appendix A), where the target particles have Maxwellian energy distributions with a temperature T and a mean velocity $v_t = (2kT/M)^{\frac{1}{2}}$, for field particles of mass M . The

timescale for the change of a scalar function ϕ of the beam (test) particle with velocity v is found from

$$t_{\phi} = \phi(v) / \langle \Delta\phi(v) \rangle \quad (2.3)$$

where $\langle \Delta\phi \rangle$ (Spitzer's notation) denotes the collisional rate of change of $\phi(v)$ for the test particle averaged over species of field particle.

In particular Spitzer defines:

$$\text{The slowing down timescale } t_S = v / \langle \Delta v_{\parallel} \rangle \quad ; \quad (2.4)$$

$$\text{The deflection timescale } t_D = v^2 / \langle \Delta v_{\perp}^2 \rangle \quad ; \quad (2.5)$$

$$\text{The energy exchange timescale } t_E = E^2 / \langle \Delta E^2 \rangle \quad ; \quad (2.6)$$

where E is the kinetic energy, v_{\parallel} is the change in velocity along the original direction of motion, and v_{\perp} is the change in velocity perpendicular to the original direction of motion of the test particle. We also define one further timescale,

$$\text{The energy loss timescale } t_{EL} = E / \langle \Delta E \rangle \quad (2.7)$$

The exact evaluation from Spitzer (1962), to order m_e/m_p , for suprathermal electrons gives,

$$t_{EL} = \frac{3}{2} t_S = 2 t_D = \frac{m_e^2 v^3 [4\pi\epsilon_0]^2}{8\pi e^4 n \ln \Lambda} \quad (2.8)$$

independent of v_t and (with $v_e = (2kT/m_e)^{\frac{1}{2}} = v_t (M=m_e)$),

$$t_E = \frac{m_e^2 v^3 [4\pi\epsilon_0]^2}{8\pi e^4 n \ln\Lambda} \frac{v^2}{v_e^2} \quad (2.9)$$

which $\rightarrow \infty$ as $v_e \rightarrow 0$, and where n is the plasma density, e is the charge on an electron, ϵ_0 is the permittivity of free space, and $\ln\Lambda$ is the Coulomb logarithm.

Frank et al (1983) and Frank and King (1984) interpreted the energy exchange timescale as the rate at which an electron loses energy to the background (field) particles. The energy exchange timescale is, however, a dispersion timescale, representing the rate at which the distribution of individual particle energies, in an initially mono-energetic beam, spreads. Frank and King should instead have used the shorter energy loss timescale. Physically, it is obvious that a beam of single energy E can never attain an energy dispersion of order E if it is interacting with cold plasma particles ($\frac{1}{2}Mv_t^2 \rightarrow 0$). This does, not, however mean that the beam particles do not undergo a reduction in energy.

Frank and King (King 1985, private communication) have responded to this correction by suggesting that the shorter mean free path can be compensated for by a corresponding reduction in the shock height. The same number of electrons could then carry the same amount of energy to the photosphere producing the same predicted soft X-ray ratios as were previously calculated.

The situation is, however, not that simple. Firstly, to transport a significant fraction of the accreted energy flux by non-local electrons, as envisaged by Frank et al (1983) and

Frank and King (1984), a very steep temperature gradient is required i.e. a very thin cooling region, the thickness of which must be less than the mean free path of a typical thermal electron. Thus the cooling length-scale

$$\lambda_{\text{cool}} \lesssim \frac{(kT)^2 [4\pi\epsilon_0]^2}{8\pi e^4 n \ln\Lambda} \quad (2.10)$$

We also require for the shock model to be self-consistent, that the cooling length-scale be greater than the shock thickness i.e.

$$\lambda_{\text{cool}} \gtrsim \frac{F_s^2 [4\pi\epsilon_0]^2}{8\pi e^4 n \ln\Lambda} \quad (2.11)$$

Since $kT_s = \frac{3}{16} E$ a model of this type cannot be self consistent.

SECTION 2.5 THE BOMBARDMENT MODEL

The bombardment treatment of white dwarf accretion columns represent the opposite extreme of uniform accretion models to the shock approach described in the Sections 2.3 and 2.4. Proposed by Kuijpers and Pringle (1982), this model assumes that all the accreted energy is lost through radiation within the region in which it is thermalised. (The shock model assumes that no energy is lost in this region.) It is essentially similar to the non-thermal beam models of solar flares (Brown 1972,1973;

Emslie 1978; Brown and Craig 1984) in which suprathermal particles (in this case the accreted protons) strike a static target atmosphere. The beam particles heat the atmosphere by Coulomb collisions and the energy deposited is then radiated away locally by the atmosphere.

Kuijpers and Pringle (1982) performed an order of magnitude calculation in which the atmosphere is heated uniformly by Coulomb collisions over its entire volume, and cooled uniformly by optically thin line radiation. They obtained a mean temperature of 10^7 K for the atmosphere, somewhat lower than the shock temperature, although still considerably above the black-body temperature $\sim 10^5$ K. They concluded, therefore, that a bombardment type solution could exist and that such a solution would have a softer spectrum than the previous shock models. Thus a bombardment solution could perhaps help to resolve the 'Soft X-ray Puzzle'.

This type of model is examined more fully in Chapters 3 and 4 and for this reason we shall not discuss it further here.

ACCRETION COLUMN MODELS

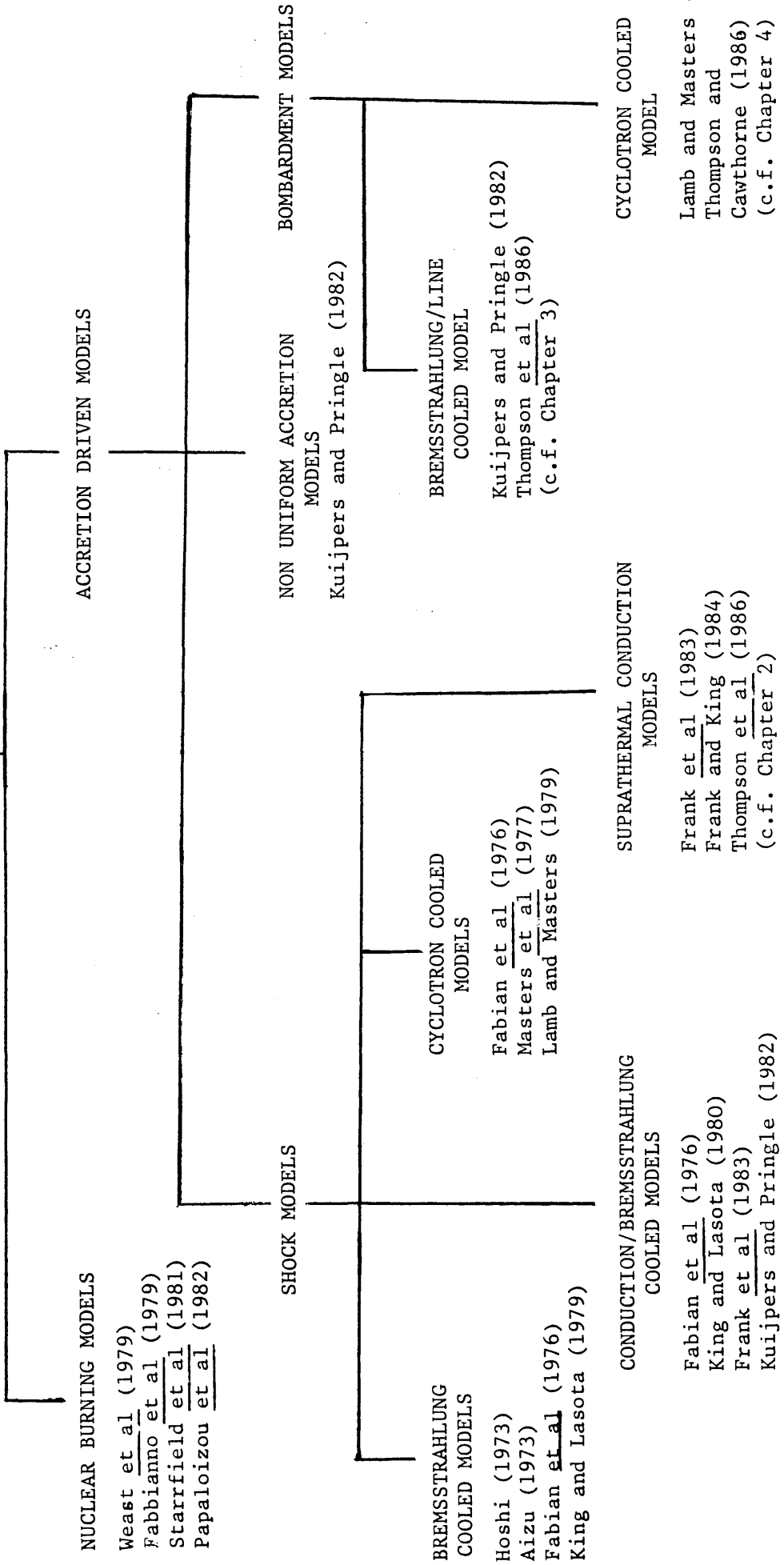


Figure 2.1: Family tree of accretion column models.

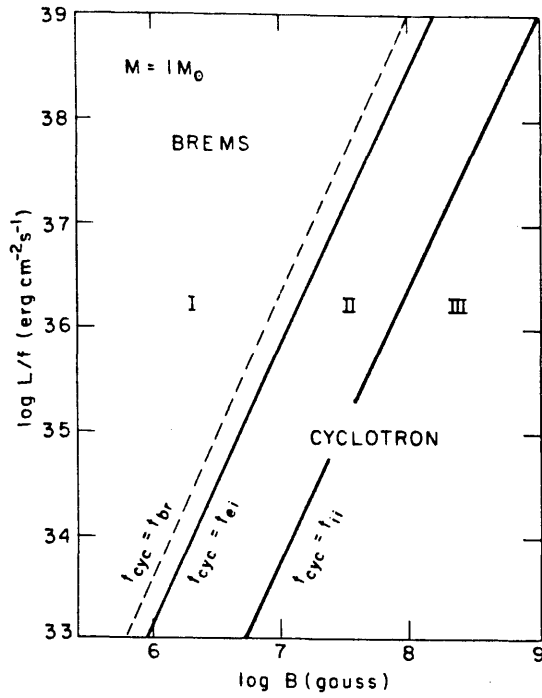


Figure 2.2: Parameter regimes in the $(B, L/f)$ plane for an $M = 1M_{\odot}$ star. (Lamb and Masters, 1979)

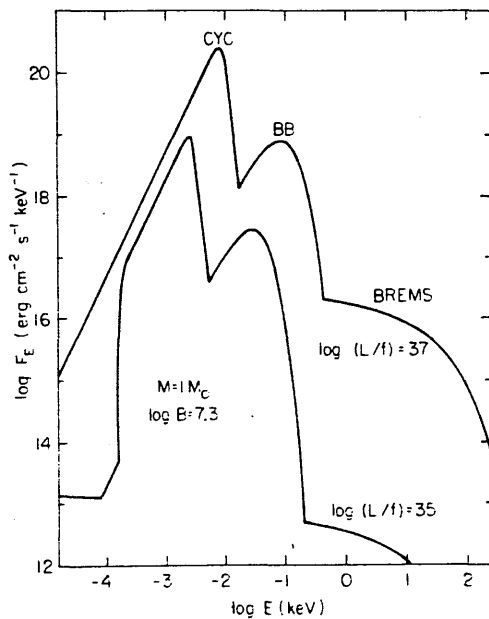


Figure 2.3: X-ray and UV spectrum produced by two different accretion rates onto a $1M_{\odot}$ degenerate dwarf having a magnetic field of $B = 2 \cdot 10^7$ gauss ($2 \cdot 10^3$ Tesla). (Lamb and Masters (1979)

CHAPTER 3

OPTICALLY THIN BOMBARDMENT MODELS

SECTION 3.1 INTRODUCTION

As we saw in the Chapter 2, most of the previous work on the 'Soft X-ray Puzzle' has centred around the study of models involving a stand off shock (e.g. Fabian et al, 1976; Lamb and Masters, 1979; Frank et al, 1983). Kuijpers and Pringle (1982), however, proposed two alternative solutions to the 'Soft X-ray Puzzle': a bombardment solution, and a non-uniform accretion model. In the first of these models, which we shall examine in this Chapter, the accreting matter is treated as a 'non-thermal' stream of protons which have mean free paths equal to the length of the dissipative region, and the Coulomb collisional energy deposition, by the 'non-thermal' accreting protons, is directly balanced by the optically thin (line) emission of a target atmosphere. Using order of magnitude estimates Kuijpers and Pringle (1982) derived a mean temperature for the column of order 10^7K , well below the shock temperature $T_s = 3.7 \cdot 10^8\text{K}$, though still well above the observed 'black-body' temperature $\sim 10^5\text{K}$.

In this Chapter we examine the bombardment solution of Kuijpers and Pringle. In Section 3.2, we show that Kuijpers and Pringle used an incorrect value for the Coulomb mean free path of the protons in their bombardment model. When the correct value is used, we find (Section 3.3) that the existence of a

solution is marginal, but the atmosphere has a 'mean' temperature around 10^5 K, lower than that found by Kuijpers and Pringle (1982), and much closer to the observed temperature of the 'black body' component of the spectrum. The fact that the temperature is close to the black body temperature does, however, cast doubt on the optically thin assumption.

In Section 3.4, we examine the bombardment solution more closely, along lines analagous to the models of solar flare heating by energetic beam collisions (Brown 1972,1973; Emslie 1978; Brown and Craig 1984). By examining the local balance of momentum and energy, we find that no pure bombardment solution exists without either a large 'top pressure' (at the gas vacuum boundary; an additional source of energy transport within the column (e.g. thermal conduction (Section 3.5)); or an additional energy loss mechanism (e.g. Cyclotron radiation (Chapter 4)).

Finally, in Section 3.6 we discuss the validity of the optically thin radiative loss curves calculated by Cox and Tucker (1969), Raymond et al (1976) and Summers and McWhirter (1979). We conclude that the large pressure (and consequent high density) in the accretion column and the large radiative flux which must be carried by a few spectral lines are likely to inhibit the atmospheres ability to radiate, and are, as a result, likely to make a bombardment / optically thin radiative solution less likely.

SECTION 3.2 COULOMB COLLISIONAL TIMESCALES

The time-scales and mean free paths of interest here are those over which suprathermal protons give up their energy to a target plasma. These can readily be derived from Spitzer's (1962) treatment, where the target (field) particles have Maxwellian distributions with temperature T . These timescales are derived in Appendix A.

There are three timescales of particular interest here. Firstly, although protons accreting onto a white dwarf may have energies E ($\geq 100\text{keV}$) much in excess of the thermal energy kT of the atmospheric plasma, they do not necessarily have speeds $v = (2E/m_p)^{\frac{1}{2}}$ in excess of the thermal speed $v_e = (2kT/m_e)^{\frac{1}{2}}$ of the atmospheric electrons. Since the relative speeds of two particles is the determining factor for the collisional mean free path, there are two limiting expressions for the proton-electron energy loss timescale.

$$t_{EL}^{pe} = \begin{cases} \frac{m_e}{m_p} \frac{[4\pi\epsilon_0]^2 m_p^2 v^3}{8\pi e^4 n \ln \Lambda} & v \gg v_e \quad (\text{cold plasma}) \quad (3.1a) \\ \frac{m_e}{m_p} \frac{3[4\pi\epsilon_0]^2 m_p^2 v^3}{32\pi^{\frac{1}{2}} e^4 n \ln \Lambda} & v \ll v_e \quad (\text{warm plasma}) \quad (3.1b) \end{cases}$$

In addition, for proton-proton collisions there is one energy loss time scale. For $v \gg v_p = (2kT/m_p)^{\frac{1}{2}}$

$$t_{EL}^{pp} = \frac{[4\pi\epsilon_0]^2 m_p^2 v^3}{8\pi e^4 n \ln \Lambda} \quad (3.2)$$

In their bombardment calculation, Kuijpers and Pringle (1982) used the proton-proton expression (Equation 3.2) to calculate the collisional mean free path of the accreting protons. However, comparison of Equations (3.1) and (3.2) shows that $t_{EL}^{pp} \leq t_{EL}^{pe}$ only if $kT \geq E(m_e/m_p)^{1/3}$ i.e. $T \geq 10^8 K$ which is not consistent with the atmospheric temperature ($\approx 10^7 K$) they derive. Instead one of Equations (3.1) should have been used, depending on the value of $(2kT/m_e)^{1/2}$ relative to $(2E/m_p)^{1/2}$. Consequently, the limit Equation (3.1a) will be applicable if $kT \leq (m_e/m_p)E$, i.e. $T \leq 6 \cdot 10^5 K$ and Equation (3.1b) will be applicable if $T \geq 6 \cdot 10^5 K$, so that the appropriate value of t_{EL}^{pe} is coupled to the atmospheric temperature which it determines. For the temperature $\approx 10^7 K$ derived by Kuijpers and Pringle, the appropriate t_{EL} would be Equation (3.1b) which is, at this temperature, about 20 times smaller than the value of t_{EL} (Equation 3.2) which they used. In the Section 3.3 we therefore re-consider the Kuijpers and Pringle result.

SECTION 3.3 GLOBAL ARGUMENT

The essence of the Kuijpers and Pringle (1982) bombardment solution is that of a global steady state, in some average sense over the accretion column, where the atmospheric plasma pressure and the optically thin radiative losses from the plasma (e.g. Summers and McWhirter, 1979) balance the rate of deposition of energy and momentum by the beam.

$$\text{i.e.} \quad 2nkT = F_0 m_p v \quad (3.3)$$

$$\text{or} \quad n = 1.5 \cdot 10^{15} \dot{M}_{13} / f_{-2} M_1^{\frac{1}{2}} R_7 T_5^{-1}$$

$$\text{and} \quad n^2 f_R(T) = F_0 E / vt_{EL} \quad (3.4)$$

where F_0 is the beam number flux, n is the electron number density, \dot{M}_{13} is the mass accretion rate in units of 10^{13} Kgs^{-1} , M_1 is the white dwarf mass measured in solar masses, R_7 is the white dwarf radius in units of 10^7 m , T_5 is the temperature in units of 10^5 K , f_{-2} is the fraction of the white dwarf's surface over which accretion is taking place measured in units of 10^{-2} and $f_R(T)$ is the radiative loss function, and where E and v are the energy and velocity of the accreting particles, and where the small corrections to n for non-hydrogenic contributions are neglected.

From Equation (3.1) we have

$$t_{EL} = \begin{cases} \frac{m_e}{m_p} \frac{[4\pi\epsilon_0]^2 m^2 v^3}{8\pi e^4 n \ln \Lambda} & v \gg v_e \\ \frac{3m_p (2\pi)^{\frac{1}{2}} [4\pi\epsilon_0]^2 (kT_e)^{\frac{3}{2}}}{8\pi e^4 n \ln \Lambda} & v \ll v_e \end{cases} \quad (3.5)$$

where the proton infall speed $v = (2GM_*/R_*)^{\frac{1}{2}}$ and M_* and R_* are respectively the stellar mass and radius. We also obtain from (3.3) and (3.4)

$$\frac{f_R(T)}{T} = \frac{2k}{n t_{EL}} \quad (3.6)$$

Therefore, taking $\ln \Lambda = 10$

$$\frac{f_R(T)}{T} = \begin{cases} 8.7 \cdot 10^{-40} M_1^{-3/2} R_7^{-3/2} & v \geq v_e \\ \frac{5.2 \cdot 10^{-31}}{T^{3/2}} & v \leq v_e \end{cases} \quad (3.7)$$

In Figure 3.1 we have plotted $f_R(T)/T$ using the results for cosmic abundances of Raymond et al (1976), and the results for solar abundances of Cox and Tucker (1969) and Summers and McWhirter (1979), as a function of T . We have also graphed the right hand side of Equation (3.7) for $M_1 = 0.8, 1.0, \text{ and } 1.2$, assuming a white dwarf mass-radius relation $R_7 = 0.87/M_1^{1/3}$. Steady state solutions may exist where the heating and radiative loss function curves intersect. Also shown (dashed line) is the value the right hand side of Equation (3.7) would have if $t_{EL} = t_{EL}^{pp}$ were the correct expression, as assumed by Kuijpers and Pringle (1982) - the intersection with $f_R(T)/T$ near $T = 10^7 K$ indicating their solution. From Figure 3.1 it can be seen, however, that the correct steady state intersection points occur either at very low temperatures $\approx 10^4 K$ or (for $M_1 > 0.9$) at temperatures in the range $5 \cdot 10^4 K \lesssim T \lesssim 2 \cdot 10^5 K$. (The slightly surprising fact that this temperature is much less than that found by Kuijpers and Pringle, in spite of the fact that the correction to the collision rate increases the energy deposition rate, can be explained by the fact that the density of the radiating plasma and the radiative loss rate per particle both increase as the temperature decreases- c.f. Equations (3.3) and (3.4)). These values are much closer to spectral observations and, if correct, could help to resolve the 'soft X-ray puzzle'.

Unfortunately, the situation is not quite so simple.

Firstly, these solutions are so cool that the optically thin assumption is at best marginally justified. This can be seen by comparing the temperatures obtained from Figure 3.1 with the minimum black body value obtained in the optically thick limit - i.e the limit in which all the accreted energy flux is radiated as black body radiation, viz.

$$T_b = 1.2 \cdot 10^5 M_1^{\frac{1}{2}} (\dot{M}_{13}/f_{-2})^{\frac{1}{4}} \quad (3.8)$$

(shown in the top left of Figure 3.1.). Thus, unless $\dot{M}_* \ll 10^{13} \text{Kgs}^{-1}$ or $f \gg 10^{-2}$, the bombardment solution yields such a low temperature that absorption in the XUV lines results in the accretion column becoming sufficiently optically thick to cast doubt on the assumptions made in the model.

Secondly, since the optically thin condition and the existence of any intersection at all in Figure 3.1 are so marginal, it is necessary to consider more closely the meaning of the average temperature found from Equation (3.7). In particular, it should be noted that the Kijpers and Pringle momentum balance Equation (3.4) is only accurate at the base of the column, where all the beam momentum has been lost, while their energy balance Equation (3.5) is only accurate at the top of the column, where E and v are as yet unmodified by collisions. It is, therefore, not clear how the 'average' temperature so derived relates to the actual structure of the column. This is considered further in the next Section.

SECTION 3.4 THE SPATIAL STRUCTURE OF A BOMBARDED COLUMN.

We now consider the possibility of a bombardment solution which is in a local steady state at each point in its structure. To do this, we must use, not just the mean collisional time-scale (Equation 3.1), but rather consider the full collisional evolution of the descending proton stream. We expect from Figure (3.1) that throughout most of the structure, the temperature will satisfy the cold target condition (c.f. Equation (3.1a)) for which the beam evolution depends only on the column density $N = \int_0^1 n dz$, measured downward from the effective source of the stream (described completely by Emslie (1978) and Brown and Craig (1984)). For a proton of initial energy E_0 (at $N=0$), the energy $E(N)$ evolves according to

$$E(N) = (E_0^2 - 2CN)^{\frac{1}{2}} \quad (3.9)$$

where

$$C = \frac{2\pi e^4 \ln \Lambda}{[4\pi\epsilon_0]^2} \frac{m_p}{m_e} \quad (3.10)$$

We neglect gravity throughout (c.f. Frank et al, 1983).

Since protons are essentially not deflected in a cold plasma (their deflection time-scale $t_D \gg t_{EL}$ their energy loss time scale), their vertical number flux remains constant at its incident value F_0 until the protons stop which occurs, in the cold plasma approximation, at

$$N_{\max} = E_0^2 / 2C \quad (3.11)$$

Using the analyses of Emslie (1978) and Craig and Brown (1984), it is then straightforward to obtain the equations for local balance of beam and atmospheric pressures, and of collisional heating and optically thin radiative losses, viz. respectively

$$nT = \frac{F_0 (2m_p E_0^2)^{\frac{1}{2}}}{2k} \left\{ 1 - (1 - \eta)^{\frac{1}{2}} + p_0 \right\} \quad (3.12)$$

and

$$f_R(T) = \frac{CF_0}{E_0 (1 - \eta)^{\frac{1}{2}}} \quad (3.13)$$

where

$$\eta = N/N_{\max} = \frac{2CN}{E_0^2} \quad (3.14)$$

and

$$p_0 = P_0 / F_0 (2m_p E_0)^{\frac{1}{2}} \quad (3.15)$$

is an atmospheric 'top pressure' ($2nkT$ at $N=0$), measured in units of the beam ram pressure, which we have introduced to generalise the Kuijpers and Pringle treatment. We are effectively allowing the top of the accretion column to be situated in a region of finite gas pressure (e.g. the atmosphere

of the primary star) rather than in a vacuum. Elimination of F_0 between Equations (3.12) and (3.13), as in Section 3.3, then gives with Equation (3.10)

$$\frac{f_R(T(\eta))}{T} = \phi(\eta) = \frac{2\pi k e^4 \ln \Lambda}{m_e m_p (GM_*/R_*)^{3/2}} \left[\frac{1}{(1-\eta)^{1/2} \{1+p_0-(1-\eta)^{1/4}\}} \right] \quad (3.16)$$

The dimensional factor (outside []) in Equation (3.16) is a factor $2^{3/2}$ larger than that in the modified Kuijpers and Pringle (1982) global solution (Equation 3.6). Further the dimensionless ([]) spatial factor in Equation (3.16) has a minimum value of $27/(4(1+p_0)^3)$ at $\eta = 1-(2/3(1+p_0))^4$ if $p_0 < \frac{1}{2}$, and of $1/p_0$ at $\eta=0$ if $p_0 > \frac{1}{2}$. Consequently, if $p_0 = 0$, as in the Kuijpers and Pringle solution (and in Section 3.3) then the right hand side of Equation (3.16) is everywhere a factor of $27/2^{1/2}$ or more larger than the right hand side of Equation (3.7), and no steady state solution for $T(N)$ can exist for any N . The situation is clearly shown in Figure 3.2 which, for the typical case of $M_1 = 1.0$, shows (a) a plot of the right hand side of Equation (3.16) as a function of η - for a variety of values of p_0 , and (b) a plot of the left hand side of (3.16) as a function of T . To find the steady state bombardment solution temperature $T(N)$, at depth N in the accretion column, for a chosen p_0 , the procedure is to calculate the η corresponding to N , find the resulting $\phi(\eta)$ at this η from Figure 3.2(a) then project this value of $\phi(\eta)$ horizontally onto the $f_R(T)/T$ curve in Figure 3.2(b). If any intersections occur, these represent a possible local steady state temperature for that N .

Inspection of Figure 3.2 shows that no steady state is possible anywhere unless $p_0 > 0.4$, i.e. the top pressure exceeds about 40% of the beam ram pressure. For $p_0 = 1.0$ two classes of solution formally exist over the range of η up to $\eta = 0.7$ only. (The singularity in the heating function at $\eta = 1$ (Equation 3.11) is not a major concern and disappears when a small spread is introduced to the accretion energy E_0 .) These classes of solution comprise: (i) solutions in which $T(N)$ increases with increasing depth N and lie in the range $T = 1.3 \cdot 10^4 \text{K}$ to $1.6 \cdot 10^4 \text{K}$, and can be discounted because they are well below T_b for a plausible \dot{M}_* ; and (ii) solutions in which $T(N)$ decreases with increasing depth N and lie in the range $1.6 \cdot 10^4 \text{K}$ to $2 \cdot 10^4$ and so are again in the optically thick regime, which invalidates the solution. If p_0 is increased still further, two further, similar, classes of solution exist but the hotter (type ii) solution is almost entirely within the temperature range $T = 10^5 \text{K}$ to $3 \cdot 10^5 \text{K}$. The cooler (type i) solution can again be neglected on the grounds of optical thickness. Furthermore, solutions in which $T(N)$ increases with increasing N require that $n(N)$ decreases as N goes up and so cannot be matched to the photosphere, nor can they be expected to be convectively stable. The hot solutions, with decreasing $T(N)$ as N increases, can, on the other hand, probably be matched on to a photosphere and are likely to be convectively stable, although they are likely to be radiatively unstable on this portion of the $f_R(T)$ curve (c.f. Cox and Tucker, 1969).

The only possible bombardment solutions in which the beam energy deposition is balanced purely by optically thin

radiation, therefore, demand a high atmospheric top pressure. Physically, the reason for this is that Coulomb collisions produce a non-zero heating per unit mass as $N \rightarrow 0$, independent of n . It is, therefore, necessary for both $T(N \rightarrow 0)$ and $n(N \rightarrow 0)$ to be finite and non-zero in order to balance this input radiatively.

What could such a top pressure mean physically? We first note that local energy balance is required only on some finite length scale and that energy description on a smaller scale requires a kinetic treatment. Thus our top pressure could in fact be the pressure one mean free path away.

We therefore consider the mean free path of an ambient electron $\lambda_e \sim t_{EL}^{ee} v_e$, where

$$t_{EL}^{ee} = \frac{[4\pi\epsilon_0]^2 [kT]^2}{2\pi e^4 n \ln\Lambda v_e} \quad (3.17)$$

is the electron - electron Coulomb collisional timescale (c.f. Equation 2.8), and where $v_e = (2kT/m_e)^{1/2}$. Thus,

$$\lambda_e \sim \frac{[4\pi\epsilon_0]^2 [kT]^2}{2\pi e^4 n \ln\Lambda} \quad (3.18)$$

and the column density through which an electron passes between collisions is

$$N_e \sim n \lambda_e \sim \frac{[4\pi\epsilon_0]^2 [kT]^2}{2\pi e^4 \ln\Lambda} \quad (3.19)$$

Using Equation (3.12) it can easily be seen that the value of p_0 one mean free path from the top of the atmosphere is given

by

$$\begin{aligned}
 p_0 &\sim (1 - (1 - N/N_{\max})^{\frac{1}{4}}) \\
 &= \left(1 - \left(1 - \frac{m [kT]^2}{m_e E^2} \right)^{\frac{1}{4}} \right) \gtrsim 3 \cdot 10^{-6} \quad (3.20)
 \end{aligned}$$

On the other hand, p_0 can never exceed unity, the pressure which is reached when the beam is entirely stopped (c.f. Equation 3.3).

Clearly, if a large p_0 is rejected, bombardment solutions are only tenable if they also involve some other form of energy transport such as conduction or convection to redistribute energy within the column (considered in Section 3.5), additional radiative processes such as cyclotron radiation (c.f. Chapter 4) or anomalously high line losses (c.f. Section 3.6). It should be noted, however, that the amount of energy flux which would have to be transported is not necessarily comparable to the accretion flux but is probably only the difference between the energy input and the radiative loss functions (Figure 3.2).

SECTION 3.5 THE SPATIAL STRUCTURE OF THE BOMBARDED COLUMN INCLUDING THERMAL CONDUCTION

In this Section we examine the effect of thermal conduction on the possible existence of a beam heated model atmosphere for a radially accreting white dwarf. We show that the inclusion of thermal conduction allows a self consistent steady state solution to be found, in which the energy that cannot be

radiated in the bombarded region is conducted to a point further down in the atmosphere where it can be radiated away. The resulting temperature structure is similar to that derived by Frank et al (1983) for a conduction/bremsstrahlung cooled shock model, in that all the accreted energy is emitted as optically thin radiation and none is conducted into the photosphere. In addition, we estimate the range of accretion rates for which this type of model is appropriate.

In order to do this we reconsider the energy and momentum continuity equations. As before, we assume a plane parallel atmosphere so that conservation of momentum gives us.

$$\frac{dP}{dz} = -F_0 m_p \frac{dv}{dz} + m_p g n \quad (3.21)$$

where g is the surface gravity of the white dwarf. (We shall see a posteriori that the contribution to the hydrostatic pressure due to gravity at the bottom of the column will no longer be negligible and we, therefore, retain this term in Equation (3.21).) Conservation of energy gives

$$\frac{dF_{\text{COND}}}{dz} = n^2 f_R(T) - F_0 \frac{dE}{dz} \quad (3.22)$$

where F_{COND} is the total energy flux conducted out of a unit volume. We again choose to introduce the column density, $N = \int_0^1 n dz$, so that Equation (3.21) reduces to

$$P(N) = F_0 m_p (v_0 - v(N)) + m_p g N \quad (3.23)$$

(where v_0 is the velocity of the beam at $N=0$, and $P(0)=0$) and Equation (3.22) becomes

$$\frac{dF_{\text{COND}}}{dN} = n f_R(T) - F_0 \frac{dE}{dN} \quad (3.24)$$

Before we can determine the structure of the model atmosphere we still require to determine the form of the energy loss rate, $\frac{dE}{dN}$, and the conductive flux, F_{COND} .

Firstly, as was shown in Section 3.2, the accreting material loses energy by Coulomb collisions to both protons and electrons so that the total energy loss timescale is

$$t_{\text{EL}} = \frac{1}{(1/t_{\text{EL}}^{\text{pe}} + 1/t_{\text{EL}}^{\text{pp}})} \quad (3.25)$$

and since $t_{\text{EL}}^{\text{pe}}$ takes two distinct forms in the limits of $v_b \gg v_e$ and $v_b \ll v_e$, we approximate $t_{\text{EL}}^{\text{pe}}$ by

$$t_{\text{EL}}^{\text{pe}} = t_{\text{EL}_{\text{cold}}}^{\text{pe}} + t_{\text{EL}_{\text{warm}}}^{\text{pe}} \quad (3.26)$$

which gives the correct asymptotic form. The total energy loss rate then is

$$\frac{dE}{dt} = \frac{2\pi e^4 \ln \Lambda n v m_p}{[4\pi\epsilon_0]^2 E m_e} \left[\frac{1}{1 + \frac{3\pi^{1/2}}{4} \left[\frac{m_p kT}{m_e E} \right]^{3/2}} + \frac{m_e}{m_p} \right] \quad (3.27)$$

i.e.

$$\frac{dE}{dN} = \frac{2\pi e^4 \ln \Lambda m_p}{[4\pi\epsilon_0]^2 E m_e} \left[\frac{1}{1 + \frac{3\pi^{1/2} \left[\frac{m_p kT}{m_e E} \right]^{3/2}}{4}} + \frac{m_e}{m_p} \right] \quad E > kT \quad (3.28)$$

The diffusive thermal conductive flux (i.e. for $F_{\text{COND}} \ll F_{\text{SAT}} \approx \frac{1}{6} n_e m_e v_e^3$, the saturated conductive flux) is given by

$$F_{\text{COND}} = \kappa \frac{dT}{dz} = \kappa_0 T^{2.5} \frac{dT}{dz} \quad (3.29)$$

where κ is the coefficient of thermal conductivity and where $\kappa_0 = 10^{-11} \text{ Jm}^{-1} \text{ s}^{-1} \text{ K}^{-3.5}$, (Spitzer, 1962). (We have assumed here that the conductive length scale \ll the electron mean free path.)

In order to determine the structure of the accretion column we require, therefore, to solve four first order ordinary differential equations (Equations 3.21, 3.24, 3.28, 3.29), one of which, Equation (3.21), is analytically integrable. i.e. we require to solve the system of equations

$$\frac{dE}{dN} = \frac{2\pi e^4 \ln \Lambda m_p}{[4\pi\epsilon_0]^2 E m_e} \left[\frac{1}{1 + \frac{3\pi^{1/2} \left[\frac{m_p kT}{m_e E} \right]^{3/2}}{4}} + \frac{m_e}{m_p} \right] \quad E > kT ; \quad (3.30)$$

$$\frac{dF_{\text{COND}}}{dN} = n f_R(T) - F_0 \frac{dE}{dN} ; \quad (3.31)$$

$$\frac{dT}{dN} = \frac{F_{\text{COND}}}{\kappa_0 T^{2.5} n} ; \quad (3.32)$$

with

$$2nkT = F_0 (2m_p E_0)^{\frac{1}{2}} (1 - (E/E_0)^{\frac{1}{2}}) + m_p g N \quad (3.33)$$

This was done numerically using a variable step Gear method (NAG routine D02EHF) subject to the 4 boundary conditions - 3 at $N=0$:

- 1) $E = E_0$ - by definition;
- 2) $n = 0$ - by definition;
- 3) $F_{\text{COND}} = 0$ - since no energy can be conducted into the vacuum above the atmosphere;

and 1 at some $N \neq 0$ where T is small ($\sim 10^5 \text{K}$):

- 4) $F_{\text{COND}} = 0$ - this is necessary to allow the atmosphere to be matched onto a photosphere.

The correct solution was found by altering the value of T at the top of the atmosphere until condition (4) was satisfied.

The inclusion of thermal conduction allows us to find a steady state structure for the accretion column, although at a somewhat higher temperature ($T \sim 10^7 - 10^8 \text{K}$) than that suggested in Section 2.2 and 2.3. Figures (3.3) to (3.8) show examples of the temperature structure of the column, and the variation of pressure and the downward conductive flux with column depth, for white dwarf masses $M_1 = 1.0$ and 1.2 and accretion rates per unit fractional area $\dot{M}_*/f = 3 \cdot 10^{12}$, $3 \cdot 10^{11}$, $2.9 \cdot 10^{10}$ and $5.5 \cdot 10^{10} \text{Kgs}^{-1}$. We can see that the higher temperature within the proton stopping region considerably increases the proton stopping length, with the result that the assumption made in Sections (2.2) and (2.3), that the effect of gravity on the pressure is negligible, is no longer valid (justifying the

inclusion of gravity in Equation (3.33).

Although we have calculated a temperature structure for the atmosphere, we still require to determine the accretion rates for which the model is self consistent. We can deduce an empirical lower limit to the accretion rates for which the model is valid by examining the change in the length of the purely conductive part of the column. As the accretion rate is reduced, the extent of this region is reduced, and in fact goes to zero in Figures (3.5) and (3.8). These structures, with an accretion rate $\dot{M}_*/f \sim 4 \cdot 10^{10} \text{Kgs}^{-1}$ represent the lower bound of the accretion rate. For accretion rates below these values the bottom of the column requires to be treated by a straight forward bombardment model, incorporating the effect of gravity.

To determine the upper limit, we must first examine the relationship between bombardment models and shock models of the type examined by Frank et al (1983). Physically, any matter falling onto a white dwarf will pass through a region in which its bulk kinetic energy is thermalised. Any energy that can not be radiated away within this region must be transported further down into the atmosphere by either thermal conduction or advection to a point where it can be radiated away. In the shock model (Frank et al, 1983) the energy loss within the region where the energy of the infalling material is thermalised is neglected whereas, in this bombardment model, we have neglected the effect of the advection of energy by residual motion of the accreted matter. We would expect, therefore, that this model would be a better representation than the shock model if the energy flux lost across the bombarded region exceeds the

expected advected flux from the bottom of the column.

The energy loss from the bombarded region can be determined simply by subtracting the conductive flux at the bottom of the region from the total energy flux of the accreting matter. In order to estimate the advected energy flux it is necessary to consider the Rankine - Hugoniot boundary conditions for a shock in which the total energy flux of the fluid is not continuous across the shock.

Conservation of mass, momentum and energy across the shock give:

$$\rho v = \rho_0 v_0 \quad (3.34)$$

$$P + \rho v^2 = \rho_0 v_0^2 \quad (3.35)$$

$$\frac{1}{2} (5P + \rho v^2) v = \frac{1}{2} \rho_0 v_0^3 (1 - \epsilon) \quad (3.36)$$

where P = the fluid pressure, ρ = the fluid mass density, v = the bulk fluid velocity, and ϵ = the fraction of the energy flux lost across the shock (to either conduction or radiation), and where the subscript 0 denotes the pre-shock value of a quantity. The post-shock temperature T_s is, therefore,

$$T_s = \frac{3}{16} [3 + (9 + 16\epsilon)^{\frac{1}{2}} - 8\epsilon] \left[\frac{\frac{1}{2} m_p v_0^2}{k} \right] \quad (3.37)$$

i.e.

$$\frac{kT_s}{\frac{1}{2} m_p v_0^2} = \frac{1}{32} [3 + (9 + 16\epsilon)^{\frac{1}{2}} - 8\epsilon] \quad (3.38)$$

Thus, for a given shock temperature, the fraction of the energy flux carried by advection immediately behind the shock is

$$(1 - \epsilon) = \frac{1}{2} \left[1 - \left(1 - \frac{4 kT_s}{\frac{1}{2} m_p v_0^2} \right)^{\frac{1}{2}} + \frac{8 kT_s}{\frac{1}{2} m_p v_0^2} \right] \quad (3.39)$$

and the residual advective flux from the bombarded region can be estimated, a posteriori, by evaluating Equation (3.39) for $T_s =$ the temperature immediately below the bombarded region.

Figure (3.9) shows a graph of the estimated advective flux $(1 - \epsilon)$ against the accretion rate per unit fractional area (\dot{M}_*/f) superimposed upon a graph of the fractional radiated flux from the bombarded region against accretion rate per unit fractional area. The point of intersection of the curves represent the upper limit of \dot{M}_*/f ($\sim 3 \cdot 10^{12} \text{ Kgs}^{-1}$) for which the model is self consistent. Above this value the structure of the atmosphere would be better represented by a conductive shock model (e.g. Frank et al, 1983).

The inclusion of thermal conduction does, therefore, allow a steady state structure for the accretion column to be found for accretion rates \dot{M}_*/f between $\sim 3 \cdot 10^{10} \text{ Kgs}^{-1}$ and $\sim 3 \cdot 10^{12} \text{ Kgs}^{-1}$. These values are not, however, consistent with observations of AM Her. Therefore, without some method of either increasing the efficiency of energy flow within the atmosphere, such as convection, or increasing the radiative efficiency of the atmosphere, such as cyclotron radiation or anomalously high heavy element line losses, no bombardment solution can be found

to the 'Soft X-ray puzzle' of AM Her.

SECTION 3.6 THE VALIDITY OF THE RADIATIVE LOSS CURVE

We saw in Sections 3.3 and 3.4 that no purely bombardment model for the accretion column could exist in which the beam energy deposition rate is balanced locally by optically thin line radiation. The discrepancy between the radiative losses and the beam heating rate is, however, small and the exact form of the radiative loss function is, therefore, critical to the existence of any bombardment model of the accretion column.

In this Section we discuss some of the factors most likely to affect the magnitude of the radiative line losses. In particular, we discuss the effects of:

- 1) the presence of anomalously high heavy element abundances;
- 2) the collisional de-excitation of heavy ions;
- 3) the self absorption of emission lines.

The first of these three factors would enhance the radiation losses while the others are likely to suppress them.

At temperatures between $\sim 10^4$ K and $\sim 10^7$ K the dominant radiative loss mechanism for a plasma with cosmic or solar element abundances is line radiation from the small proportion of heavy elements (e.g. C, Si, O, Fe). An increase in the abundances of these elements by a factor of 10, for example, would enhance the radiative losses from the column by a similar factor, allowing a bombardment solution to exist. Such an enhancement would, however, seem to be unlikely. Firstly,

observations of non-accreting white dwarfs (e.g. Wesmael et al, 1984) suggest that white dwarfs have similar heavy element abundances to those found in the Sun. Secondly, the atmosphere of the white dwarf in the vicinity of the accretion column is likely to be made up of previously accreted matter and, since this matter comes from the atmosphere of the main sequence companion, it is unlikely to have significantly different element abundances in its atmosphere to those found in the Sun's atmosphere. Consequently, it is unlikely that the radiative losses could be increased in this manner.

The discrepancy between the beam energy input and the energy that the atmosphere is able to radiate may, in any case, be somewhat larger than the factor ~ 10 suggested in Sections 3.3 and 3.4.

The difference between the energy deposition rate and the radiative loss curve is at a minimum at the peak of the radiative loss curve ($T \sim 10^5 \text{K}$) which corresponds to a density in the atmosphere $n \sim 10^{24} \dot{M}_{13} / f_{-2} M_1^{\frac{1}{2}} R_7^{-\frac{5}{2}} \text{m}^{-3}$. This peak is due to the CIV (1549) and OVI (1033) lines. For these transitions, however, the collisional de-excitation rate becomes comparable to the radiative de-excitation rate at densities $\sim 10^{21} - 10^{22} \text{m}^{-3}$ (Summers 1985). The low density approximation (i.e. the assumption that collisional de-excitation is negligible), made by Cox and Tucker (1969), Raymond et al (1976) and Summers and McWhirter (1979), is clearly no longer valid and the ability of the atmosphere to radiate is reduced.

In addition, the problem of dissipating the energy from the atmosphere may further be exacerbated by self absorption of

radiation near the centres of CIV (1549) and OVI (1033) lines. From Raymond and Doyle (1981), we would expect the spectral flux at the centre of these lines

$$F(1549) \sim F(1033) \sim 10^{11} - 10^{12} (M_1^{8/3} \dot{M}_{13}/f_{-2}) W_m^{-2} \text{\AA}^{-1} \quad (3.40)$$

(assuming a line width of a few \AA). This compares with the flux from a black-body spectrum at a temperature of $5 \cdot 10^5 \text{K}$ of

$$F \sim 10^9 W_m^{-2} \text{\AA}^{-1} \quad (3.41)$$

Thus, the optical depths of both the CIV and OVI lines would be significantly greater than unity ($\tau \sim 10 - 100$), further reducing the atmosphere's ability to radiate.

It seems, therefore, somewhat unlikely that the line radiative losses could be enhanced sufficiently to allow the existence of a low temperature bombardment solution of the type described in Sections 3.3 and 3.4. In addition, such an atmosphere would tend to produce strong emission lines which have not been observed. It should be noted, however, that for higher temperatures ($T \sim 10^7 \text{K}$), where the dominant emission lines are those of iron and silicon, the problems of collisional de-excitation and line self absorption disappear. The problem of the discrepancy between the beam energy input and the ability of a solar element abundance plasma to radiate does, however, still remain.

SECTION 3.7 CONCLUSIONS

In this Chapter we re-examined the bombardment model for white dwarf accretion columns, proposed by Kuijpers and Pringle (1982), correcting the Coulomb timescale used in their calculation. Kuijpers and Pringle over-estimated the timescale for a proton beam being stopped by a cold plasma. The correction of this error improves their average solution in that the resulting temperature is reduced from $\sim 10^7\text{K}$ to $\sim 10^5\text{K}$ which is in better agreement with observations. Detailed calculations, equating, locally, the energy deposition by the beam to optically thin radiative losses and the beam momentum deposition rate to the gas pressure does not, however, produce a solution. Indeed no solution of this kind can ever exist without the inclusion of a non-zero 'top-pressure', since at column density $N = 0$ the collisional deposition rate per unit mass is finite, while the rate of energy loss through optically thin radiation is zero. The introduction of a large top pressure does permit a bombardment solution to exist, allowing the optically thin radiation losses to be finite at $N=0$. On the basis of the argument given in Section 3.4, concerning mean free paths, such an effect is likely to be small and certainly cannot exceed the beam ram pressure. It is, therefore, unlikely that a pure bombardment / optically thin radiation solution exists.

The existence of the Kuijpers and Pringle type global solution does suggest, though, that by invoking some other kind of energy transport process, such as thermal conduction, to redistribute energy within the column, a modified bombardment

solution may still be possible. However, as we showed in Section 3.5, although conduction does allow a structure for the atmosphere to be found, the model is only valid for accretion rates very much less than those inferred for AM Her. stars. Therefore, for these accretion rates the structure of the accretion column would be better represented by a shock model of the kind described by Frank et al (1983).

A significant increase in the radiative losses would move the bombardment model towards a steady state solution. This could be achieved either by the inclusion of cyclotron radiation (considered Chapter 4) or by an enhancement of heavy element line losses due to anomalously high heavy element abundances. The increase in the abundances required to achieve a steady state solution may, however, be significantly greater than the factor of ~ 10 suggested by the calculation in Section 3.4, since the densities involved here are sufficiently high that the use of the 'low density' radiative loss curve $f_R(T)$ will over-estimate the true losses both because of self absorption, near the line centres, and because of suppression of the line by collisional de-excitation. It is, therefore, unlikely that the 'Soft X-ray Puzzle' can be explained in terms of a self-consistent steady-state bombardment / optically thin line radiation model.

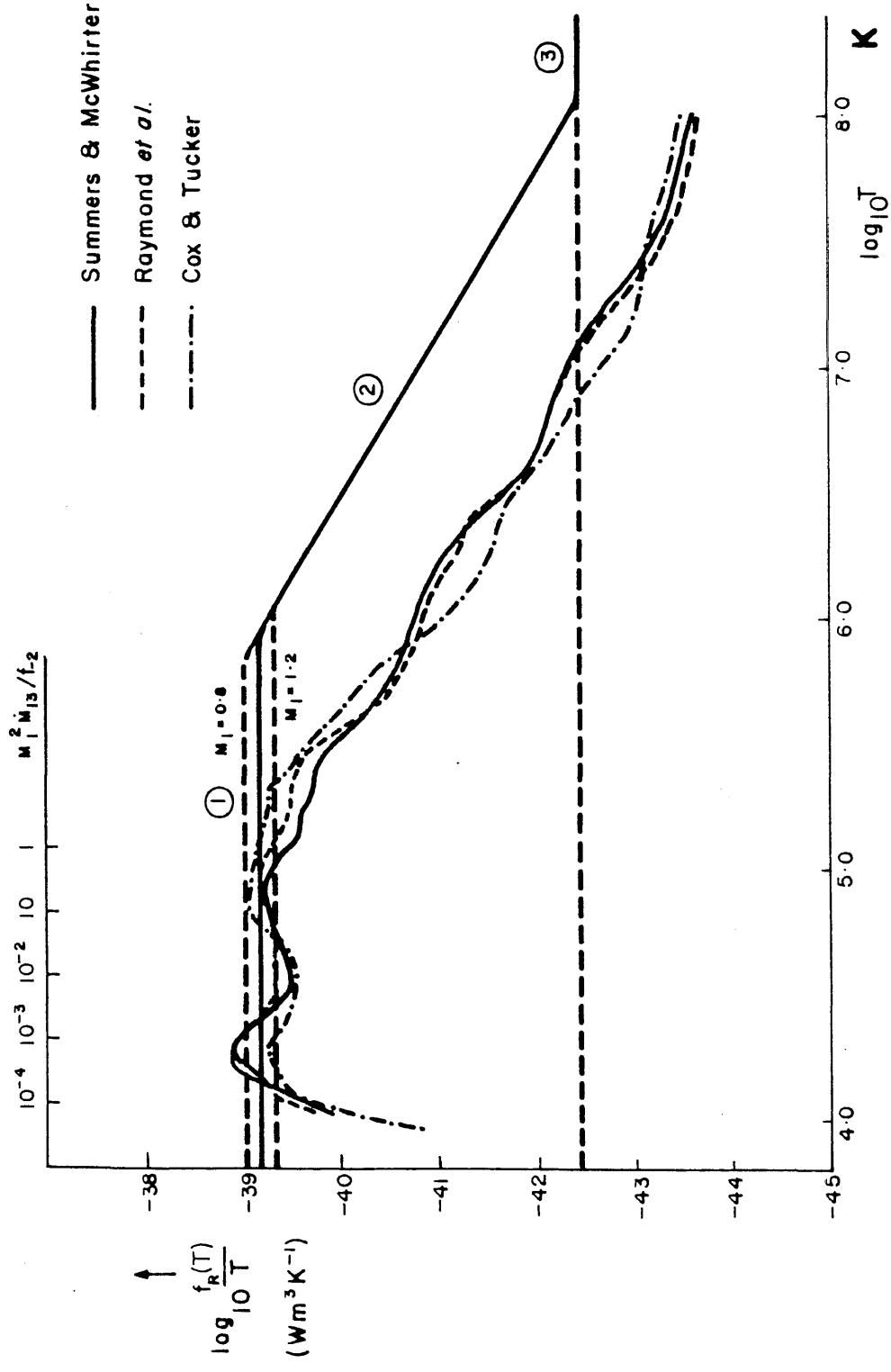


Figure 3.1: The curves of $f_r(T)$ against temperature are obtained from the calculations of Summers and McWhirter (1979) Raymond *et al.* (1976) and Cox and Tucker (1969). The solid piecewise straight line represents the values of k/nt_{BL} for a $1M_{\odot}$ white dwarf in the cold (1), warm (2) and hot (3) target approximations. The intersection of the dotted extension to region three with the radiative loss curves illustrates the original Kuijpers and Pringle (1982) solution. The dotted lines in region (1) illustrate the value of k/nt_{BL} for $M = 0.8$ and 1.2

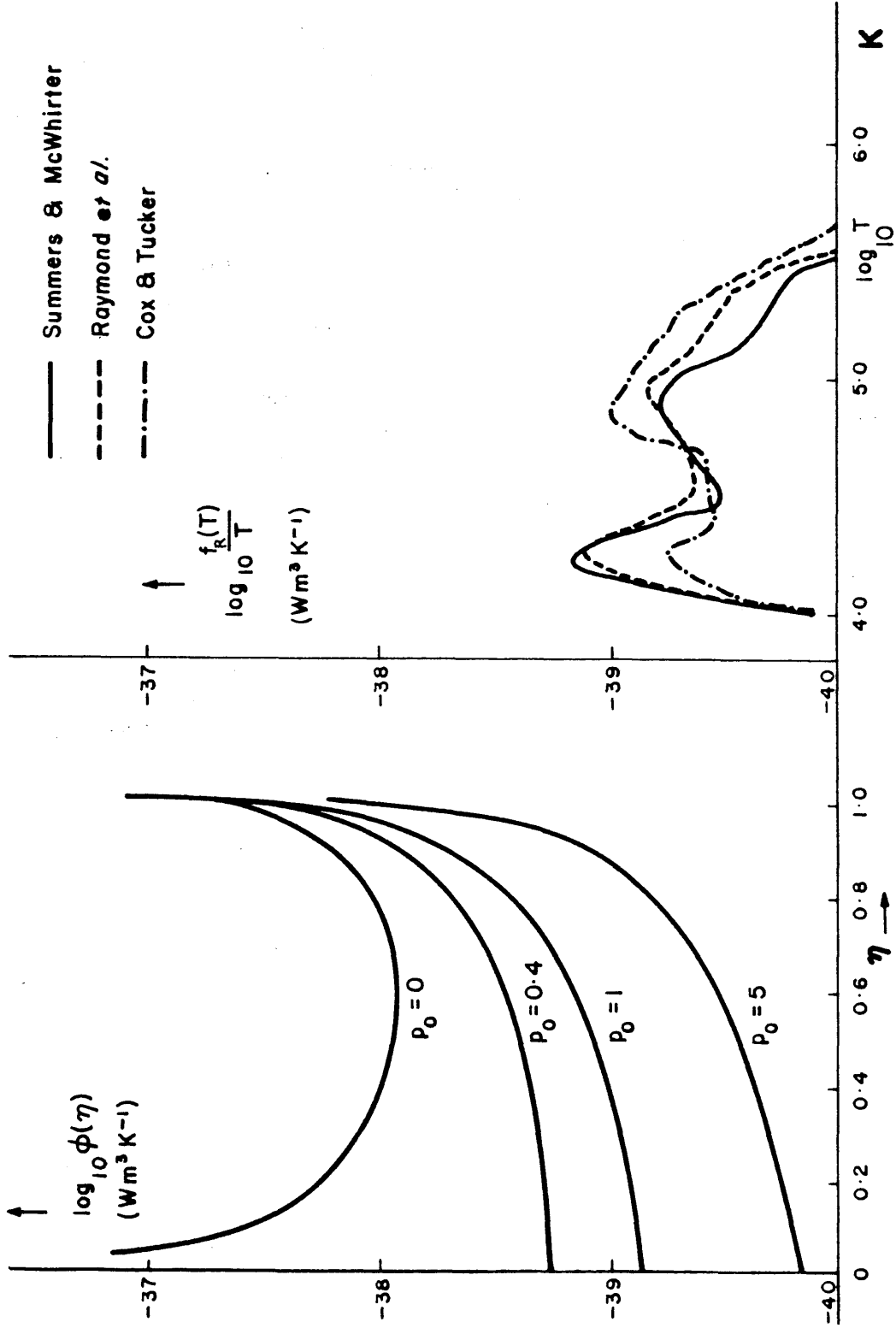


Figure 3.2: The right hand graph shows $f_R(T)/T$ as a function of temperature T . The left hand graph shows $\phi(\eta)$ against η for $p_0 = 0, 0.4, 1$ and 5 . The positions where $\phi(\eta) = f_R(T)/T$ denote the existence of an equilibrium solution for those particular values of η and T

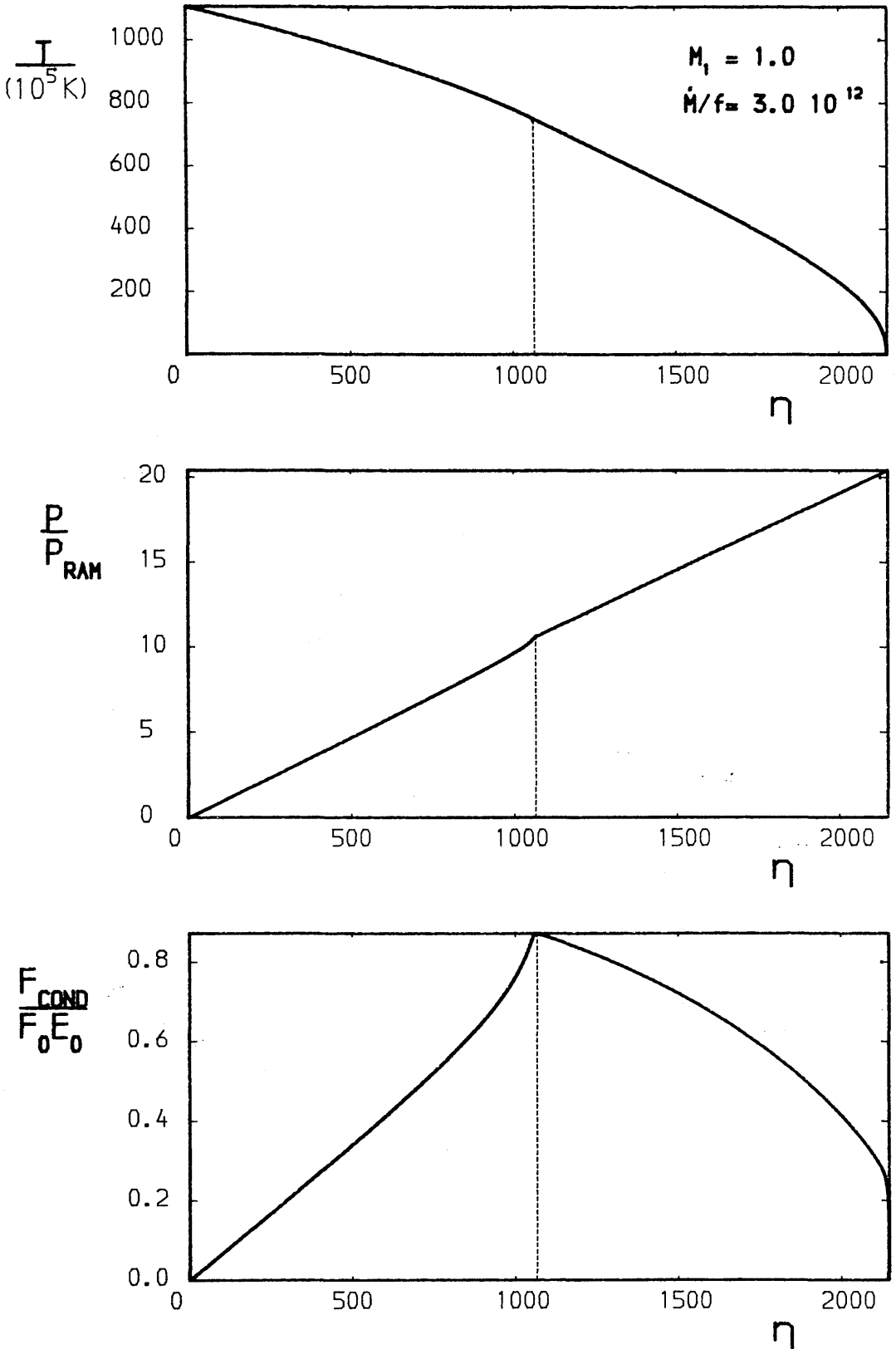


Figure 3.3: These graphs illustrate the variation of Temperature, Pressure and Conductive Flux with $\eta = N/N_{\text{max}}$ for a conduction cooled bombarded accretion column for a white dwarf mass = $1M_{\odot}$ and an accretion rate per unit fractional accreting area of $\dot{M}_*/f = 3 \cdot 10^{12} \text{ Kgs}^{-1}$. The dotted line denotes the depth at which the beam heating is terminated.

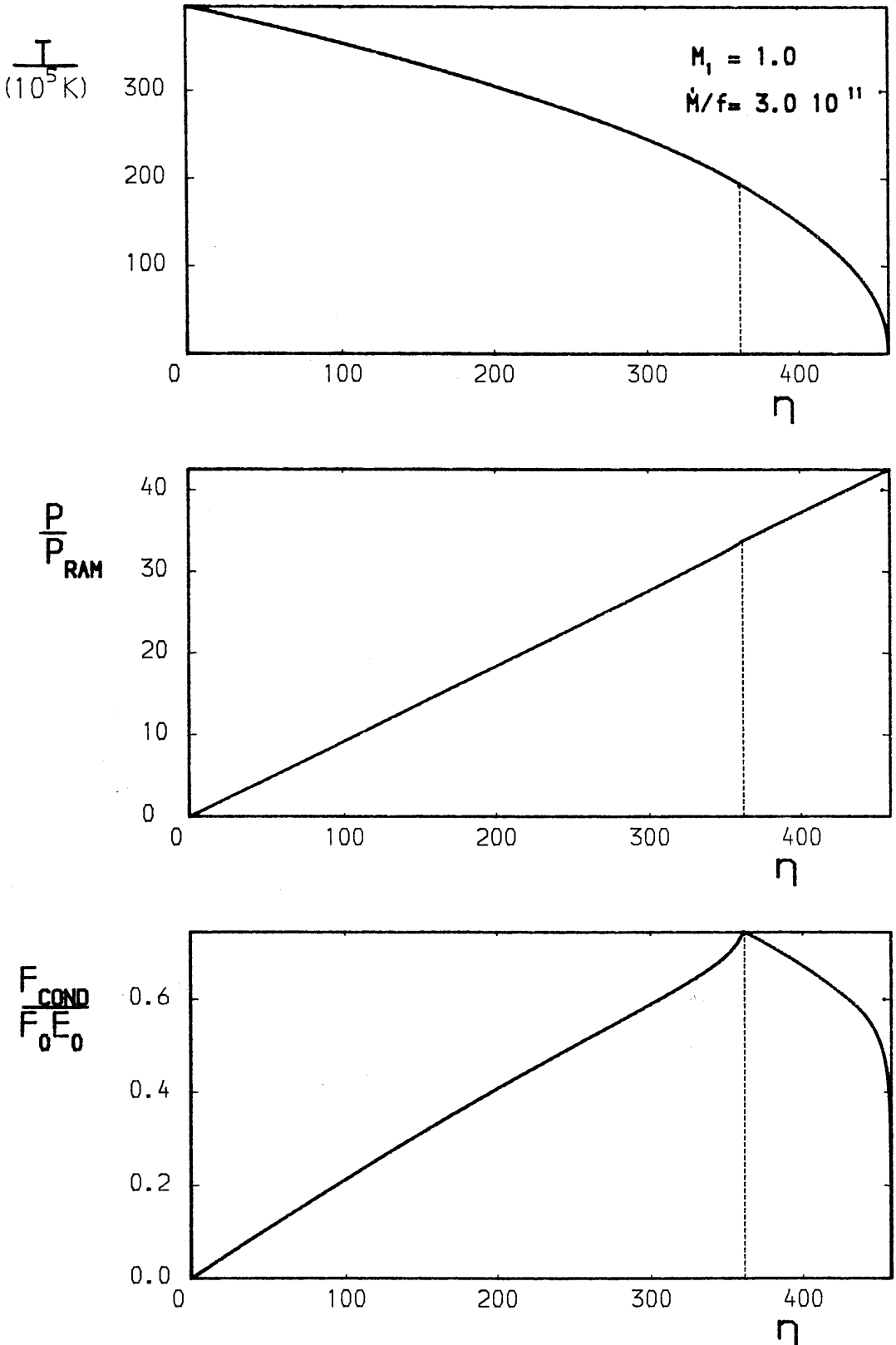


Figure 3.4: These graphs illustrate the variation of Temperature, Pressure and Conductive Flux with $\eta = N/N_{\text{max}}$ for a conduction cooled bombarded accretion column for a white dwarf mass = $1M_{\odot}$ and an accretion rate per unit fractional accreting area of $\dot{M}_*/f = 3 \cdot 10^{11} \text{ Kgs}^{-1}$. The dotted line denotes the depth at which the beam heating is terminated.

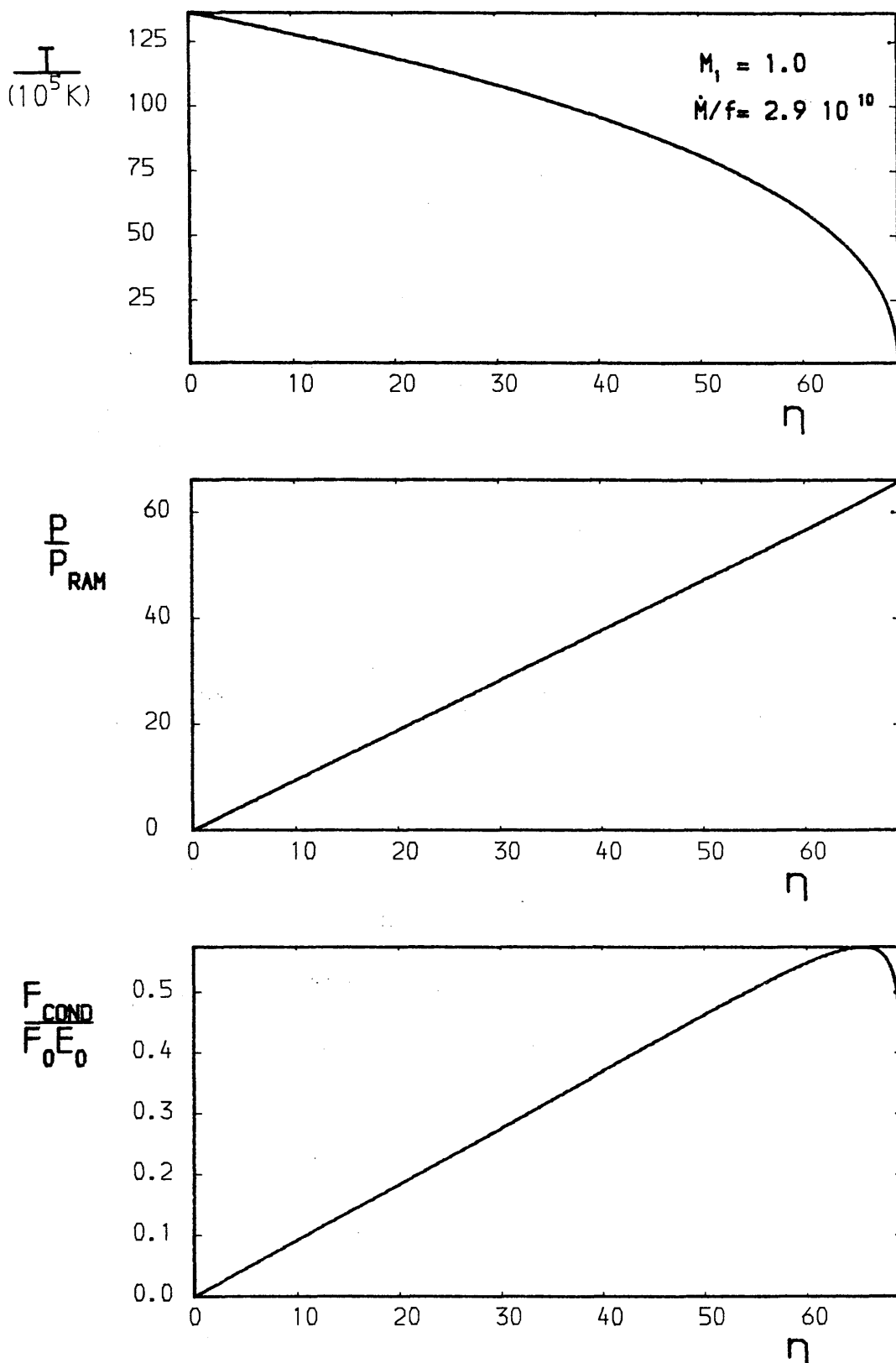


Figure 3.5: These graphs illustrate the variation of Temperature, Pressure and Conductive Flux with $\eta = N/N_{\text{max}}$ for a conduction cooled bombarded accretion column for a white dwarf mass = $1M_{\odot}$ and an accretion rate per unit fractional accreting area of $\dot{M}_*/f = 2.9 \cdot 10^{10} \text{ Kgs}^{-1}$.

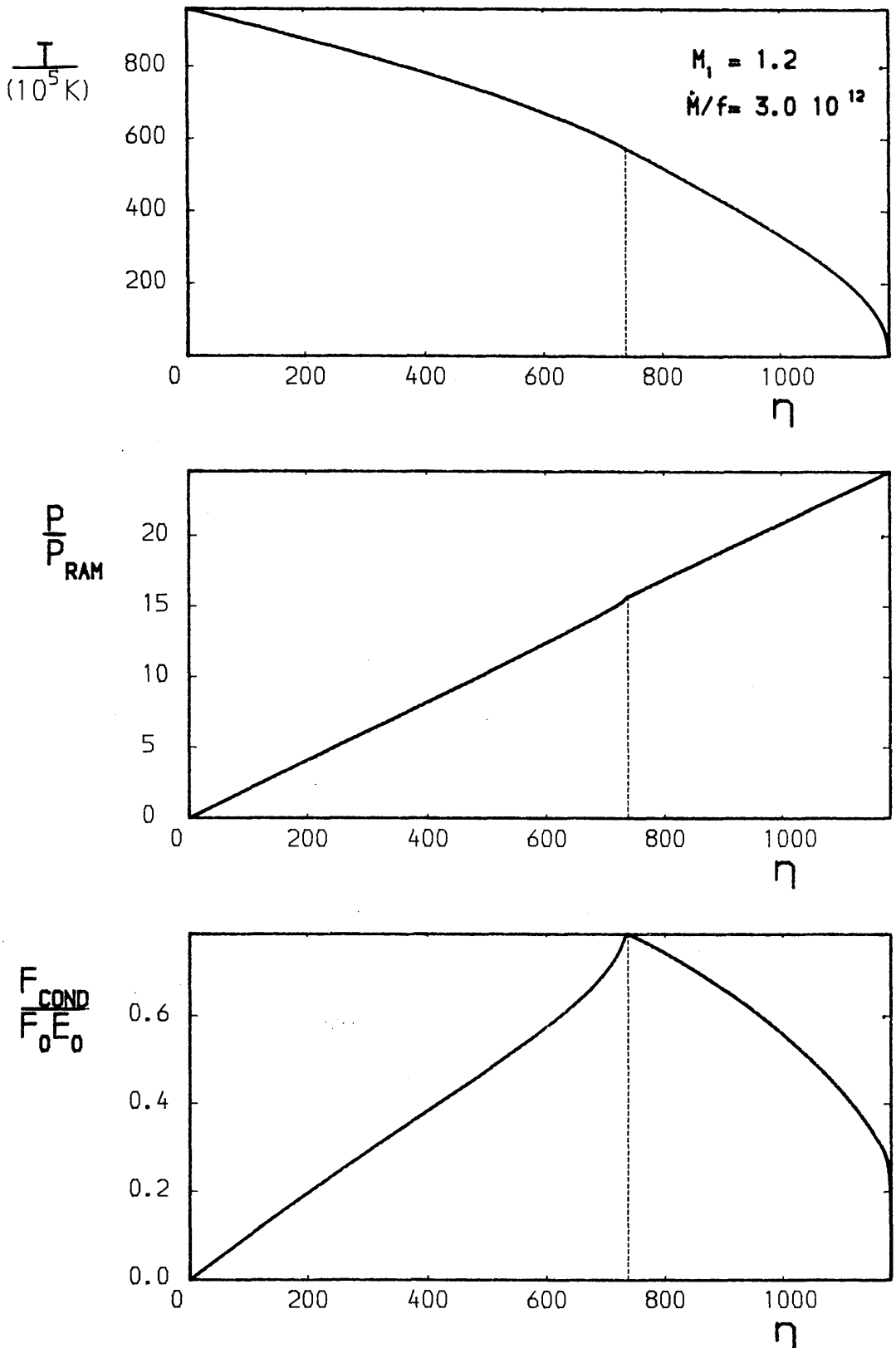


Figure 3.6: These graphs illustrate the variation of temperature, Pressure and Conductive Flux with $\eta = N/N_{max}$ for a conduction cooled bombarded accretion column for a white dwarf mass = $1.2M_{\odot}$ and an accretion rate per unit fractional accreting area of $\dot{M}_*/f = 3 \cdot 10^{12} \text{ Kgs}^{-1}$. The dotted line denotes the depth at which the beam heating is terminated.

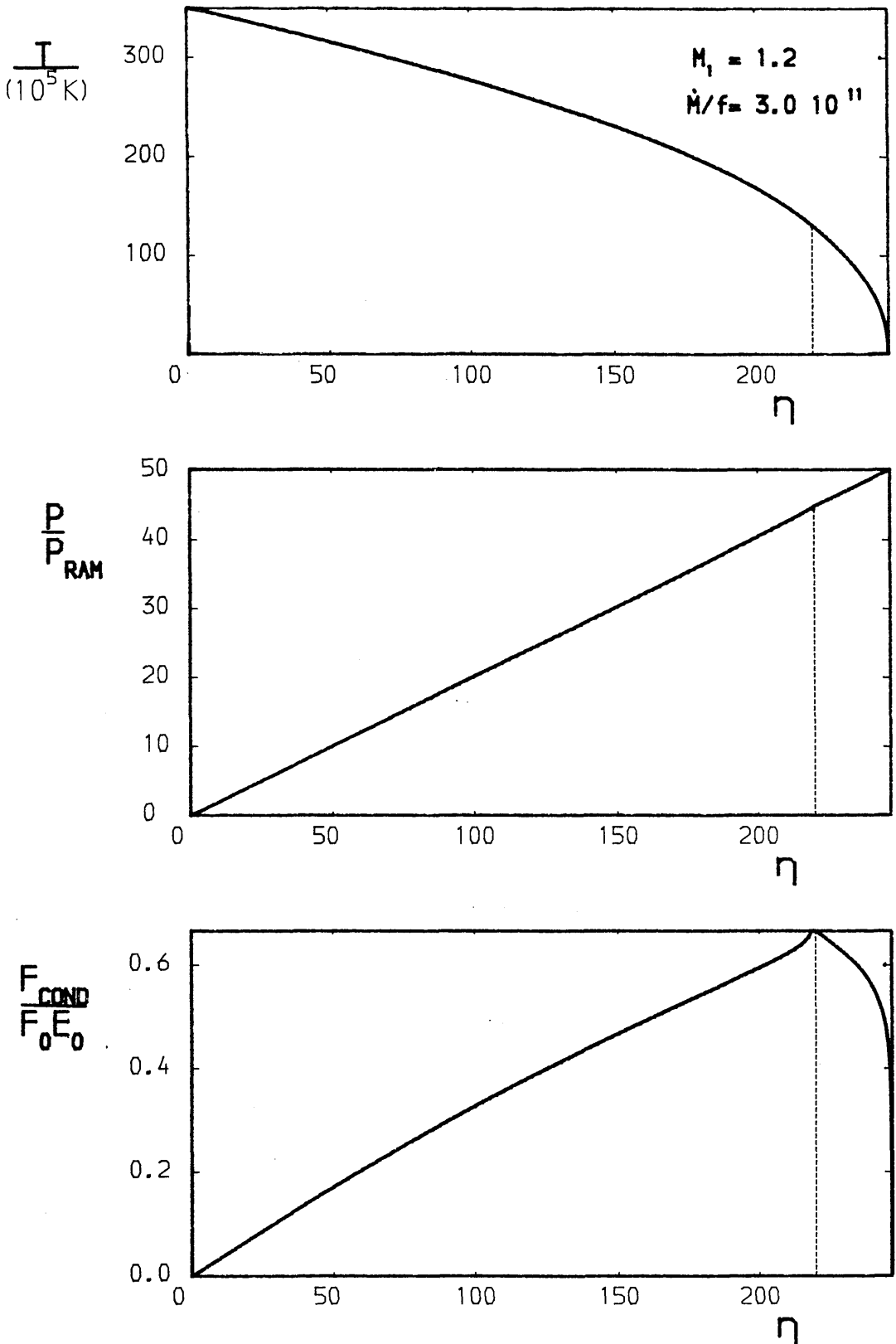


Figure 3.7: These graphs illustrate the variation of Temperature, Pressure and Conductive Flux with $\eta = N/N_{\text{max}}$ for a conduction cooled bombarded accretion column for a white dwarf mass = $1.2M_{\odot}$ and an accretion rate per unit fractional accreting area of $\dot{M}_*/f = 3 \cdot 10^{12} \text{ Kgs}^{-1}$. The dotted line denotes the depth at which the beam heating is terminated.

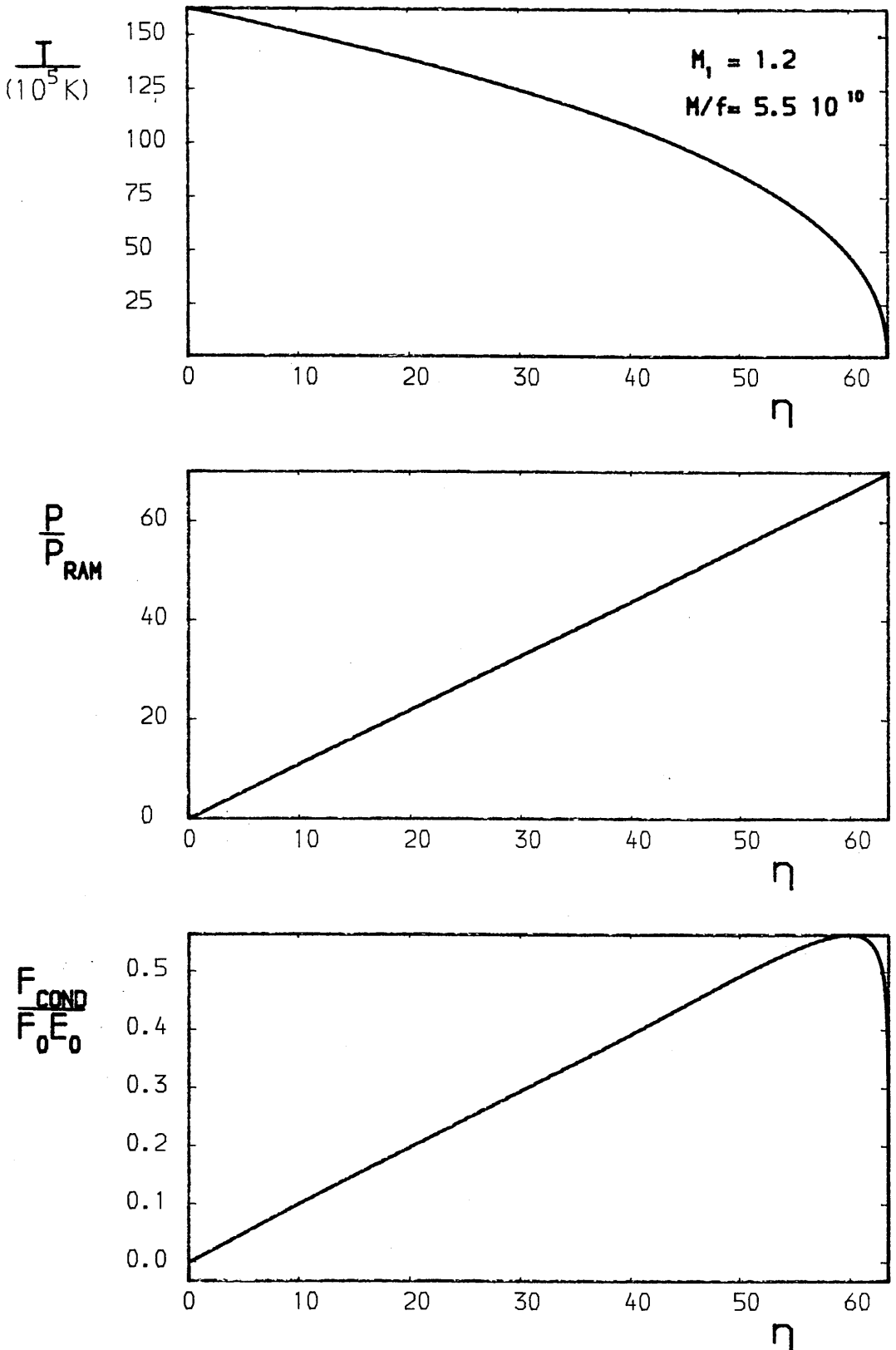


Figure 3.8: These graphs illustrate the variation of Temperature, Pressure and Conductive Flux with $\eta = N/N_{\text{max}}$ for a conduction cooled bombarded accretion column for a white dwarf mass = $1.2M_{\odot}$ and an accretion rate per unit fractional accreting area of $M_*/f = 5.5 \cdot 10^{10} \text{ Kgs}^{-1}$.

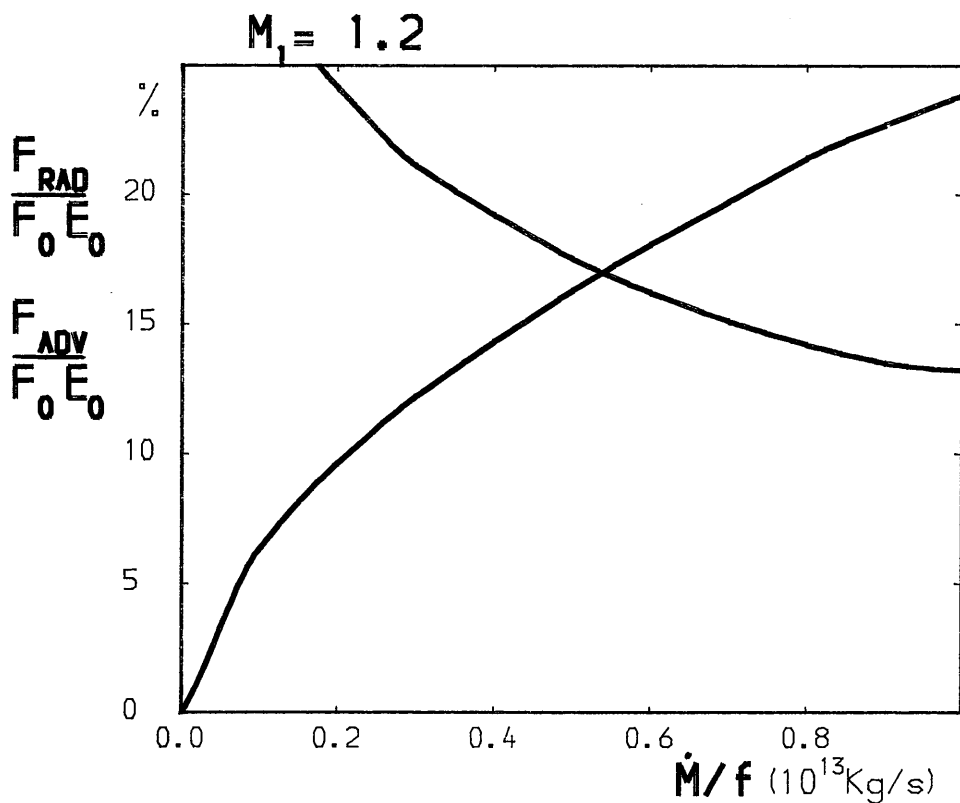
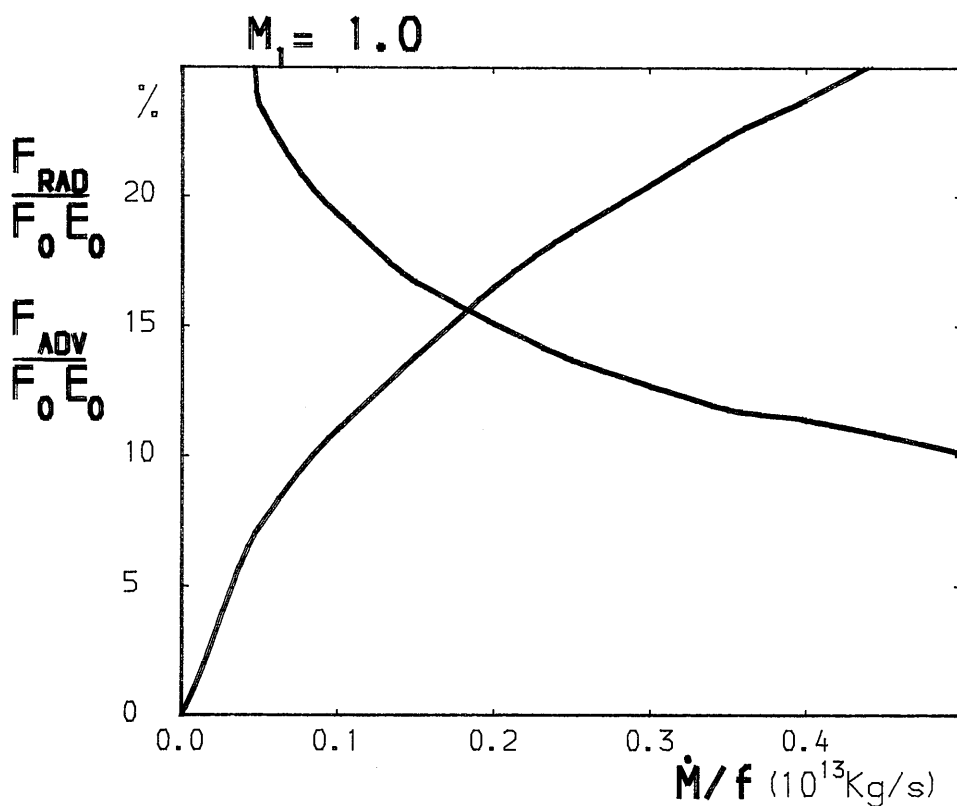


Figure 3.9: Graphs of the energy flux radiated within the bombarded region of the accretion column (black) and the advective flux expected from the base of the column (red) against the accretion rate per unit fractional area.

CHAPTER 4

CYCLOTRON COOLED BOMBARDMENT MODELS

SECTION 4.1 INTRODUCTION

In Chapter 3 we examined bombardment models of white dwarf accretion columns which are cooled solely by optically thin line radiation. We concluded that, for the accretion parameters inferred observationally for AM Her. stars, no steady state temperature structure could exist for a model of this type. The large magnetic field associated with AM Her. objects ($B \sim 10^3 - 10^4$ Tesla, Lamb and Masters, 1979; King and Lasota, 1980; Chanmugam, 1980; Barrett and Chanmugam, 1984) does suggest, however, that cyclotron losses may be important and the polarization observations of Wickramasinghe and Visvanath (1980) tend to confirm this. Indeed, some authors (e.g. Patterson et al, 1984) believe that the 'Soft X-ray Puzzle' can be explained in terms of the inflowing matter passing through a strong adiabatic shock and being subsequently cooled by cyclotron radiation.

In this Chapter we discuss for what accretion parameters optically thick cyclotron radiation can balance the accreted energy flux at a temperature $T \lesssim 10$ Kev, and whether these parameters are consistent with observations. We calculate the cyclotron emissivity due to mildly relativistic electrons in a thermal plasma and use this to estimate the optically thick cyclotron flux from a uniform temperature, plane parallel

atmosphere of thickness equal to the Coulomb collisional stopping length of the accreting protons. This allows us to estimate the range of accretion parameters for which a cyclotron cooled 'bombardment' model is possible.

In Section 4.5 we calculate a crude, piecewise uniform temperature structure for the accretion column, and in Section 4.6 we show that the predicted ratio of soft to hard X-rays agrees well with the observed ratio ~ 10 (Fabbianno et al, 1981). We also show, however, that for the observed optical flux to agree with that predicted by a cyclotron cooled model the cyclotron emitting region would have to be hidden from view.

Finally, we conclude that, in view of the good agreement between the predicted and the observed hard/soft X-ray ratio, a more detailed treatment should be undertaken.

SECTION 4.2 THE CYCLOTRON OPACITY DUE TO MILDLY RELATIVISTIC ELECTRONS.

In order to calculate the opacity of the atmosphere we adopt the strategy used in Chanmugam (1980).

For radiation of frequency very much greater than the plasma frequency $\omega_p = (n_e e^2 / \epsilon_0 m_e)^{1/2}$ (where n_e is the number density of electrons), the emissivity can be obtained by summing the contributions from each electron. The energy emitted per unit frequency per unit time by an electron of velocity components $\beta_{\parallel} c$ and $\beta_{\perp} c$ parallel and perpendicular to the magnetic field is,

$$\eta_{\omega} = \frac{e^2 \omega^2}{8\pi\epsilon_0 c} \left[\sum_{n=1}^{\infty} \left\{ \left(\frac{\cos\theta - \beta_{\parallel}}{\sin\theta} \right)^2 J_n(z) + \beta_{\parallel}^2 J_n'(z)^2 \right\} \delta(y) \right] \quad (4.1)$$

(Bekefi, 1966).

$$\text{Where: } z = \gamma\omega\beta_{\perp} \sin\theta / \omega_c \quad ; \quad (4.2)$$

$$y = n\omega_c / \gamma - \omega (1 - \beta_{\parallel} \cos\theta) \quad ; \quad (4.3)$$

θ = the angle between the line of sight of an observer and the magnetic field;

$$\gamma = (1 - \beta_{\perp}^2 - \beta_{\parallel}^2)^{-\frac{1}{2}}, \text{ the lorentz factor;}$$

$J_n(z)$ is a Bessel function of order n and $J_n'(z) = dJ_n(z)/dz$

The relativistic Maxwell-Boltzmann distribution for electrons of energy E and momentum \underline{p} is given by

$$f(\underline{p}) = n_e f_0 e^{-E/kT} \quad (4.5)$$

$$\text{where } 1/f_0 = 4 m_e^2 c k T K_2(\mu) \quad (4.5)$$

and where $\mu = m_e c^2 / kT$ and $K_2(\mu)$ is a modified Bessel function (Bekefi, 1966).

The total emissivity is, therefore, given by combining Equations (4.1) and (4.4)

$$j(\theta, \omega) = \frac{n_e f_0 m_e^2 c^2 e^2 \omega^2}{[4\pi\epsilon_0]} \left[\sum_{n=1}^{\infty} \int_{-1}^1 \int_0^1 \left\{ \left(\frac{\cos\theta - \beta_{\parallel}}{\sin\theta} \right)^2 J_n^2(z) + \beta_{\perp}^2 J_n'(z)^2 \right\} \delta(y) e^{-\gamma\mu} \gamma^5 \beta_{\perp} d\beta_{\perp} d\beta_{\parallel} \right] \quad (4.6)$$

which yield by integration

$$j(\theta, \omega) = \left[\frac{\omega^2}{\omega_c c} \right] \left[\frac{\pi \mu^2}{2 K_2(\mu)} \right] \left[\sum_{n=1}^{\infty} \int_{-1}^1 \left\{ \left(\frac{\cos \theta - \beta_n}{\sin \theta} \right) J_n^2(z) \right. \right. \\ \left. \left. + \beta_n^2 J_n'(z)^2 \exp \left\{ \frac{-\mu n \omega_c / \omega}{1 - \beta_n \cos \theta} \right\} \frac{n^3 (\omega_c / \omega)^4}{(1 - \beta_n \cos \theta)^4} d\beta_n \right\} \right] \quad (4.7)$$

By Kirchoff's law the absorption co-efficient

$$\alpha(\omega, \theta) = \frac{j(\omega, \theta)}{B_\omega(T)} \quad (4.8)$$

where $B(T) = \frac{\omega^2 kT}{8\pi c^2}$ is the Rayleigh-Jeans intensity per polarisation mode. i.e.

$$\alpha(\omega, \theta) = \left[\frac{\omega^2}{\omega_c c} \right] \phi(\omega, \theta) \quad (4.9)$$

where

$$\phi(\omega, \theta) = \left[\frac{\pi \mu^2}{2 K_2(\mu)} \right] \left[\int_{-1}^1 \sum_{n=1}^{\infty} \left\{ \left(\frac{\cos \theta - \beta_n}{\sin \theta} \right)^2 J_n^2(z) \right. \right. \\ \left. \left. + \beta_n^2 J_n'(z)^2 \right\} \exp \left\{ \frac{-\mu n \omega_c / \omega}{(1 - \beta_n \cos \theta)} \right\} \frac{n^3 (\omega_c / \omega)^4}{(1 - \beta_n \cos \theta)^4} d\beta_n \right] \quad (4.10)$$

with

$$z = \frac{n \sin \theta}{(1 - \beta_w \cos \theta)} \left[(1 - \beta_w)^2 - \left(\frac{\omega}{n \omega_c} \right)^2 (1 - \beta_w \cos \theta)^2 \right]^{\frac{1}{2}} \quad (4.11)$$

The values of the Bessel function $J_n(z)$ and its derivative $J'_n(z)$ were calculated either using the integral representation

$$J_n(z) = \frac{1}{\pi} \int_0^\pi \cos(z \sin \theta - n\theta) d\theta \quad (4.12)$$

and the relation

$$J'_n(z) = J_{n-1}(z) + \frac{n}{z} J_n(z) \quad (4.13)$$

(in Sections 4.2 and 4.3), or using the approximation of Wild and Hill (1971)

$$J_n(n\zeta) = \frac{\zeta^n \exp[n(1-\zeta^2)^{\frac{1}{2}}] \left[1 + \frac{0.50330}{n(1-\zeta^2)^{\frac{3}{2}}} \right]^{-1/6}}{(2\pi n)^{\frac{1}{2}} (1-\zeta^2)^{\frac{1}{4}} [1+(1-\zeta^2)^{\frac{1}{2}}]^n} \quad (4.14)$$

$$\begin{aligned} \zeta J'_n(n\zeta) &= (1-\zeta^2)^{\frac{1}{2}} J_n(n\zeta) \left[1 + \frac{\zeta^2}{n(1-\zeta^2)} \right]^{\frac{3}{2}} \\ &\times \left[(1-\zeta^2) + \frac{1.19300}{n} \right]^{\frac{1}{6}} \left[1 - \frac{1}{5n^{\frac{2}{3}}} \right] \end{aligned} \quad (4.15)$$

ϕ was evaluated numerically as a function of $x = \omega / \omega_c$ for particular values of θ . Some examples of the results of such calculations are given in Figure 4.1a and 4.1b, which show the contributions made by each of the first dozen or so harmonics for $\theta = 30^\circ$ and 75° respectively, and $kT = 10\text{KeV}$ ($T \approx 10^8\text{K}$). The values of ϕ , obtained by summing the contributions made by each harmonic, are also shown. Figure 4.2 shows the variation of the value of ϕ with θ .

SECTION 4.3 THE COLLISIONAL STOPPING LENGTH OF THE ACCRETING PROTONS

The accreted protons impinge on the background atmosphere with a velocity of order their free fall velocity,

$$v_0 = \left[\frac{2GM_*}{R_*} \right]^{1/2} = 5.5 \cdot 10^6 M_1^{2/3} \text{ ms}^{-1} \quad (4.16)$$

where $R_* = 0.87 \cdot 10^7 M_1^{-1/3} \text{ m}$, and M_1 is the mass of the white dwarf in solar masses.

The mean time for each of these protons to lose their energy is

$$t_{\text{EL}} = \left\{ \begin{array}{l} \frac{m_e}{m_p} \frac{m_p^2 v^3 [4\pi\epsilon_0]^2}{8\pi e^4 n_e \ln\Lambda} \quad v \gg v_e \quad \text{i.e. } T \geq 10^6 \quad (4.17a) \\ \frac{m_e}{m_p} \frac{3m_p^2 v_e^3 [4\pi\epsilon_0]^2}{32\pi^2 e n_e \ln\Lambda} \quad v_e \gg v \gg v_e (m_e/m_p)^{1/3} \\ \quad \text{i.e. } 10^6 \text{K} \geq T \geq 10^8 \text{K} \quad (4.17b) \\ \frac{m_p^2 v^3 [4\pi\epsilon_0]^2}{8\pi e^4 n_e \ln\Lambda} \quad v_e (m_e/m_p)^{1/3} \gg v \gg v_p \\ \quad \text{i.e. } 10^8 \text{K} \geq T \geq 10^9 \text{K} \quad (4.17c) \end{array} \right.$$

(Spitzer, 1962; c.f. Section 3.2 and Appendix A), where $v_e = \left(\frac{2kT}{m_e}\right)^{\frac{1}{2}}$, the electron thermal velocity, and $v_p = \left(\frac{2kT}{m_p}\right)^{\frac{1}{2}}$, the proton thermal velocity.

Cyclotron losses, because of the effect of self-absorption, will only be important if the cyclotron lines are significantly broadened by some process. As we show in Appendix B, the collision frequency ($\nu_c < 10^9$ Hz) for the atmospheric electrons is too small for any substantial collisional broadening of cyclotron lines produced by electrons in a $B \sim 10^3$ T field (typical for radially accreting white dwarfs) to occur. Cyclotron radiation can, therefore, only be important if the lines are significantly Doppler broadened. i.e. if the accretion column has a temperature $\geq 10^8$ K. Yet much above 10^8 K, Equation (4.17) shows that energy would be lost preferentially to atmospheric protons rather than electrons and, as in the 'shock' model, energy would be transferred to electrons and radiated away only as the matter settles onto the photosphere. Consequently, the case of interest here is that for which $T \approx 10^8$ K (4.17b or 4.17c). We choose here to make use of Equation (4.17c), firstly for simplicity of calculation, and secondly because the stopping length for the beam $v_0 t_s$ derived using (4.17c) represents the maximum stopping length for the beam. The energy loss rate is, therefore,

$$\frac{dE}{dt} = - \frac{K \ln \Lambda n_e v^2}{v_z E} \quad (4.18)$$

where $K = \frac{2\pi e^4 \ln \Lambda}{[4\pi\epsilon_0]^2}$, $\ln \Lambda$ is the Coulomb logarithm ~ 10 , and v_z

is the component of velocity along the magnetic field lines. In this, the hot target, case it is necessary to take account of the pitch angle scattering of the beam protons on the ambient protons (c.f. Emslie 1978).

From Emslie (1978), the rate of deflection of the infalling protons (scattering off protons)

$$\frac{d\bar{v}_z}{dt} = - \frac{K \ln \Lambda n_e v^2}{E^2} \quad (4.19)$$

At this point we again introduce the variable $N = \int_0^1 n dz$, the column density, where $N=0$ defines the top of the atmosphere. Thus, Equations (4.18) and (4.19) become

$$\frac{dE}{dN} = - \frac{K v \ln \Lambda}{E v_z} \quad (4.20)$$

and

$$\frac{dv_z}{dN} = - \frac{K v}{E^2} \quad (4.21)$$

On combining Equations (4.20) and (4.21) we find that the maximum column density required to stop an accreting proton is

$$N_s = 7.84 \cdot 10^{25} M_1^{8/3} \text{ m}^{-2} \quad (4.22)$$

SECTION 4.4 THE ESTIMATION OF THE CYCLOTRON LOSSES

We adopt a crude model for the atmosphere in which the energy of the accreting material is balanced by the cyclotron emission from a uniform temperature atmosphere of thickness equal to the Coulomb collisional stopping length of the accreting protons (l_s). We consider, therefore, a uniform temperature slab of material with a magnetic field normal to its surface. The accreting material, therefore, strikes the surface of the atmosphere normally.

The optical depth of such a slab, for an observer looking at an angle θ to the normal, is

$$\tau_{\omega}(\theta) = \int_0^{l_s} \frac{\alpha(\omega, \theta)}{\cos \theta} dz \quad (4.23)$$

which combined with Equation (4.9) gives

$$\tau_{\omega}(\theta) = \frac{\phi(\omega, \theta)}{\cos \theta} \int_0^{l_s} \left[\frac{\omega^2}{\omega_c c} \right] dz \quad (4.24)$$

i.e.

$$\tau_{\omega}(\theta) = \frac{N_s e}{\epsilon_0 B c} \frac{\phi(\omega, \theta)}{\cos \theta} = 4.7 \cdot 10^5 M_1^{8/3} B_4^{-1} \frac{\phi(\omega, \theta)}{\cos \theta} \quad (4.26)$$

where $N_s = \int_0^{l_s} n dz$, and B_4 is the magnetic field expressed in units of 10^4 Tesla.

The combined emission from the lower cyclotron harmonics will form a Rayleigh-Jeans tail up to some $\omega_{cr}(\theta)$ at which the optical depth $\tau_{\omega}(\theta)$ is equal to 1. Above this frequency, due to the rapid, approximately exponential, decrease of ϕ with ω , only a small amount of energy will be radiated away. The total power per unit solid angle per unit area emitted by the slab is, therefore,

$$I(\theta) = \frac{1}{3} \frac{kT \omega^3}{8 \pi^3 c^2} \quad (4.26)$$

and the total energy flux emitted by the slab from one surface is

$$F = 2\pi \int_0^{\pi/2} I(\theta) \cos \theta \sin \theta d\theta \quad (4.27)$$

Table 4.1 shows typical values of $\nu_{cr}(\theta) = \omega_{cr}/2\pi$ and $I(\theta)$ for fields of 10^3 , $3 \cdot 10^3$ and 10^4 Tesla and for $kT = 10\text{KeV}$. Figure 4.3 shows the largest values of accretion rate and magnetic field for which a simple bombardment solution, where energy is deposited by the in-falling protons directly into the atmospheric electrons which then radiate the energy away, is viable, i.e. where $kT \approx 10\text{KeV}$. Although the limiting curve lies somewhat below that shown in Lamb and Masters (1979), the region does include acceptable parameters for radially accreting white dwarfs. This can be clearly seen by comparing the typical accreted energy flux $F_{acc} = 1.6 \cdot 10^{14} M_1^2 \dot{M}_{13}/f_{-3} \text{ Wm}^{-2}$ with the values of emitted power as a function of temperature and magnetic field shown in Table 4.2.

Above 10^8K , a fraction $(1 + T_8^{1.5})^{-1}$ (where T_8 is the temperature in units of 10^8K) of the energy of the accreting protons is lost directly to the electrons. Therefore, at larger accretion rates the corresponding fraction of accreted energy can be emitted from the region, which in the simple shock model is treated as a discontinuity. If this fraction is appreciable, as Table 4.2 indicates it can be, one might expect the observed temperature and hard X-ray luminosity to be lower than expected for $kT \sim 30\text{KeV}$. This we shall confirm later.

SECTION 4.5 THE TEMPERATURE STRUCTURE OF A CYCLOTRON COOLED ACCRETION COLUMN

In Section 4.4 we used a 'global' energy balance argument, similar to that used by Kuijpers and Pringle (1982) in the case of a line cooled column (see Section 3.3), to determine a 'mean' temperature for a cyclotron cooled accretion column. In this Section we extend this model to allow us to determine a piecewise uniform temperature structure for the column. This we achieve by increasing the number of layers in the bombarded atmosphere.

In addition, the results of Section 4.4 suggest that we might expect the temperature to be $\sim 10^8\text{K}$. We, therefore, include a correction to the energy input in each layer to take account of diffusive thermal conduction. The inclusion of thermal conduction also allows us to examine the extent to which the column can be lengthened by this process, and the effect of this

lengthening on the spectral softness ratio. (c.f. Section 4.6).

As previously, we will consider a plane parallel atmosphere and as before we obtain from the local conservation of momentum and energy, respectively,

$$\frac{dP}{dz} = F_0 m_p \frac{dv}{dz} + m_p g n \quad (4.28)$$

and

$$\frac{dF_{\text{COND}}}{dz} = F_0 \frac{dE}{dz} + R(z) \quad (4.29)$$

where $F_{\text{COND}} = \kappa_0 T^{2.5} \left(\frac{dT}{dz} \right)$ is the diffusive conductive flux, F_0 is the beam number flux density, g is the surface gravity of the white dwarf, $R(z)$ represents the radiative energy losses per unit volume.

It can be verified that, for the accretion number fluxes of interest here, the contribution of gravity to Equation (4.28) is small and we can, therefore, neglect this term. So that

$$\frac{P(N)}{P_{\text{RAM}}} = (1 - \epsilon^2)^{\frac{1}{2}} \quad (4.30)$$

where $P_{\text{RAM}} = F_0 (2m_p E_0)^{\frac{1}{2}}$, the ram pressure of the beam and $\epsilon = E(N)/E_0$, where E_0 is the initial energy of the beam particles.

The radiative loss term in the energy Equation, $R(z)$ can be replaced by an optically thin bremsstrahlung component $n^2 f_R(T)$ and a cyclotron component $n \phi_{\text{cyc}}$. Equation (4.29) becomes

$$\frac{dF_{\text{COND}}}{dz} = F_0 \frac{dE}{dz} + n^2 f_R(T) + n \phi_{\text{cyc}} \quad (4.31)$$

which can be re-written in terms of the column density as

$$\frac{dF_{\text{COND}}}{dN} = F_0 \frac{dE}{dN} + n f_R(T) + \phi_{\text{cyc}} \quad (4.32)$$

To solve this Equation (4.32) we shall replace each term by its mean value over finite intervals in N and use a Newton-Raphson procedure to determine the mean value of T for each layer. Clearly, the conduction term, because of its dependence on the rate of change of T with N ($F_{\text{COND}} = \kappa_0 T^{2.5} n \frac{dT}{dN}$), depends on the temperature of neighbouring layers. We, therefore, treat this as a correction term, calculating it from an initial temperature structure. We then solve Equation (4.32) for the temperature of each layer and re-calculate the conductive flux. This process is repeated until a satisfactory temperature structure is found, i.e. one in which the temperature of each layer does not vary significantly between successive calculations.

Beam energy deposition :-

We anticipate from the results of Section 4.4 that the temperature of the layers within the column will be typically $\sim 10^8$ K. We, therefore, adopt the hot target approximation (Equation 4.17c), for the energy deposition rate

$$\frac{dE}{dt} = \begin{cases} -\frac{K n_e v \ln \Lambda}{E} & E > 0 \\ 0 & E \leq 0 \end{cases} \quad (4.33)$$

i.e.

$$\frac{dE}{dN} = \begin{cases} -\frac{K \ln \Lambda}{E} & E > 0 \\ 0 & E \leq 0 \end{cases} \quad (4.34)$$

where

$$K = \frac{2\pi e^4}{[4\pi\epsilon_0]^2}$$

which, neglecting the small correction due to pitch angle scattering gives, on integration,

$$\epsilon = \begin{cases} (1 - \xi)^{\frac{1}{2}} & \xi < 1 \\ 0 & \xi > 1 \end{cases} \quad (4.35)$$

where $\xi = N/N_{\max}$ and where $N_{\max} (= E_0^2 / 2K \ln \Lambda)$ is the maximum column depth to which a proton of energy E_0 can penetrate.

Thus, the mean energy deposition rate per unit volume is given by $\frac{F_0 E_0 \Delta \epsilon}{N_{\max} \Delta \xi}$ where

$$\Delta \xi = \xi_L - \xi_U \quad (4.36)$$

and

$$\Delta\varepsilon = \varepsilon_L - \varepsilon_U = \begin{cases} (1 - \xi_L)^{\frac{1}{2}} - (1 - \xi_U)^{\frac{1}{2}} & \xi_L, \xi_U < 1 \\ - (1 - \xi_U)^{\frac{1}{2}} & \xi_U < 1, \xi_L \geq 1 \\ 0 & \xi_U, \xi_L \geq 1 \end{cases} \quad (4.37)$$

where subscripts L and U denote respectively the value at the lower and upper faces of any layer.

Bremsstrahlung / line emission :-

Again, since we expect temperatures $\sim 10^8$ K we need only consider the bremsstrahlung dominated region of the radiative loss curve. We obtain from Allen (1973) for a plasma with cosmic abundances,

$$f_R(T) = 1.64 \cdot 10^{-40} T^{\frac{1}{2}} \quad (4.38)$$

Thus the bremsstrahlung loss term from Equation (4.32) becomes

$$nf_R(T) = 1.64 \cdot 10^{-40} nT^{\frac{1}{2}} \quad (4.39)$$

and substituting from Equation (4.30) we obtain

$$nf_R(T) = 2.10 \cdot 10^{-2} (1 - \varepsilon^2)^{\frac{1}{2}} T_8^{-\frac{1}{2}} M_1^2 \frac{F_0 E_0}{N_{\max}} \quad (4.40)$$

where T_8 is the temperature expressed in units of 10^8 K. The mean

value of the bremsstrahlung emissivity over a layer is, therefore,

$$n f_R(T) = 2.10 \cdot 10^{-2} \left(1 - \frac{(\epsilon_U^{\frac{1}{2}} + \epsilon_L^{\frac{1}{2}})}{2} \right) T_8^{-\frac{1}{2}} M_1^2 \frac{F_0 E_0}{N_{\max}} \quad (4.41)$$

Cyclotron Emission :-

The cyclotron emission per unit volume per unit frequency per steradian is

$$j(\theta, \omega) = \left[\frac{\omega^2}{\omega_c} \right] \left[\frac{kT \omega_c^3}{8\pi^3 c^2} \right] \left[\left(\frac{\omega}{\omega_c} \right)^2 \phi(\omega, \theta) \right] \quad (4.42)$$

where $\phi(\omega, \theta)$ is given by Equation (4.10) Thus, the total emitted energy per unit volume is

$$j = \int_0^\pi \int_0^\infty j(\omega, \theta) d\omega 2\pi \sin\theta d\theta \quad (4.43)$$

Self-absorption does, however, mean that not all of this energy will necessarily escape. We, therefore, approximate the total emitted flux from the upper surface of a layer by

$$\begin{aligned}
 F_{\text{layer}} &= \int_0^{\pi/2} \int_0^{\omega_s} 2\pi B_{\omega}(T) \sin\theta \cos\theta \, d\omega \, d\theta \\
 &+ \int_0^{\pi/2} \int_{\omega_s}^{\infty} j(\theta, \omega) 2\pi \sin\theta \, d\omega \, d\theta \, \Delta z
 \end{aligned}
 \tag{4.44}$$

where Δz is the thickness of the layer and ω_s is the angular frequency for which the layer, has optical depth 1, i.e. we assume that the flux at angular frequencies above ω_s is approximately the optically thin emissivity integrated along the line of sight. In addition, we choose to neglect downward emission of cyclotron radiation at the optically thick wavelengths. (We shall discuss this assumption later.)

In general the actual escaping flux from a given layer will be less than if it were totally isolated, since the matter lying above a particular layer will tend to absorb the flux at lower frequencies. We, therefore, define ω_a to be the frequency at which the optical depth of the overlying material is unity and neglect the contribution to the emitted flux below this frequency. Thus, the total escaping energy flux is

$$\begin{aligned}
 F_{\text{cyc}} &= \int_0^{\pi/2} \int_0^{\omega_s} 2\pi B_{\omega}(T) \sin\theta \cos\theta H(\omega_a) \, d\omega \, d\theta \\
 &+ \int_0^{\pi/2} \int_{\omega_s}^{\infty} j(\theta, \omega) H(\omega_a) 2\pi \sin\theta \, d\omega \, d\theta \, \Delta z
 \end{aligned}
 \tag{4.45}$$

We make two further simplifying approximations. Firstly, we replace $j(\omega, \theta)$ with a mean $j(\theta) = j(\omega, 45^\circ)$, and, secondly, we approximate the optically thin tail of $j(\omega, \theta)$ by an exponential of the form

$$\phi(\omega, \theta) = \phi(\omega_s, \theta) \exp(-\omega/\omega_0) \quad (4.46)$$

where

$$\omega_0 = \left[\frac{\phi(\omega, \theta)}{|d\phi/d\omega|} \right]_{\omega=\omega_s} \quad (4.47)$$

Although these approximations were introduced primarily to facilitate calculation of F_{cyc} in a realistic time, inspection of Figures 4.1a and 4.1b demonstrate that the decrease in ϕ is approximately exponential and inspection of Table 4.2 suggests most of the energy emitted from the column is emitted between $\theta = 45^\circ$ and $\theta = 60^\circ$.

We, therefore, have in Equation (4.32)

$$\begin{aligned} \phi_{\text{cyc}} &= \frac{F_{\text{cyc}}}{N_{\text{max}} \Delta\xi} \\ &= \left[2.8 \cdot 10^{-2} x_s^3 (1 - (x_a/x_s)^3)^3 B_4^3 + 7.9 \cdot 10^6 x_s^2 B_4^2 \frac{\phi_1^2(x_s)}{|d\phi_1/dx|_{x_s}} \right] \\ &\times T_8 M_1^{2/3} f/M_{13}^{-1} \left[\frac{F_0 E_0}{N_{\text{max}}} \right] \quad x_a \ll x_s \quad (4.48) \end{aligned}$$

and

$$\phi_{\text{cyc}} = \frac{F_{\text{cyc}}}{N_{\text{max}} \Delta \xi}$$

$$= \left[7.8 \cdot 10^6 x_s^2 B_4^2 \frac{\phi_1^2(x_s)}{|d\phi_1/dx|_{x_s}} \right]$$

$$T_8 M_1^{2/3} f/\dot{M}_{13}^{-1} \frac{F_0 E_0}{N_{\text{max}}} \quad x_a > x_s \quad (4.49)$$

where

$$\phi_1(x) = \phi(x\omega, 45^\circ) \quad (4.50)$$

Conductive Flux :-

The change in the diffusive conductive flux across a finite element of the atmosphere is given by

$$\Delta F_{\text{COND}} = F_{\text{COND}_U} - F_{\text{COND}_L} \quad (4.51)$$

where

$$F_{\text{COND}} = \kappa_0 T^{2.5} \frac{dT}{dz} = \kappa_0 n T^{2.5} \frac{dT}{dn} \quad (4.52)$$

with $\kappa_0 = 10^{-11} \text{Wm}^{-1} \text{K}^{-3.5}$ (Spitzer, 1962).

In order to calculate the conductive fluxes, we require to know the temperature gradient at the interface between two layers. Clearly, in this calculation, this gradient will be formally infinite because of the temperature discontinuity at the interface. We, therefore, replace the temperature gradient at the interface between the $n-1^{\text{th}}$ and the n^{th} layers by its mean value between the centre of the layers, so that

$$\frac{dT}{dN} = \frac{T_n - T_{n+1}}{\Delta N} \quad (4.53)$$

where ΔN is the separation of these centres of the two layers. Thus, the conductive flux from the $n-1^{\text{th}}$ layer to the n^{th} layer is

$$F_{\text{COND}_i} = 1.448 \cdot 10^{11} \frac{P_i [T_{n-1}^{2.5} - T_n^{2.5}]}{N_{\text{max}} [\xi_{n-1} - \xi_n]} \quad (4.54)$$

where P_i is the pressure at the interface, and ξ_{n-1} and ξ_n are, respectively, the values of ξ corresponding to the centre of each layer.

The nett change in conductive flux across the n^{th} layer is, therefore,

$$F_{\text{COND}_U} - F_{\text{COND}_L} = 5.3 \cdot 10^{-2} M_1^{-10/3} (F_0 E_0)$$

$$\times \left[\frac{[1-\epsilon_U^{1/2}] [T_{8n-1}^{2.5} - T_{8n}^{2.5}]}{[\xi_{n-1} - \xi_n]} - \frac{[1-\epsilon_L^{1/2}] [T_{8n}^{2.5} - T_{8n+1}^{2.5}]}{[\xi_n - \xi_{n+1}]} \right] \quad (4.55)$$

Thus, the rate of change of conductive flux in Equation (4.32) becomes

$$\frac{dF_{\text{COND}}}{dN} = \frac{F_{\text{COND}_U} - F_{\text{COND}_L}}{N_{\text{max}} (\xi_U - \xi_L)} \quad (4.56)$$

and Equation (4.32) becomes, for the n^{th} layer,

$$5.3 \cdot 10^{-2} M_1^{-10/3} \left[\frac{[1-\epsilon_U^{1/2}] [T_{8n-1}^{2.5} - T_{8n}^{2.5}]}{\xi_{n-1} - \xi_n} - \frac{[1-\epsilon_L^{1/2}] [T_{8n}^{2.5} - T_{8n+1}^{2.5}]}{\xi_n - \xi_{n+1}} \right] \frac{1}{\xi_U - \xi_L}$$

$$= \frac{\epsilon_U - \epsilon_L}{\xi_U - \xi_L} + 2.1 \cdot 10^{-2} \left[1 - \frac{(\epsilon_U + \epsilon_L)}{2} \right] T_8^{-1/2} M_1^2 + \phi_{\text{cyc}}(T_{8n}, x_{s_n}) \frac{N_{\text{max}}}{F_0 E_0}$$

(4.57)

where x_s is determined by

$$\tau(x_{s_n}) = 5.91 \cdot 10^5 B_4^{-1} (\xi_U - \xi_L) \phi_1(x_{s_n}) = 1 \quad (4.58)$$

We have, therefore, a system of $2I$ equations in the dimensionless variables x_s and T_g , where I is the number of layers within the atmosphere). While it may be possible to solve the entire system of equations simultaneously, we choose to adopt a simpler, iterative, approach. We assume an initial temperature structure for the atmosphere and determine the conductive term on the left hand side of Equation (4.57). We then treat this as a constant, and solve Equations (4.57) and (4.58) to determine a new temperature structure. We then use this to recalculate the conductive flux and repeat the process until an 'acceptable' solution is found, i.e. one which is both self consistent and satisfies the appropriate boundary conditions at the top and bottom.

Equation (4.57) is effectively a second order ordinary differential equation in T . We, therefore, require two boundary conditions to determine the structure of the atmosphere. These are:

$$F_{\text{COND}} = 0 \text{ at } N = 0$$

$$F_{\text{COND}} = 0 \text{ at some unspecified } N \text{ for which } T \text{ is small.}$$

These are essentially the same conditions as were used in Section 3.5.

We impose the first condition simply by setting the conductive flux across the upper face of the top layer of the column equal to zero. The second condition requires us to match the column onto a low temperature 'photosphere'

This we achieve by noting, firstly, that the bottom of the column will have no beam energy input. Secondly, the combination of self-absorption at small ω , due to overlying matter, and the

decrease in cyclotron emissivity with temperature result in a rapid decrease in the cyclotron flux emitted from the low lying layers of the column with column density. Consequently, the dominant loss mechanism from the bottom of the accretion column is thermal bremsstrahlung radiation, and we can neglect cyclotron losses. Below $T \sim 10^7$ K the optically thin radiative losses are, in fact, dominated by line radiation rather than bremsstrahlung radiation. It is, however, simple to show that in the present context the inclusion of line radiation will make no significant difference to the results we obtain. Equation (4.32), in this region, thus, reduces to

$$\frac{dF_{\text{COND}}}{dN} = n f_R(T) \quad (4.59)$$

combining this with Equation (4.52) gives

$$F_{\text{COND}} \frac{dF_{\text{COND}}}{dT} = \kappa_0 T^{2.5} n^2 f_R(T) \quad (4.60)$$

which, when integrated, gives

$$\left[\frac{F_{\text{COND}}}{F_0 E_0} \right]^2 = 2.8 \cdot 10^{-3} M_1^{-4/3} T_8^2 + \text{constant} \quad (4.61)$$

i.e. applying the lower boundary condition we have

$$\frac{F_{\text{COND}}}{F_0 E_0} = 5.3 \cdot 10^{-2} M_1^{-2/3} T_8 \quad (4.62)$$

Substituting Equation (4.62) into Equation (4.52) gives

$$\frac{dT_8}{d\xi} = \frac{0.397 M_1^{8/3}}{T_8^2} \quad (4.63)$$

which when integrated yields

$$T_8 = (0.60 M_1^{8/3} \xi)^{2/3} + \text{constant} \quad (4.64)$$

The constant is evaluated by imposing the constraint that T_8 , in the analytic and piecewise uniform temperature parts of the solution should be continuous at the centre of the lowest layer of the piecewise uniform temperature part of the column. The structure can then be determined by calculating a piecewise uniform temperature solution down to some ξ , where the radiative losses are dominated by the bremsstrahlung, then adding the analytic, 'matched', part of the solution.

The structure of a column of this kind was determined for $B_4 = 1$, $M_1 = 1$ and $\dot{M}_{13}/f = 5 \cdot 10^{-2}$.

Figure 4.4a shows the temperature structure of the column. The red histogram denotes the structure excluding conduction, the black histogram denotes the structure including conduction, and the black dotted line denotes the analytic segment of the

conduction solution. Figure 4.4a clearly demonstrates that the thermal conduction has two effects. Firstly, it reduces the temperature of the atmosphere (the peak in temperature around $\xi = 0.9$ being reduced by approximately 0.2) and, secondly, it lengthens the column by a factor ~ 5 . Figure 4.4b, which shows the downward conductive flux as a function of ξ , demonstrates that in fact approximately 20% of the total energy is radiated below the point where the beam is cut off. As we shall see in Section 4.6 this extension of the column does have a significant effect on the soft/hard X-ray ratio, predicted by a cyclotron cooled bombardment model.

It should, however, be emphasized that due to the simplifying assumptions made within the model, some of which are at best marginally justified, this model cannot give more than a crude estimate of the temperature structure of the atmosphere. For example, we have neglected the effect of advection of energy from the bombarded region which the analysis in Section 3.5 (Equation 3.39) suggest would be of order 45% of the accreted flux, greater than the conductive flux. This means that a treatment including both advection and conduction i.e. a radiative shock model would perhaps be more appropriate.

We have also neglected the contribution to the radiative losses due to cyclotron emission towards the stellar surface. At best this approximation can only be marginally justified on the grounds that the downward emission is unlikely to exceed the upward emission and therefore should not represent more than a factor of 2 in the total radiative losses from the column. The omission of this effect is, however, likely to affect the

structure of the lower part of the column and should, therefore, be included in a future calculation. The inclusion of this effect, however, requires a more elaborate treatment of the radiative transport within the column and the reprocessing of the cyclotron radiation in the photosphere than is presented here and is, therefore, beyond the scope of this thesis.

Finally, the discretisation technique is reasonable only if the temperature does not vary greatly over the width of one layer. While this is true over most of the column, it is not clear whether it will be true for the top layer. The very much greater energy loss rate per unit volume very close to the top of the column due to the lack of self absorption is likely to result in a thin layer at the top of the column which is very much cooler than the rest of the column. The narrowness of the cyclotron lines at temperatures much below 10^8 K would, however, suggest that this effect might be small, since the Rayleigh-Jeans tail would only fill out with emissions from regions with temperatures $\sim 10^8$ K

Clearly the inadequacies of the model should be dealt with by a more accurate determination of cyclotron losses and radiative transport. However, this simple model does demonstrate one very important feature of the model - that of the lengthening of the column by energy transport processes. As we shall demonstrate in the Section 4.6, such a lengthening allows good agreement to be achieved between the observed and predicted soft/hard X-ray ratios.

SECTION 4.6 COMPARISON WITH OBSERVATIONS.

In this Chapter we have so far only been concerned with demonstrating that the bombarded atmosphere of a white dwarf can dissipate energy fluxes as large as 10^{14} Wm^{-2} by cyclotron radiation, for atmospheric temperatures of about 10^8 K and magnetic fields of 10^4 T . Soft X-ray fluxes of this magnitude have been inferred for AM Herculis (Tuohy et al, 1978) and are usually supposed to originate from the reprocessing of hard X-rays (King and Lasota, 1980) or cyclotron radiation (Lamb and Masters, 1979). The soft X-ray luminosity does, however, exceed that in the hard X-rays by at least a factor ~ 10 (Fabbianno et al, 1981; Heise et al, 1986), so that, the reprocessing of hard X-rays cannot be the dominant source of soft X-ray flux. In this Section we examine the observational constraints on the cyclotron flux and discuss the limits these place on the acceptability of the two models described earlier in this Chapter.

We compute first the ratio of the soft X-ray flux (assumed comparable to the accreted energy flux) to the hard X-ray flux (assumed equal to the thermal bremsstrahlung flux).

From Allen (1973) we have that the total power emitted from a given volume as bremsstrahlung is

$$\epsilon_{\text{HARD}} = 1.64 \cdot 10^{-40} \text{ g T}^{\frac{3}{2}} \int n_e^2 \text{ dv} \quad \text{Wm}^{-3} \quad (4.65)$$

where g is the gaunt factor ≈ 1 .

i.e.

$$\epsilon_{\text{HARD}} = 5.94 \cdot 10^{-18} \text{ T}^{-\frac{1}{2}} \text{ A} \int_0^N n_c P \text{ dN} \quad \text{Wm}^{-3} \quad (4.66)$$

where N_c is the length of the column, P is the gas pressure and A is the surface area of the column. If we equate the soft X-ray flux to the accreted energy flux we have,

$$\epsilon_{\text{SOFT}} = \epsilon_{\text{ACC}} = F_0 m_p v_0^3 A \quad (4.67)$$

Therefore, in the case of the single uniform temperature slab described in Section 4.4, if we integrate Equation (4.66), we obtain

$$\epsilon_{\text{HARD}} = 9.90 \cdot 10^{-19} P_{\text{RAM}} A N_s \quad (4.68)$$

where P_{RAM} is the ram pressure of the beam $= F_0 m_p v_0$ and N_s is the Coulomb collisional stopping length of the protons, so that

$$\frac{\epsilon_{\text{SOFT}}}{\epsilon_{\text{HARD}}} = 5.05 \cdot 10^{18} T^{\frac{1}{2}} v_0^{\frac{1}{2}} N^{-1} = 385 T^{\frac{1}{2}} M_1^{-2} \quad (4.69)$$

This suggests that such a model would predict a soft to hard X-ray ratio $\sim 10^2$ - 10^3 , which is considerably larger than the ratio ~ 10 suggested by observations (Fabbianno *et al.*, 1981). This, however, does not necessarily preclude the existence of a column of this type on observational grounds. The inclusion of energy transport processes such as thermal conduction (see Section 4.5) can significantly lengthen the accretion column. This increases the bremsstrahlung (hard X-ray flux) while leaving the cyclotron flux almost unchanged. For example, the column described in Section 4.5 loses approximately 10% of the accreted energy as hard X-rays, which gives a ratio of hard X-rays to soft X-rays $\frac{\epsilon_{\text{SOFT}}}{\epsilon_{\text{HARD}}} \approx 10$, much closer to the observed

value.

The soft/hard X-ray ratio is not the only constraining factor on any cyclotron cooled model of an accretion column. For the uniform temperature layer considered in Section 4.4, with temperature $T \approx 10^8 \text{K}$ and $B \approx 10^4 T$, one would expect a flux at $\nu \approx 1.5 \cdot 10^{15} \text{Hz}$ ($\lambda = 2000 \text{\AA}$)

$$\frac{kT \nu^2}{D^2 c^2} [4\pi R^2 f] = 3 \cdot 10^{-26} M_1^{-2/3} f_{-2} W_m^{-2} \text{Hz}^{-1} \quad (4.70)$$

where $D = 100 \text{pc}$ is the estimated distance of AM Her.

The region $1000 - 3000 \text{\AA}$ was observed by Raymond et al (1979) using I.U.E., and the eclipsed component of the flux in the range $2000 - 3000 \text{\AA}$ was found to be less than $10^{-28} W_m^{-2} \text{Hz}^{-1}$. If the soft X-rays do arise from reprocessed cyclotron radiation then it is clear that the cyclotron source is not directly visible - (as was noted by Raymond et al, 1979)

At first sight it would appear that this problem could be resolved by assuming (within the model) a smaller value for the fractional area over which the white dwarf accretes. Such a change is, however, likely to result in higher temperatures, more efficient energy transport, and a lower soft/hard X-ray ratio, producing once more a 'Soft X-ray Puzzle'.

It is clear, though, that the inclusion of optically thick cyclotron losses is likely to produce an enhancement of the soft X-ray flux and may, therefore, contribute to a resolution of the 'Soft X-ray Puzzle'.

Finally, we note that the presence of cyclotron lines in the optical spectrum of the VV Puppis, which has been used to

suggest that this star must have a shock temperature $\sim 10\text{keV}$, and hence an unusually low mass for the white dwarf (Wickramasinghe and Meggitt, 1982). However, the source of the lines must be in a region where $B \approx 3 \cdot 10^3 \text{T}$, and Table 4.2 shows that the observed flux (of order 10^{12}Wm^{-2}) is quite compatible with a 10keV bombardment solution for $1M_{\odot}$ white dwarf. The column density of the bombardment model also agrees with the results of Barrett and Chanmugam (1985).

SECTION 4.7 CONCLUSIONS AND DISCUSSIONS.

In this Chapter we have calculated the optical depth due to cyclotron self absorption of a uniform temperature slab of plasma of thickness equal to the Coulomb collisional stopping length for protons falling freely onto a white dwarf star, as a function of frequency and angle of observation. We have shown that, for an acceptable choice of parameters, the energy input due to accretion, $\sim 10^{14} \text{Wm}^{-2}$, can be balanced by the optically thick cyclotron radiation from a uniform temperature atmosphere (slab) at a temperature $\sim 1-2 \cdot 10^8 \text{K}$, less than the shock temperature of the infalling material. In addition, we also determined a crude temperature structure for a cyclotron cooled bombarded white dwarf atmosphere.

These two simple approaches do allow us to demonstrate two very important points about cyclotron cooled accretion columns. Firstly, we have shown that the normal assumption made in shock models of accretion columns that no energy loss takes place

within the bombarded (or shock) region may not be valid. i.e. we have demonstrated that there is in fact a significant amount of energy loss within the region where the bulk of the kinetic energy of the accreting matter is thermalised and the region can no longer be treated as a fluid discontinuity.

Secondly, we have shown that the inclusion of thermal conduction within the cyclotron model leads to reasonable agreement between the predicted and observed soft/hard X-ray ratios.

It should be stressed that these models take no account of the advection of energy by the residual bulk motion of the accreting material, the details of the process of transferring thermal energy from the atmospheric protons to the atmospheric electrons, or the effect of the downward emission and subsequent reprocessing of radiation. The inclusion of these processes would require a more detailed radiative shock treatment, which is beyond the scope of this thesis.

In the absence of such a model, the agreement between the observed and predicted soft/hard X-ray ratios does suggest that the inclusion of cyclotron radiation within the accretion column model may contribute to a resolution of the 'Soft X-ray Puzzle'.

Table 4.1: Typical values of $\nu_{cr}(\theta) = \omega_{cr}/2\pi$ and $I(\theta)$ for magnetic fields of 10^3 , $3 \cdot 10^3$ and 10^4 Tesla and $kT = 10$ Kev

θ	10^3 Tesla		$3 \cdot 10^3$ Tesla		10^4 Tesla	
	ν_{cr} (Hz)	$I(\theta)Wm^{-2}ster^{-1}$	ν_{cr} (Hz)	$I(\theta)Wm^{-2}ster^{-1}$	ν_{cr} (Hz)	$I(\theta)Wm^{-2}ster^{-1}$
75°	$3.0 \cdot 10^{14}$	$1.6 \cdot 10^{11}$	$8.1 \cdot 10^{14}$	$3.2 \cdot 10^{12}$	$2.4 \cdot 10^{15}$	$8.2 \cdot 10^{13}$
60°	$2.7 \cdot 10^{14}$	$1.2 \cdot 10^{11}$	$7.3 \cdot 10^{14}$	$2.3 \cdot 10^{12}$	$2.2 \cdot 10^{15}$	$6.3 \cdot 10^{13}$
45°	$2.3 \cdot 10^{14}$	$7.2 \cdot 10^{10}$	$6.4 \cdot 10^{14}$	$1.6 \cdot 10^{12}$	$1.9 \cdot 10^{15}$	$4.1 \cdot 10^{13}$
30°	$1.9 \cdot 10^{14}$	$4.1 \cdot 10^{10}$	$5.4 \cdot 10^{14}$	$9.4 \cdot 10^{11}$	$1.6 \cdot 10^{15}$	$2.4 \cdot 10^{13}$
15°	$1.5 \cdot 10^{14}$	$2.0 \cdot 10^{10}$	$4.2 \cdot 10^{14}$	$4.4 \cdot 10^{11}$	$1.3 \cdot 10^{15}$	$1.3 \cdot 10^{13}$

Table 4.2: The power emitted by the uniform temperature layer described in Section 4.4. and the corresponding predicted soft X-ray ratio as a function of the temperature of the column and its magnetic field.

T	F(Wm ⁻²)				$\frac{L_{\text{SOFT}}}{L_{\text{HARD}}}$
	B 10 ³ Tesla	3 10 ³ Tesla	10 ⁴ Tesla	10 ⁴ Tesla	
10 Kev	2.5 10 ¹¹	5.2 10 ¹²	1.4 10 ¹⁴	3.8 10 ²	
15 Kev	6.9 10 ¹¹	1.4 10 ¹³	3.7 10 ¹⁴	4.7 10 ²	
20 Kev	1.5 10 ¹²	2.9 10 ¹³	7.6 10 ¹⁴	5.4 10 ²	
25 Kev	2.7 10 ¹²	5.3 10 ¹³	1.4 10 ¹⁵	6.1 10 ²	
30 Kev	4.7 10 ¹²	9.1 10 ¹³	2.3 10 ¹⁵	6.7 10 ²	

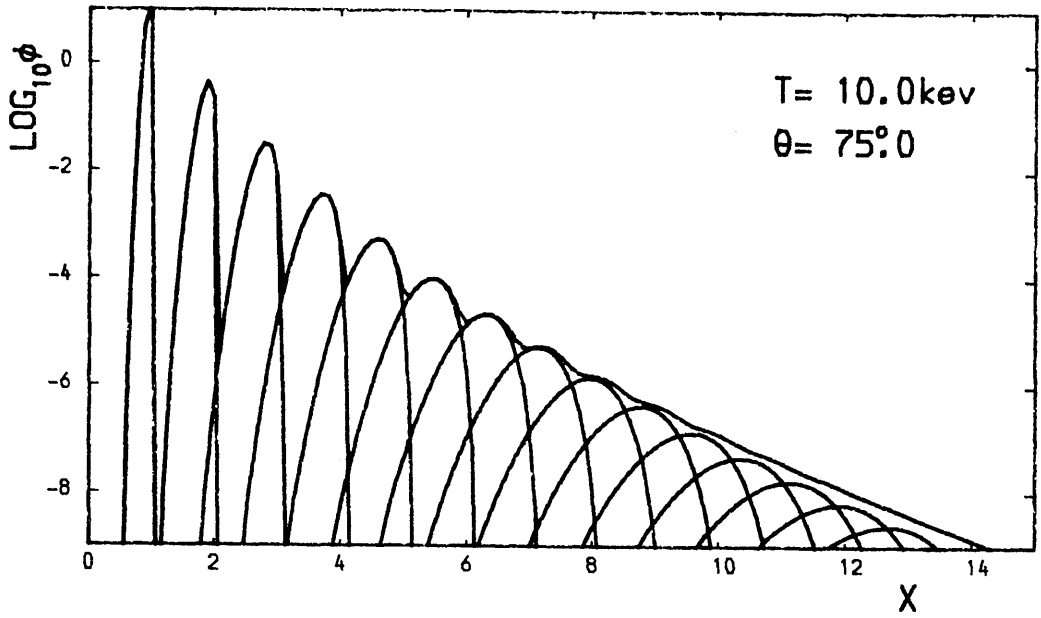


Figure 4.1a

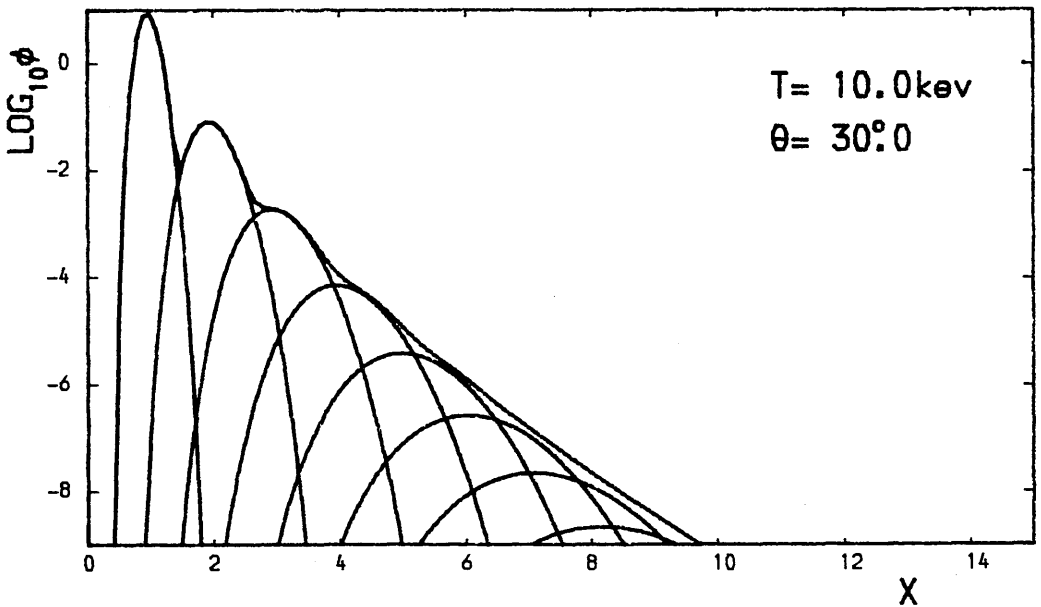


Figure 4.1b

Figure 4.1: These figures show the value of ϕ (the optical depth in units of the plasma parameter Λ) up to $x = 15$ as well as the individual contributions of each of the first few harmonics to the value of ϕ for a temperature of 10 KeV and angles of observation $\theta = 75^\circ$ (1a) and 30° (1b).

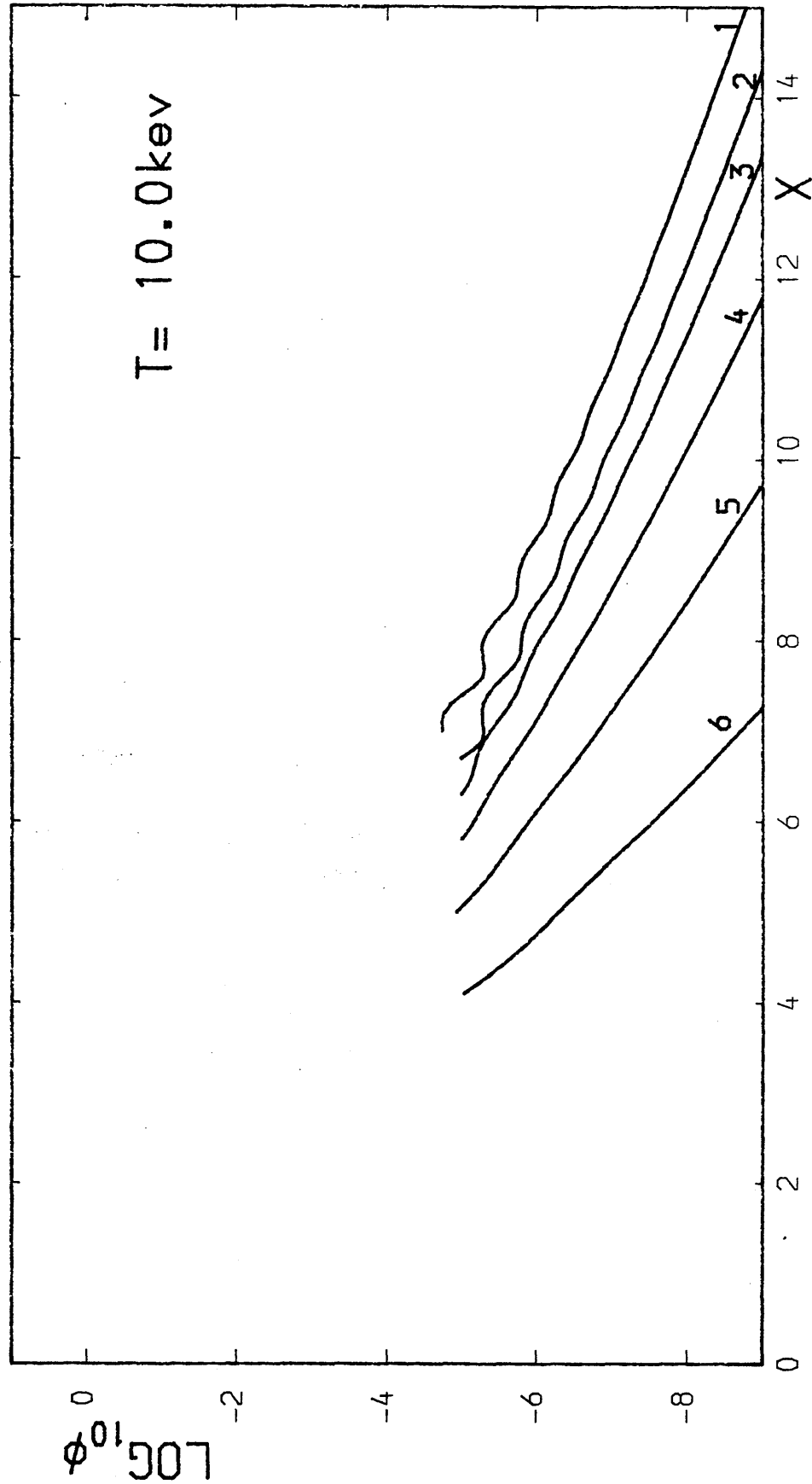


Figure 4.2: This figure illustrates the variation of ϕ (the optical depth in units of the plasma parameter Λ) with angle θ . Each curve corresponds to the value of ϕ for a different θ . Curve 1 corresponds to $\theta = 90^\circ$, curve 2 corresponds to $\theta = 75^\circ$, curve 3 corresponds to $\theta = 60^\circ$, curve 4 corresponds to $\theta = 45^\circ$, curve 5 corresponds to $\theta = 30^\circ$, and curve 6 corresponds to $\theta = 15^\circ$

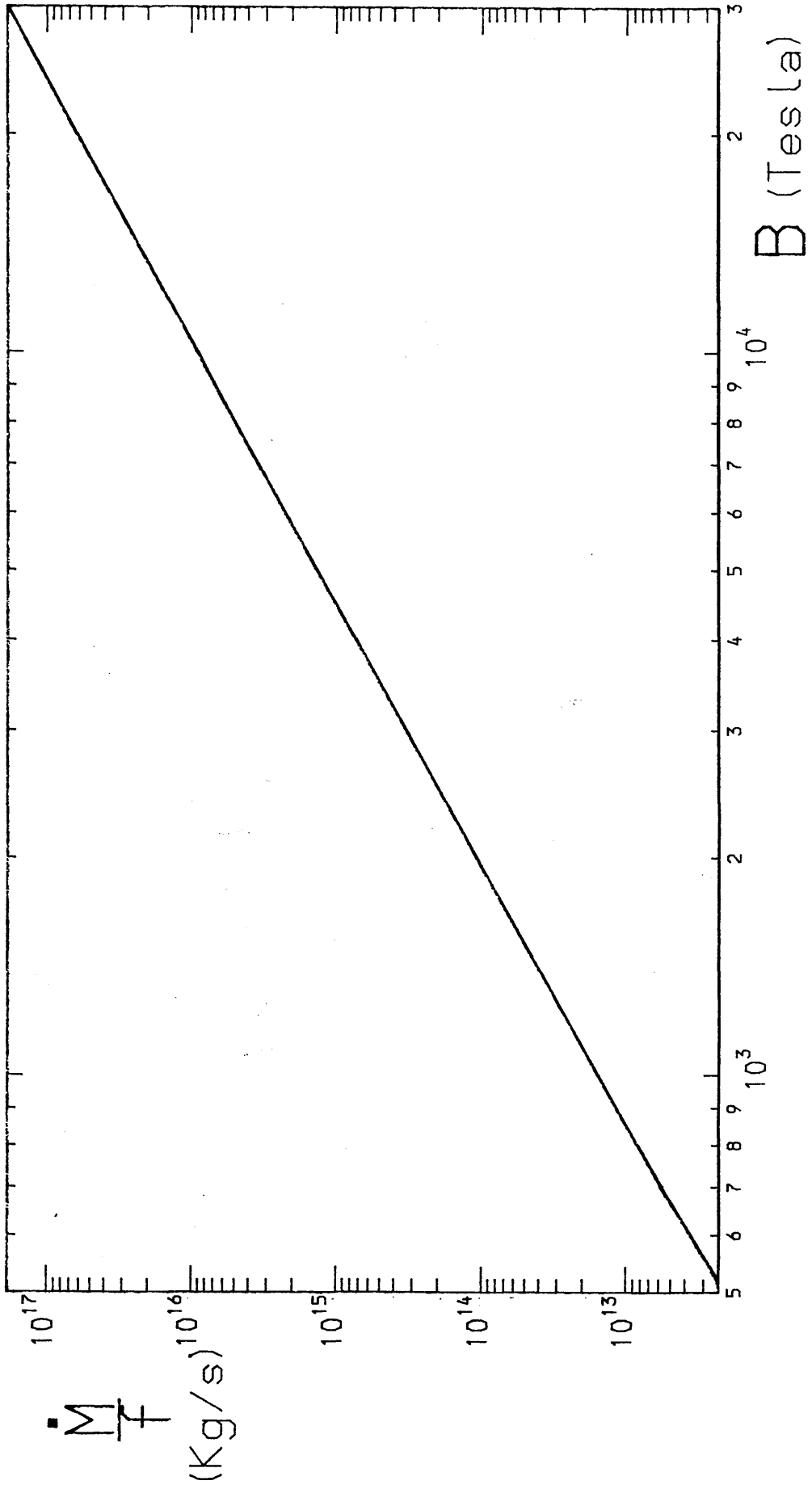


Figure 4.3: The region below the curve illustrates the values of the accretion rate and the magnetic field for which the energy deposited into the electrons by the accreting material can be dissipated 'locally' as optically thick cyclotron radiation.

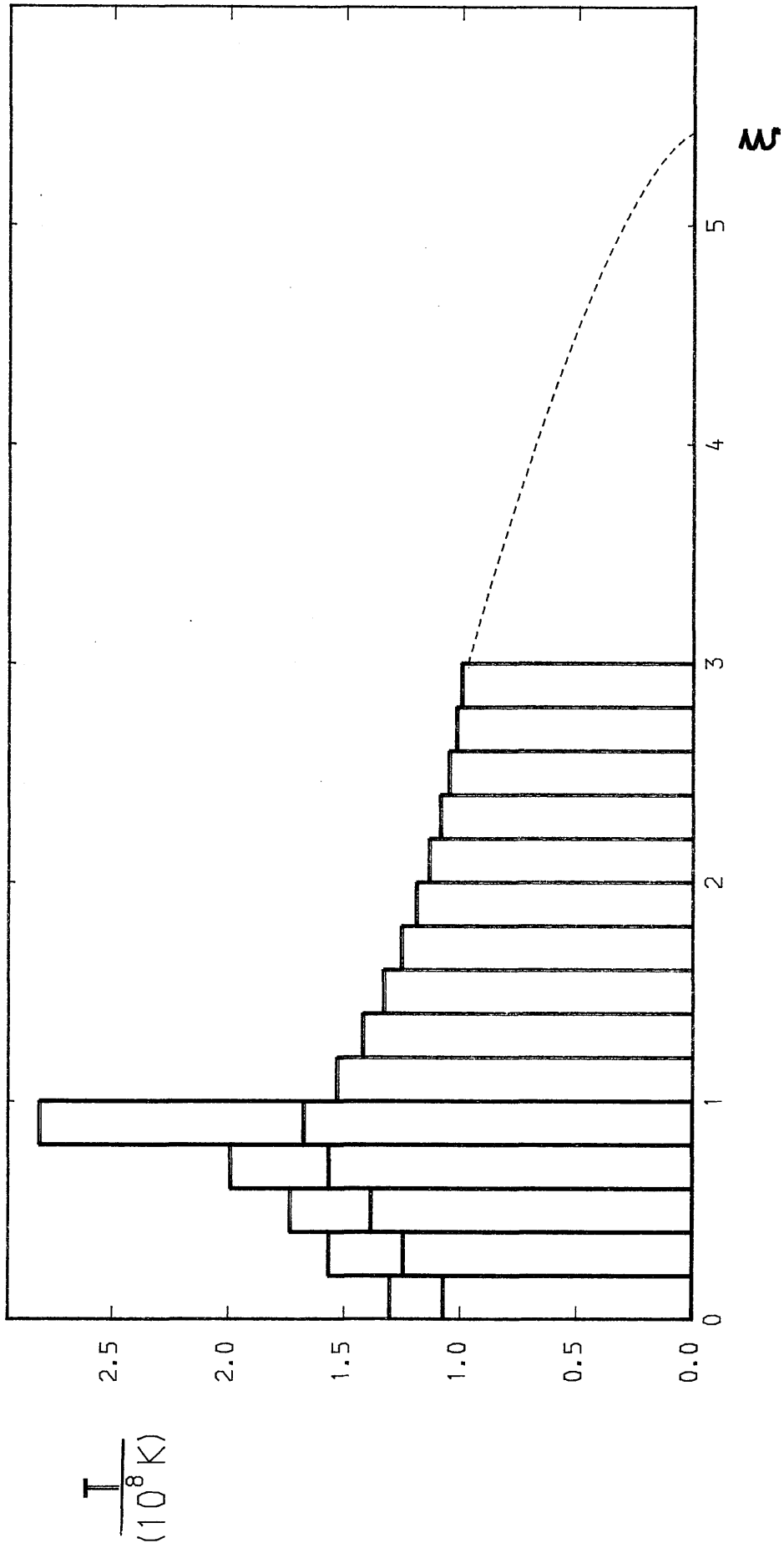


Figure 4.4a: The temperature structure derived for the cyclotron cooled bombardment model described in Section 4.5. The red histogram is the temperature structure excluding thermal conduction and the black histogram is the structure including conduction. The smooth dotted line is the analytic part of the solution which matches onto a photosphere.

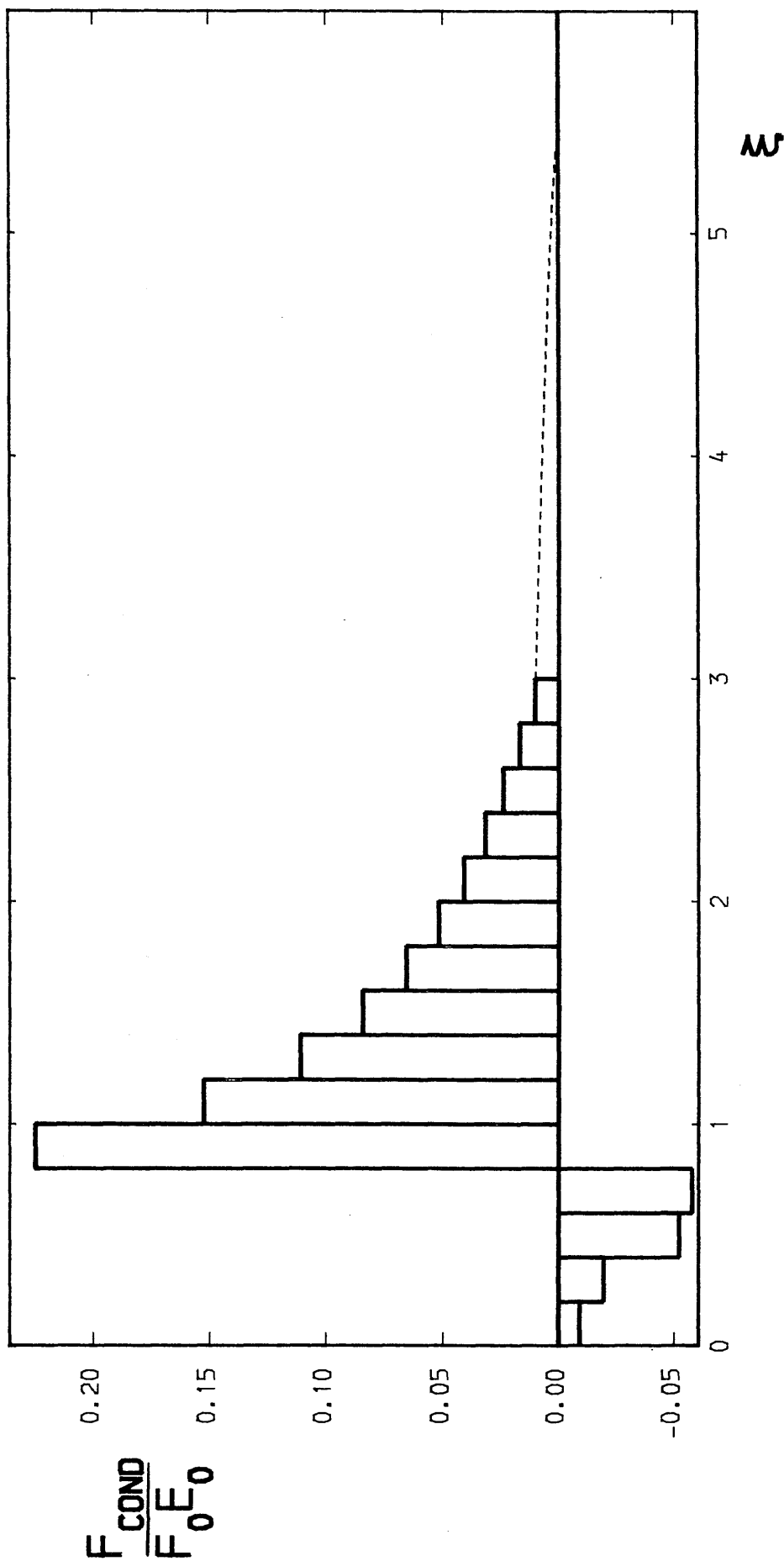


Figure 4.4b: The downward conductive flux corresponding to the temperature structure, including thermal conduction, shown in Figure 4.4a

CHAPTER 5NON-THERMAL EMISSION PROCESSESSECTION 5.1 INTRODUCTION

In Chapters 3 and 4 we examined the thermal optically thin line/bremsstrahlung and optically thick cyclotron emission from a bombarded white dwarf atmosphere. We then determined whether or not these emission processes are sufficiently efficient to balance the heating of the atmosphere by accreting protons. Bombardment models of white dwarf accretion columns, such as those described in Chapters 3 and 4, have a great deal in common with beam models of solar flare heating (e.g. Brown, 1972,1973; Emslie, 1978; Brown and Craig, 1984). These similarities would suggest that the non-thermal emission processes associated with solar flares might also be present in accreting white dwarf stars. In this Chapter we examine two such processes:- non-thermal Lyman- α emission; and non-thermal bremsstrahlung emission.

The emission of non-thermal Lyman- α radiation was suggested some time ago (Orall and Zirker, 1976; Canfield and Chang, 1985) as a method of detecting 'low' energy (10Kev - 1Mev) protons in solar flares. This radiation results from 'beam' protons picking up electrons by charge exchange during collisions with chromospheric hydrogen atoms. These 'beam' hydrogen atoms are excited by further collisions and radiated by normal dipole transitions. The resulting L_{α} emission is, however, doppler

shifted redwards by the motion of the beam. This produces a red excess in the L_α line and allows, in principle, the flux and energy of the non-thermal protons to be determined.

In Section 5.2, using essentially the same method as that described in Canfield and Chang (1985) we calculate the non-thermal L_α spectrum. We show that while in the white dwarf case it is, in principal, possible to gain information about the accretion rate and the energy distribution of the infalling protons, in practice, the flux is likely to be too small to be detectible above the continuum.

Emslie and Brown (1985) pointed out that a beam of suprathermal protons of energy E_0 and number flux F_0 , scattering off essentially stationary thermal electrons, will produce the same bremsstrahlung spectrum as a beam of suprathermal electrons of energy $\frac{m_e}{m_p} E_0$ and number flux $\frac{m_p}{m_e} F_0$. In the case of solar flares this offers the attractive possibility of a proton beam carrying a specified amount of energy and producing a given bremsstrahlung spectrum with a current 1/2000th of that of the equivalent electron beam. In the case of AM. Her objects this 'inverse' bremsstrahlung process has the attraction of being a possible source of radiation with an energy $\sim 100\text{eV}$, close to the temperature of the soft X-ray component of the characteristic spectrum.

In Section 5.3 we pose the question 'Can sufficient energy be emitted in the form of inverse bremsstrahlung to contribute significantly to the soft X-ray component of the spectrum of a radially accreting white dwarf star?'. We determine the fraction of the energy of a suprathermal proton that can be lost in the

form of inverse bremsstrahlung and calculate the spectrum of the resultant radiation.

SECTION 5.2 NON THERMAL LYMAN- α EMISSION

In this Section we calculate the non-thermal Lyman- α emission from protons being accreted onto a static white dwarf atmosphere using essentially the method outlined in Canfield and Chang (1985). We represent the accreting protons by a vertical downwards beam. Some of these protons become suprathermal hydrogen atoms by either picking up free electrons, or by charge exchange collisions with neutral, atmospheric, hydrogen atoms. Some of these 'beam' hydrogen atoms will, in turn, be in the first excited state and will produce L_α radiation.

The intensity of L_α emission per unit wavelength displacement $\Delta\lambda$ for an observer looking along the accretion column is given by

$$\phi(\Delta\lambda) d(\Delta\lambda) = \frac{dE}{4\pi} \int_0^\infty n_2^*(E,z) A_{21} dz \quad (5.1)$$

where z is the distance downward from the top of the column, n_2^* is the number density of beam hydrogen atoms in the second energy level per unit beam energy E , and A_{21} is the transition rate for a hydrogen atom between the second and the first energy levels. Since $d(\Delta\lambda) = \lambda_\alpha dv/c = \lambda_\alpha (2m_p E)^{-\frac{1}{2}} dE/c$ Equation (5.1) can be written as

$$\phi(\Delta\lambda) = \frac{(2m_p c^2)^{\frac{1}{2}} E^{\frac{1}{2}}}{(4\pi\lambda_\alpha)} \int_0^\infty n_2^*(E,z) A_{21} dz \quad (5.2)$$

where λ_α is the line centre wavelength of L_α radiation.

In order to determine $\phi(\Delta\lambda)$ we need only determine $n_2^*(E,z)$. We must, therefore, calculate the rate at which hydrogen atoms in the first excited state are created and destroyed.

We obtain from conservation of the number of suprathermal particles

$$n_p^*(E,z) v_0 dE_0 = \sum n_i^*(E,z) v_i dE \quad (5.3)$$

or alternatively

$$F/v = \sum n_i^* v_i dE \quad (5.4)$$

where F is the total number flux per unit energy of non-thermal particles, and where we have dropped the explicit (E,z) dependence (i.e. $n_i^* \equiv n_i^*(E,z)$). In addition, since equilibrium is reached on a length scale short compared to a beam proton (or hydrogen) mean free path, the rate of creation of suprathermal hydrogen atoms, in a given excited state, must be equivalent to the rate of destruction in that given state. So that

$$n_i^* D_i = \sum_{j \neq i} n_j^* C_{ji} \quad (5.5)$$

where D_i denotes the rate of destruction of beam hydrogen in the i th level and C_{ji} denotes the rate of creation of suprathermal hydrogen in the i th level from the j th state.

Equations (5.3) and (5.4) give us $m+1$ equations in the $m+1$ unknowns n_i^* (in practice we have three equations in three n_i^* s). We can, therefore, in principle determine n_2^* from these equations. In order to simplify the calculation we can, however, use the relative importance of the various competing atomic processes to make some simplifying approximations. We make essentially the same simplifications as were used by Canfield and Chang (1985), although, as we shall show, because of the high densities in the accretion column, these simplifications may not be valid throughout the entire length of the column. They are, however, valid in the region of the column which is most likely to exhibit non-thermal L_α emission, i.e. the top of the column.

Firstly, we make the approximation that the spontaneous radiative de-excitation from the first excited state is much faster than any of the other processes (e.g. collisional ionisations) destroying beam hydrogen in the ground state, so that the population of the excited state is much less than that of the ground level. Thus, Equation (5.4) becomes

$$F/v = n_1^* + n_p^* \quad (5.6)$$

Secondly, since we expect the accretion column to be somewhat hotter than the solar chromosphere and therefore more fully ionised, we do not follow Canfield and Chang (1985) in

neglecting the creation of beam hydrogen atoms by radiative recombination. We do, however, follow them in neglecting the creation of hydrogen by di-electronic recombination and by spontaneous de-excitation of n_2^* . We also include the creation of beam hydrogen by charge exchange in collisions with atmospheric hydrogen atoms. Thus Equation (5.4) becomes

$$n_1^* D_1 = n_p^* C_{p1} \quad (5.7)$$

where

$$D_1 = (n_H^H Q_{1p} + n_e^e Q_{1p} + n_p^p Q_{1p}) v_b \quad (5.8)$$

$$C_{p1} = (n_e^e Q_{e1} + n_H^H Q_{H1}) v_b \quad (5.9)$$

where ${}^\alpha Q_{ij}$ denotes the cross-section for the transition between the i th and j th levels by a collision with a particle of species α , and $Q_{\alpha i}$ denotes the cross-section for the production of an i th level hydrogen atom by a collision with a particle of type α . (Where necessary ${}^e Q_{ij}$ and Q_{ei} have been averaged over electron thermal velocities.)

Combining Equations (5.6) and (5.7) we get

$$n_p^* = (F/v) (D_1 / (C_{p1} + D_1)) \quad (5.10)$$

and

$$n_1^* = (F/v) (C_{p1} / (C_{p1} + D_1)) \quad (5.11)$$

The value of n_2^* can then be determined from the processes that link the first excited state of hydrogen to the ground state and the fully ionised state. So that

$$n_2^* \approx (C_{p2} n_p^* + C_{12} n_1^*) / D_2 \quad (5.12)$$

where

$$C_{p2} = (n_H Q_{H2} + n_e Q_{e2}) v_b \quad (5.13)$$

$$C_{12} = (n_H^H Q_{12} + n_p^P Q_{12} + n_e^e Q_{12}) v_b \quad (5.14)$$

$$\text{and} \quad D_1 = (n_H^H Q_{2p} + n_p^P Q_{2p} + n_e^e Q_{2p}) v_b + A_{21} \quad (5.15)$$

Thus, by Equations (5.10), (5.11) and (5.12), Equation (5.2) becomes

$$\phi(\Delta\lambda) = \frac{(2m_p c^2)^{\frac{1}{2}}}{(4\pi\lambda_\alpha)} E^{\frac{1}{2}} \int_0^\infty \frac{(C_{p2} D_1 + C_{p1} C_{12})}{(C_{p1} + D_1) D_2} \frac{F}{nv} dN \quad (5.16)$$

i.e

$$\phi(\Delta\lambda) = \frac{m_p c}{(4\pi\lambda_\alpha)} \int_0^\infty \frac{(C_{p2} + C_{12} (C_{p1}/D_1))}{(1 + (C_{p1}/D_1)) D_2} \frac{F}{n} dN \quad (5.17)$$

Before we can calculate $\phi(\Delta\lambda)$, we require only to determine

C_{p2} , C_{12} , C_{p1} , D_1 , and D_2 . These can, given a knowledge of the temperature, density, and ionisation at any point in the atmosphere, be calculated using Equations (5.8), (5.9) and (5.13-5.15). In view of the fact that no standard models of accretion columns exist we adopt a uniform temperature structure with Saha ionisation. The density was determined from the atmospheric pressure

$$P(N) = P_{RAM} [1 - (\overline{E(N)}/\overline{E}_0)^2] \quad (5.18)$$

where $\overline{E(N)}$ (calculated using Equation (3.30)) is the mean energy of the beam protons at a column density N , \overline{E}_0 is the mean energy of the protons at $N=0$, and P_{RAM} is the beam ram pressure. The values of the cross sections used are given in Table 5.1.

The values of $\phi(\Delta\lambda)$ were calculated for a white dwarf mass $= 1M_{\odot}$, an accretion rate $\dot{M}_* = 10^{13} \text{Kgs}^{-1}$, over a fraction of the surface area $f = 10^{-2}$, with atmospheric temperatures $T = 10^5, 10^6, 10^7 \text{K}$. We did this for both mono-energetic beams and beams which had an initial parabolic spread in energies with half width ΔE i.e

$$F_0(E_0) = F_0 (aE_0^2 + bE_0 + c) \quad |E_0 - \overline{E}_0| < \Delta E_0 \quad (5.19)$$

$$F_0(E_0) = 0 \quad |E_0 - \overline{E}_0| \geq \Delta E_0 \quad (5.20)$$

where

$$\begin{aligned} a &= -3/(4\Delta E^3) \\ b &= -2\overline{E}_0 a \\ c &= [\overline{E}_0^2 - \Delta E^2] a \end{aligned} \quad (5.21)$$

and F_0 is the total number flux of non-thermal particles integrated over energies. The results of these calculations are shown in Figures 5.1-5.3

Qualitatively, all these results show the same three main features. Firstly, and of most interest here, there is a peak around 1237\AA . This is due to the radiative recombination of free electrons with the beam protons near the top of the accretion column where the density, and consequently the collisional ionisation rates, are small. Below this thin region (thickness $\frac{\Delta N}{N_s} \sim 3 \cdot 10^{-9} T_6^2 M_1^{4/3} f_{-2}^2 M_{13}^{-2}$, where N_s is the distance in which the beam stops), the rate at which beam hydrogen atoms in the first excited state are collisionally ionised becomes greater than the rate at which they radiatively de-excite. This results in the non-thermal L_α emission being suppressed and accounts for the second feature in the spectrum, the dip in the centre (λ between 1222\AA and 1235\AA). Thirdly, there is a large increase in the flux close to $\lambda_\alpha = 1215\text{\AA}$. Although this up-turn represents a considerable fraction of the L_α emission, it is, in part, an artifact of the computational method which takes no account of the beam merging with the thermal background as E tends to kT but instead allows E , for all protons, to tend to zero. As we shall see later the flux from this part of the spectrum would in any case be too low to be observable, and as can be seen from the results for different energy spreads it is unlikely to yield any useful information about the infalling material anyway. We, therefore, concentrate for the rest of this Section on the first feature.

Two pieces of information can, in principle, be determined from the small bump around 1237\AA . Firstly, because of the narrowness of the region from which this part of the spectrum is emitted, the half width of the bump, $d\lambda$, directly reflects the initial spread in the energies of the beam particles ΔE . ΔE can be calculated using the relationship

$$d\lambda = (2m_p E)^{\frac{1}{2}} \frac{\Delta E}{c} \lambda_\alpha \quad (5.22)$$

Secondly, the temperature of the top of the emitting region can also, in principle, be determined from increase in the intensity of the radiation with temperature. This is due to the decrease in density and increase in penetrating power of the beam with temperature. These extend the region at the top of the atmosphere within which this spectral feature is produced.

Before either of these quantities can be calculated we must, however, verify that the flux that we expect at the earth

$$F = \frac{4\pi R_*^2 f}{4\pi D^2} \phi(\Delta\lambda) \quad (5.23)$$

(where R_* is the white dwarf radius and D is the distance to the source ($\sim 100\text{pc}$)) is observable. The maximum possible flux (corresponding to a monoenergetic beam striking an atmosphere with $T \sim 10^8\text{K}$)

$$F_{\max} \sim 10^{-24} \text{ W m}^{-2} \text{ \AA}^{-1} \quad (5.24)$$

is several orders of magnitude below the observed background

flux.

$$F_{\text{back}} \sim 10^{-16} \text{ W m}^{-2} \text{ \AA}^{-1} \quad (5.25)$$

(Raymond et al, 1979). The same is also true of the peak close to the rest frequency.

Therefore, although information about the accreting matter and the accretion column could, in principle, be gained from non-thermal L_{α} emission, in practice we expect the non-thermal L_{α} flux to be several orders of magnitude too small to be observable.

SECTION 5.3 NON THERMAL INVERSE BREMSSTRAHLUNG EMISSION

Boldt and Serlimistos (1969), Hudson (1973) and Emslie and Brown (1985) pointed out, in connection with the solar flare problem, that a beam of suprathemal protons striking a cold atmosphere (the electron thermal velocity $v_e \ll v_b$, the beam velocity) will accelerate the atmospheric electrons causing them to emit non-thermal 'inverse' bremsstrahlung with a characteristic energy $\varepsilon = E_b m_e / m_p$ (where E_b is the beam proton energy). In the case of radially accreting white dwarfs, we might expect, therefore, the infalling material to produce non-thermal 'inverse' bremsstrahlung with $\varepsilon \sim 90\text{eV}$, close to the temperature of the soft X-ray component of their spectrum.

In this Section we calculate the fraction of the energy of a suprathemal proton that can be radiated as inverse

bremsstrahlung and the resulting emission spectrum. We determine whether such a radiation mechanism could contribute significantly to the large soft X-ray flux observed from AM Her. objects.

The number of photons emitted per unit energy ϵ during the lifetime of a non-thermal proton is given by

$$\frac{dv_p(\epsilon, E)}{d\epsilon} = \int_{\frac{m_p}{m_e} \epsilon}^{E_0} \frac{n_e Q_B(\epsilon, E m_e/m_p) v_p}{|dE_p/dt|} dE_p \quad (5.26)$$

where

$$\frac{dE_p}{dt} = \frac{2\pi e^4 n_e v_p \ln \Lambda}{[4\pi\epsilon_0]^2 E_p} \frac{m_p}{m_e} \quad (5.27)$$

is the rate of loss of energy of the protons by Coulomb collisions (c.f. Equation 3.1a), Q_B is the bremsstrahlung cross-section differential in ϵ , given by the Bethe-Heitler formula:

$$Q_B(\epsilon, E) = \frac{8 r_e^2 m_e c^2}{3 E \epsilon 137} \log \left(\frac{1+(1-\epsilon/E)^{\frac{1}{2}}}{1-(1-\epsilon/E)^{\frac{1}{2}}} \right) \quad (5.28)$$

(Heitler, 1954), and where E_0 is the initial energy of the beam, v_p is the velocity of a proton with energy E_p , n_e is the electron number density, and r_e is the classical electron radius.

Thus, changing variable to $x = \frac{m_e E_p}{m_p \epsilon}$

$$\frac{dv_p}{d\epsilon} = \frac{[4\pi\epsilon_0]^2}{2\pi e^4 \ln \Lambda} \frac{m_p}{m_e} \frac{8}{3} \frac{r_m^2 c^2}{137} \int_1^{x_0} \log \left(\frac{1+(1-1/x)^{\frac{1}{2}}}{1-(1-1/x)^{\frac{1}{2}}} \right) dx \quad (5.29)$$

where $x_0 = \frac{m_e E_0}{m_p \epsilon}$. So that the energy emitted per unit ϵ range is given by

$$\frac{d\eta_p}{d\epsilon} = \frac{dv_p}{d\epsilon} = \frac{[4\pi\epsilon_0]^2 E_0}{2\pi e^4 \ln \Lambda} \frac{8}{3} \frac{r_m^2 c^2}{137} \frac{1}{x_0} \int_1^{x_0} \log \left(\frac{1+(1-1/x)^{\frac{1}{2}}}{1-(1-1/x)^{\frac{1}{2}}} \right) dx \quad (5.30)$$

The fraction of the proton beam energy emitted per unit ϵ range is, therefore, given by

$$\frac{1}{E_0} \frac{d\eta_p}{d\epsilon} = \frac{[4\pi\epsilon_0]^2}{2\pi e^4 \ln \Lambda} \frac{8}{3} \frac{r_m^2 c^2}{137} \frac{1}{x_0} \int_1^{x_0} \log \left(\frac{1+(1-1/x)^{\frac{1}{2}}}{1-(1-1/x)^{\frac{1}{2}}} \right) dx \quad (5.31)$$

and the fraction of the beam energy emitted as non-thermal bremsstrahlung is

$$\frac{\eta_p}{E_0} = \frac{[4\pi\epsilon_0]^2}{2\pi e^4 \ln \Lambda} \frac{m_e}{m_p} \frac{8}{3} \frac{r_m^2 c^2}{137} \int_1^{\infty} \frac{1}{x^3} \int_1^{x_0} \log \left(\frac{1+(1-1/x)^{\frac{1}{2}}}{1-(1-1/x)^{\frac{1}{2}}} \right) dx \quad (5.32)$$

$$\approx 2 \cdot 10^6 E_0 \quad (5.33)$$

where E_0 is measured in joules. In the case of matter falling onto a white dwarf

$$\frac{n_p}{E_0} \approx 5 \cdot 10^{-8} M_1^{4/3} \quad (5.34)$$

Figure 5.4 shows the energy spectrum of the non-thermal bremsstrahlung photons emitted by a single proton passing through a cold plasma. Clearly, however, the total energy emitted by a suprathermal proton by this mechanism represents only a small fraction of its total energy and, consequently, non-thermal inverse bremsstrahlung cannot contribute significantly to the soft X-ray component of the spectrum of radially accreting white dwarfs.

One might ask what would happen if the atmosphere were warm ($v_{th} > v_b$). As we saw in Chapters 3 and 4, a warm atmosphere allows suprathermal protons to penetrate deeper into the atmosphere. Consequently, they might be expected to emit more non-thermal radiation. Since, in these circumstances, we would have the thermal electrons scattering off the relatively stationary beam protons, the 'non-thermal' bremsstrahlung formed in this way will have the same characteristic temperature and spectrum as the thermal bremsstrahlung. The ratio of the energies contained in the 'non-thermal' and thermal contributions to the bremsstrahlung would simply be the ratio n_p^*/n_p (where n_p^* is the density of beam and n_p is the density of atmospheric protons). The only part of the column where this ratio is large is at the top of the column where the

atmospheric pressure, and, consequently, the value of n_p is small. This suggests, then, an alternative definition for the 'top pressure' defined in Chapter 3

$$P_0 = 2n_p^*kT \quad (5.35)$$

At any point in column where the pressure is lower than this, the non-thermal beam emission dominates the thermal emission and sets a lower limit on the emissivity at that point.

SECTION 5.4 CONCLUSIONS

In this Chapter we have investigated two of the non-thermal emission processes that might reasonably be expected to be present when a proton beam strikes a white dwarf atmosphere.

In Section 5.2 we suggested that, as in the case of solar flares, the emission of non-thermal Lyman- α radiation by hydrogen atoms formed in the proton beam might provide information about both the beam and the medium through which it is passing. We calculated the resultant emission spectrum for a uniform temperature atmosphere and showed that, although information about the initial spread in energy of the beam protons, and the temperature of the top of the atmosphere could, in principle, be determined, the number of photons expected was too small to be detectable above the continuum emission.

In Section 5.3 we calculated the energy spectrum of photons emitted as the result of one suprathreshold proton striking a cold

atmosphere ($v_{th} < v_b$). We showed that, although this radiation would, in the case of a radially accreting white dwarf, occur at 'soft' X-ray wavelengths ($\lambda \sim 200\text{\AA}$), the fraction of the protons total energy that can be emitted in this way is very small ($\sim 10^{-7}$) and could not contribute significantly to the soft X-ray component of the spectrum of AM Her. stars.

We also showed that for a warm atmosphere ($v_{th} > v_b$), for pressures less than $P_0 = 2n_p^*kT$, the total energy emitted, as bremsstrahlung radiation by the thermal electrons scattering off the non-thermal 'beam' protons would exceed that produced by the thermal electrons scattering off the thermal, atmospheric, protons. This produces a lower limit for the energy emitted as bremsstrahlung radiation at the top of the atmosphere. We suggest, therefore, that the value P_0 , above represents an alternative definition of the 'top pressure' to that given in Chapter 3. Such a definition would still not, however, produce a sufficiently large value of P_0 to resolve any of the problems described in that Chapter.

Table 5.1: Atomic cross-sections (m^2)

Energy (Kev)	Q_{H1} (1)	Q_{H2} (2)	e_{Q12} (3)	P_{Q12} (4)
1000	$2.6 \cdot 10^{-26}$	$2.9 \cdot 10^{-28}$	$1.6 \cdot 10^{-21}$	$2.0 \cdot 10^{-21}$
100	$6.4 \cdot 10^{-22}$	$9.0 \cdot 10^{-23}$	$1.3 \cdot 10^{-21}$	$6.2 \cdot 10^{-21}$
10	$8.7 \cdot 10^{-20}$	$7.5 \cdot 10^{-21}$		$1.4 \cdot 10^{-20}$
1.0	$1.3 \cdot 10^{-18}$	$5.1 \cdot 10^{-23}$		$3.4 \cdot 10^{-23}$
0.3	$4.9 \cdot 10^{-18}$	$1.8 \cdot 10^{-24}$		$3.0 \cdot 10^{-24}$

Energy (Kev)	H_{Q12} (5)	e_{Q1p} (6)	P_{Q1p} (4)	H_{Q1p} (7)
1000	$1.8 \cdot 10^{-22}$	$2.0 \cdot 10^{-21}$	$1.1 \cdot 10^{-21}$	$1.1 \cdot 10^{-21}$
100	$1.0 \cdot 10^{-21}$	$7.0 \cdot 10^{-21}$	$1.3 \cdot 10^{-20}$	$6.2 \cdot 10^{-21}$
10	$1.2 \cdot 10^{-21}$		$1.5 \cdot 10^{-20}$	$4.4 \cdot 10^{-21}$
1.0	$2.7 \cdot 10^{-22}$		$1.6 \cdot 10^{-22}$	$1.7 \cdot 10^{-21}$
0.3	$4.4 \cdot 10^{-23}$		$2.1 \cdot 10^{-24}$	$1.1 \cdot 10^{-21}$

Energy (Kev)	e_{Q2p} (8)	P_{Q2p} (9)	H_{Q2p} (9)	Q_{e1} (8)
1000	$3.5 \cdot 10^{-21}$	$4.9 \cdot 10^{-22}$	$1.0 \cdot 10^{-23}$	$1.1 \cdot 10^{-25}$
100	$3.3 \cdot 10^{-21}$	$4.9 \cdot 10^{-21}$	$1.0 \cdot 10^{-22}$	$8.9 \cdot 10^{-24}$
10	$1.3 \cdot 10^{-19}$	$4.9 \cdot 10^{-20}$	$1.0 \cdot 10^{-21}$	$3.2 \cdot 10^{-22}$
1.0		$4.9 \cdot 10^{-21}$	$1.0 \cdot 10^{-22}$	$4.2 \cdot 10^{-21}$
0.3		$1.5 \cdot 10^{-21}$	$3.0 \cdot 10^{-23}$	$1.4 \cdot 10^{-20}$

Table 5.1(cont)

Energy (Kev)	Q_{e2} (8)
1000	$1.4 \cdot 10^{-26}$
100	$1.3 \cdot 10^{-24}$
10	$8.5 \cdot 10^{-23}$
1.0	$1.9 \cdot 10^{-21}$
0.3	$6.5 \cdot 10^{-21}$

References:

- (1) Stier and Barnett (1965)
- (2) Bates and Dalgarno (1953)
- (3) Fite and Brackmann (1958a)
- (4) Bates and Griffing (1953)
- (5) Bates and Griffing (1954)
- (6) Fite and Brackmann (1958b)
- (7) Bates and Griffing (1955)
- (8) Allen (1973)
- (9) Canfield and Chang (1985)

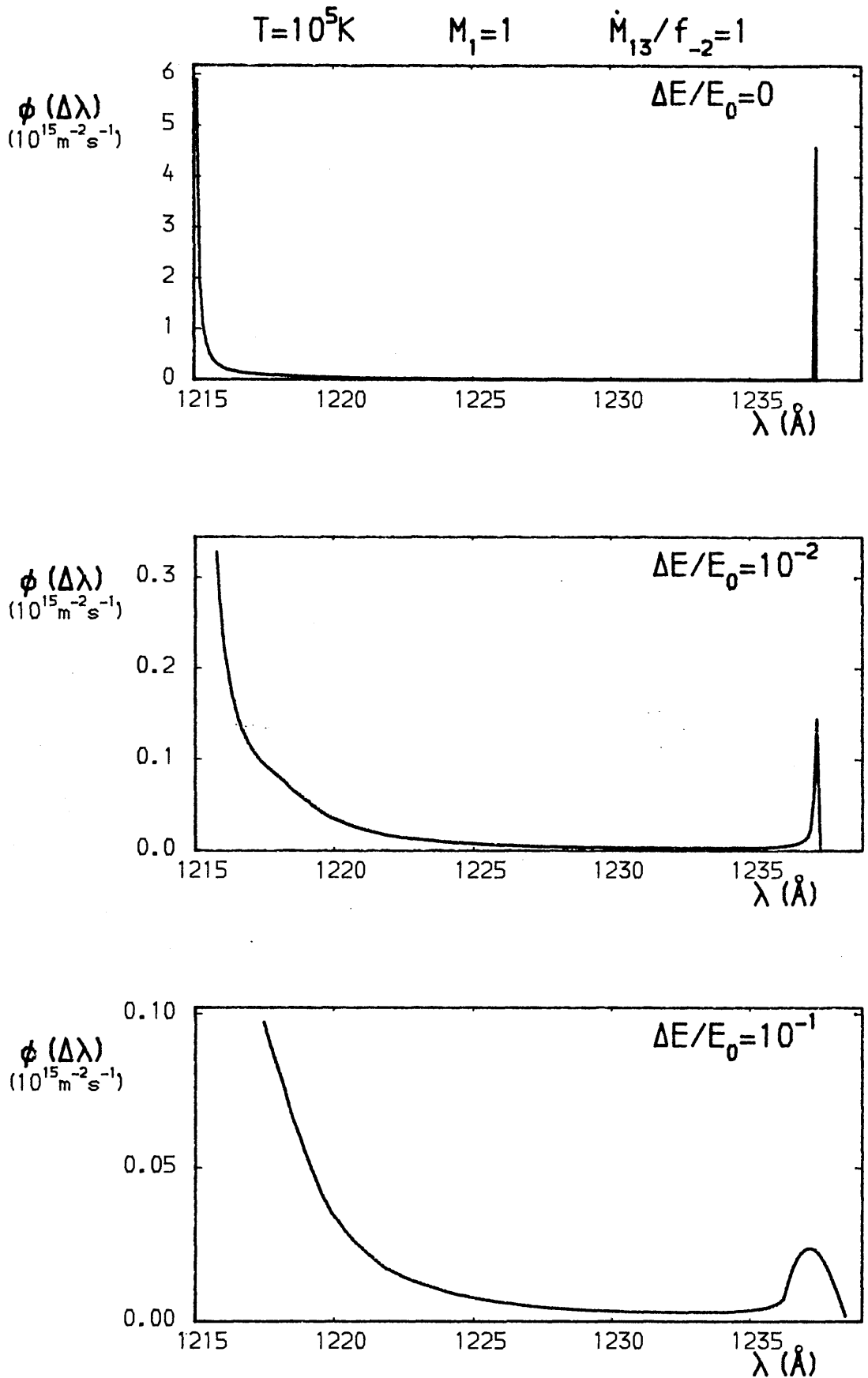


Figure 5.1: Graphs of the non thermal L_α flux produced by a uniform temperature accretion column with $T = 10^5\text{K}$, $\dot{M}_{13}/f_{-2} = 1$, $M_1 = 1$ and for spreads in the initial energy of $\Delta E/E_0 = 0, 10^{-2}$ and 10^{-1} .

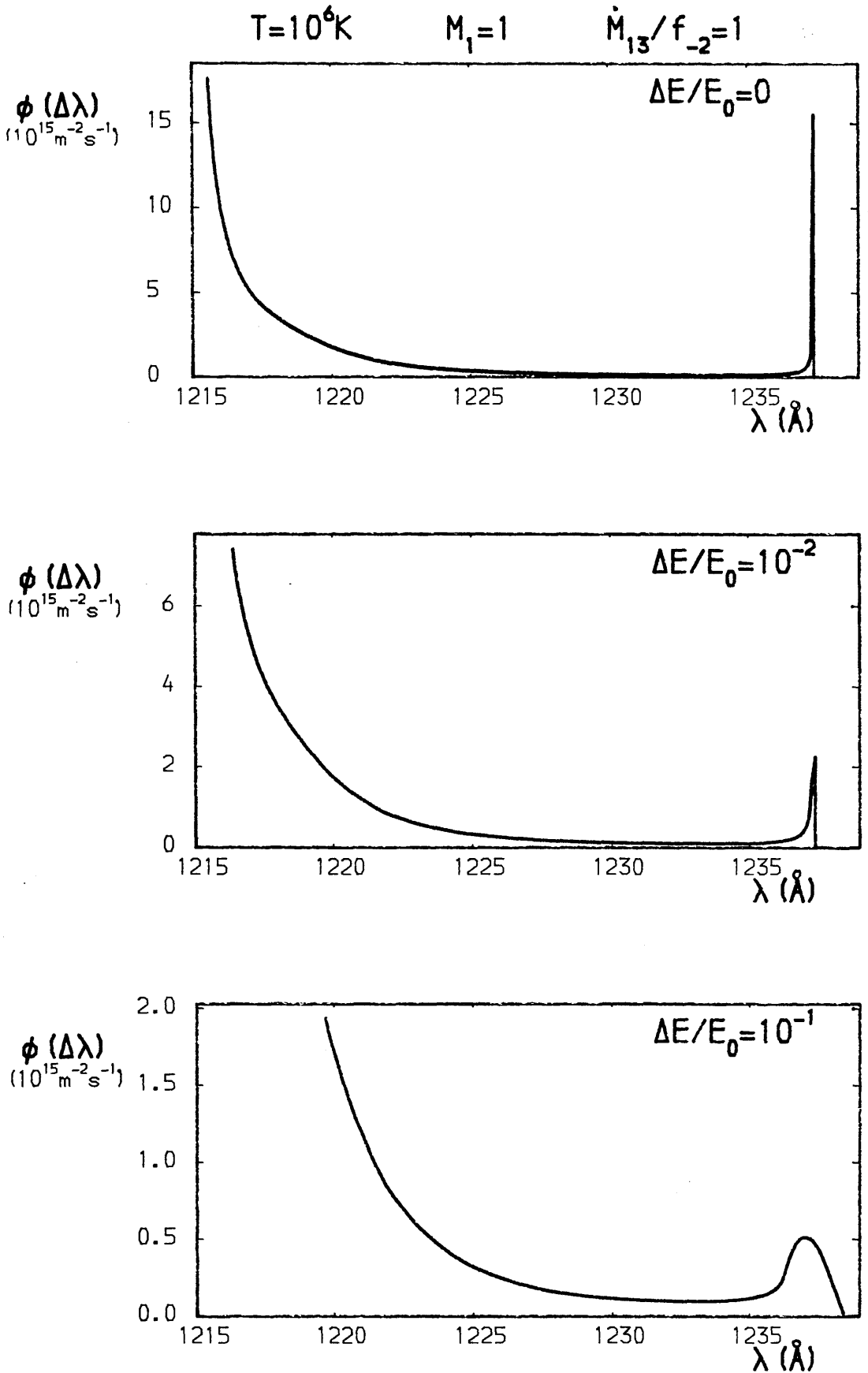


Figure 5.2: Graphs of the non thermal L_α flux produced by a uniform temperature accretion column with $T = 10^6\text{K}$, $\dot{M}_{13}/f_{-2} = 1$, $M_1 = 1$ and for spreads in the initial beam energy of $\Delta E/E_0 = 0, 10^{-2}$ and 10^{-1} .

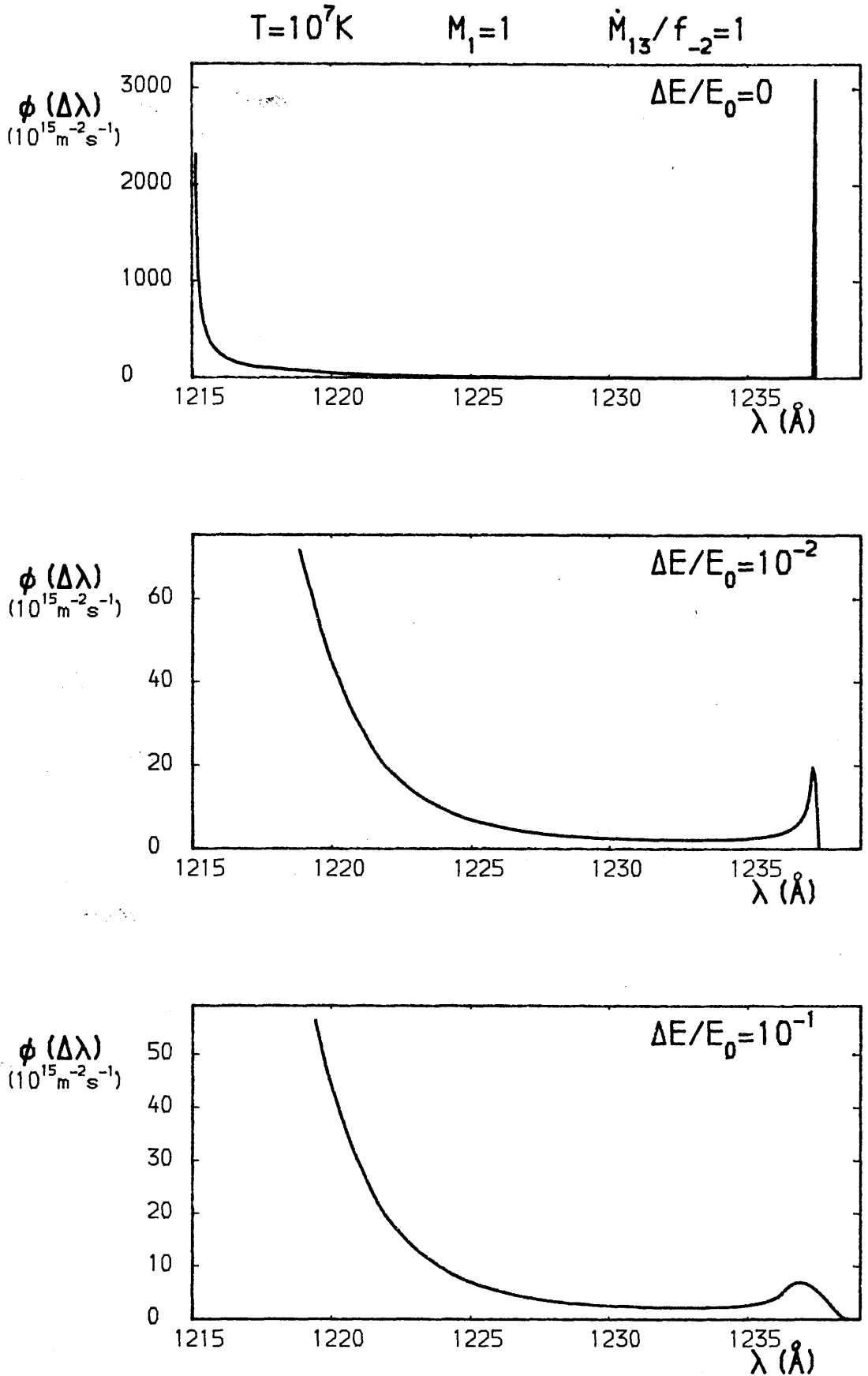


Figure 5.3: Graphs of the non thermal L_α flux produced by a uniform temperature accretion column with $T = 10^7\text{K}$, $\dot{M}_{13}/f_{-2} = 1$, $M_1 = 1$ and for spreads in the initial energy of $\Delta E/E_0 = 0, 10^{-2}$ and 10^{-1} .

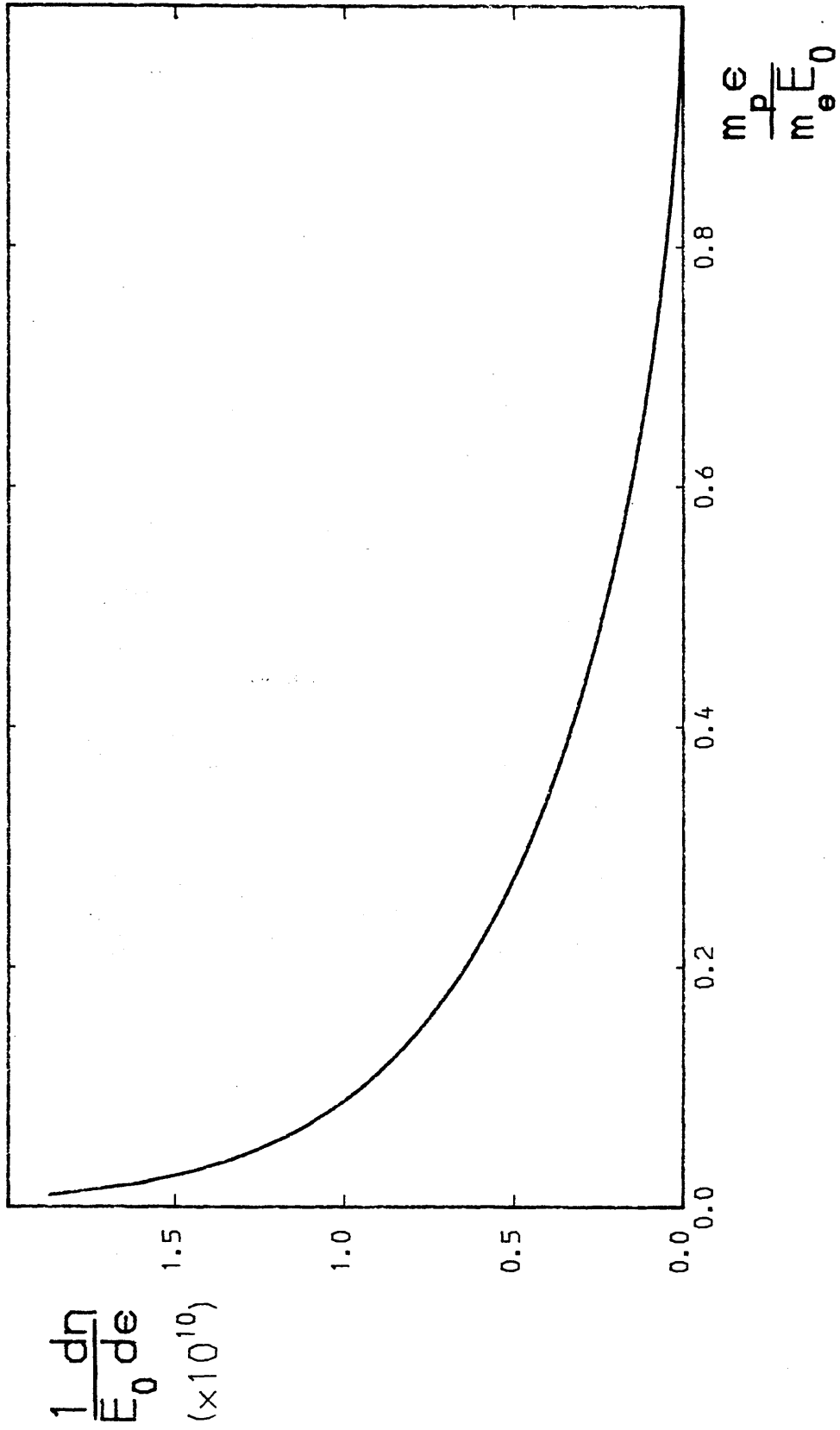


Figure 5.4: The energy spectrum of the inverse bremsstrahlung radiation produced by a proton of energy E_0 striking a cold fully ionised target atmosphere.

CHAPTER 6

CONCLUSIONS AND FUTURE WORK

In this Thesis we have examined in detail some of the non-thermal aspects of energy transport within white dwarf accretion columns. In this final Chapter we briefly summarise the conclusions we have reached in the previous Chapters and suggest two possible extensions and sequels to this research.

In Chapter 2 we examined the non-thermal electron energy transport model for a shock heated accretion column (Frank et al, 1983; Frank and King, 1984). Frank and King (1984) suggested that an adiabatic shock wave could be formed in the accreting matter sufficiently close to the white dwarf photosphere to allow the post-shock region to be cooled predominantly by the 'leaking' of hot, shock heated electrons into the photosphere of the star. They envisaged these electrons as emerging from the hot shock region into the cold photosphere where they then behave as supra-thermal particles which lose their energy by means of Coulomb collisions. This is similar to the situation that occurs in the solar transition region.

We showed that, due to a misinterpretation of the standard Coulomb collisional timescales, Frank and King (1984) overestimated the mean free path of the shock heated electrons and, consequently, the length of the accretion column. We also showed that if the correct time scales are used, the post shock cooling region would, in order to allow significant energy transport by non-thermal, 'leak', electrons, have to be thinner than the shock itself. We concluded, as a result, that no self

consistent model of the type described in Frank and King (1984) can exist.

In Chapters 3 and 4 we investigated the possibility of a bombardment solution to the structure of a white dwarf accretion column. This type of solution was first suggested by Kuipers and Pringle (1982). They derived a 'mean' temperature for such a model $\sim 10^7$ K. In Chapter 3 we showed, however, that they also had used an incorrect Coulomb collisional time scale. We repeated their calculation using the correct time scale and found that the resulting mean temperature was $\sim 10^5$ K, somewhat closer to the temperature of the observed black-body component of the spectrum of radially accreting white dwarfs. On the other hand, we found, from a more detailed investigation, that the heating rate within the column was too high to allow the energy deposited by the accreting matter to be radiated away locally, unless a large 'top pressure' (pressure at the gas vacuum boundary) was introduced. Although we suggested two possible origins (c.f. Chapters 3 and 5) of such a pressure, neither would produce a sufficiently large pressure to allow a column of this type to exist. We also examined the effect of diffusive thermal conduction on the possible existence of a self consistent, bremsstrahlung/line radiation cooled, bombardment model of white dwarf accretion columns. We showed that a steady state model of this type could be found but that it is only self-consistent for relatively low accretion rates, $\dot{M}_*/f \lesssim 10^{12} - 10^{13} \text{ Kgs}^{-2}$, roughly 3 orders of magnitude below those observed in AM Her. stars.

In Chapter 4 we considered the effect that the strong

magnetic field ($B \sim 10^3 - 10^4$ T), normally associated with radially accreting white dwarfs, has on the cooling of the 'shock' heated accreting material. We showed that on a global basis, the accreted energy flux (typically $\sim 10^{14} \text{ Wm}^{-2}$) could be radiated away within one proton mean free path by optically thick cyclotron radiation at a temperature $< 10^8 \text{ K}$, slightly lower than the shock temperature. We also derived, as a first approximation to the temperature structure of the column, a piecewise uniform temperature structure. We showed that this simple structure predicted a soft/hard X-ray ratio which is consistent with that observed in AM Her. stars. In addition, we noted that this type of solution allows an observed hard X-ray temperature $\sim 10^8 \text{ K}$ without the need for the unusually small white dwarf mass required by the cyclotron cooled shock model (Meggit and Wickramasinghe, 1982; Barrett and Channugam, 1985). We concluded, therefore, that a bombardment model of the type described in Chapter 4 may represent a solution to the 'Soft X-ray Puzzle'.

In Chapter 5, we investigated two of the non-thermal emission processes (non-thermal Lyman- α emission and inverse bremsstrahlung emission) that might be expected to be produced by a beam of supra-thermal protons striking a static atmosphere. We showed that, although the non-thermal Lyman- α emission (L_α emission produced by hydrogen atoms formed in the beam by protons 'picking up' electrons) could, in principle, be used to derive information about the energy distribution and flux of the accreting protons and the atmospheric temperature at the top of the accretion column, the emitted L_α flux is too small to be

observable.

In chapter 5 we also determined the spectrum of the inverse bremsstrahlung radiation emitted by a mono-energetic beam striking a cold static atmosphere. We calculated that for a white dwarf accretion column most of the radiation produced by this process would be emitted at energies between 10eV and 100eV and would, therefore, enhance the soft X-ray flux from the column. We also showed, however, that only 10^{-7} of the energy of the infalling material would be radiated in this manner and that, consequently, the enhancement of the soft X-ray flux would be negligible.

Finally, we would like to suggest two possible areas of future research which are logical extensions to the work presented here. In Section 2.3 we saw that the cyclotron cooled shock model predicts the correct three component form for the spectrum produced by a white dwarf accretion column. Similarly, in Chapter 4 we saw that the cyclotron cooled bombardment model, despite some rather large approximations, gives reasonable values for the soft/hard X-ray ratios, as well as giving the correct three component form for the emitted spectrum. Both these models do, however, have their limitations. Firstly, in deriving the temperature structure for the bombarded column, we made some approximations that are at best marginally justified. For example, we ignored the effect of advection energy from the bottom of the bombarded region. However, using the argument outlined in Section 3.5, we might expect the advected flux to be $\sim 40\%$ of the total accreted energy flux. Similarly, we neglected the effect of cyclotron radiation towards the photosphere,

although we might reasonably expect this to represent $\sim 50\%$ of the total cyclotron losses. In addition to the inaccuracies introduced by these approximations, the bombardment model is itself not a totally appropriate treatment. For example, in the bombardment model we consider two sets of ions, a set of moving, accreting, ions which strike a completely independent set of stationary, atmospheric, ions. In reality, however, there is no distinction between the atmospheric ions and the beam ions, as the atmosphere is made up of beam ions which have been slowed down.

The shock treatment, on the other hand, takes account of the fact that the accreting material and the atmosphere on to which it is accreting are one and the same, but takes no account of the fact that some of the accreted energy could be lost in the shock itself. As we saw in Chapter 4, radiative losses from the shock are likely to be important. Clearly, what we require, ideally, is a globally self-consistent treatment which smoothly models the transition of the cold supersonic fluid, through collisional shock, into a hot subsonic fluid, as well as incorporating the effects of radiative losses from the shock itself. Such a radiative shock model requires a full kinetic treatment, of the type described by Zeldovitch and Raizer (1966), for the shock (equivalent to the bombarded region) which must then turn smoothly into a fluid treatment for the remainder of the column.

A calculation of this type represents a major undertaking due to the difficulties not only in handling the kinetic equations but also in modelling both the upward and downward

cyclotron emission. It is, however, possible to comment, qualitatively, on some aspects of the results we could expect from this type of calculation. As far as the cyclotron aspects are concerned, since both the cyclotron cooled bombardment model and the cyclotron cooled shock model predict the correct three component spectrum, it is likely that the radiative shock model will also have this type of spectrum. In addition, since the radiative shock model incorporates downward emission of cyclotron radiation and extra energy transport processes, which were ignored in the bombardment model, we would expect bremsstrahlung and cyclotron temperatures in the radiative shock model to be less than that for the equivalent bombardment model. Similarly, comparing the radiative shock model with the shock model of Lamb and Masters (1979), we would expect the inclusion of the radiative losses from the shock to result in a lower temperature for the radiative shock model. Qualitatively, therefore, we expect the radiative shock model of white dwarf accretion columns to predict the correct three component spectrum, but at a lower cyclotron/hard X-ray temperature.

One question that remains unanswered is whether a model of this type could explain a reprocessed black-body flux in excess of the energy flux emitted directly by the column. The fact that the discrepancy is only a factor ~ 2 does mean, though, that this question is unlikely to be resolved without the performing a detailed calculation.

The second area for future investigation is that of non-uniform accretion models. In this Thesis we have concerned ourselves, chiefly, with uniform accretion models of white dwarf

accretion columns. In Chapter 2, however, we discussed, briefly, a non-uniform accretion model proposed by Kuijpers and Pringle (1982). They suggested that as matter enters the white dwarf's magnetosphere, the matter cools producing inhomogeneities in the flow which are preserved during the infall. If these inhomogeneities are sufficiently dense they may penetrate to a depth at which the atmosphere is optically thick. In other words, they suggested that matter accreted in lumps could penetrate into an existing, quiescent, atmosphere to a depth at which the atmospheric pressure is of order the ram pressure of the beam. At this depth the white dwarf atmosphere could be optically thick so that only the radiation emitted through the hole in the atmosphere left by the lump of material would be seen directly. The remaining radiation would, instead, be reprocessed by the surrounding atmosphere.

If such a process does occur then the black body flux would be enhanced and the soft X-ray puzzle could be resolved. Clearly, this represents another, probably more tractable, area for future research.

APPENDIX ACOULOMB COLLISIONAL TIME-SCALES

In Chapters 2 and 3 we discussed, in the context of radially accreting white dwarfs, the use of inappropriate Coulomb collisional time-scales for suprathermal particles (i.e. particles of energy $E \gg kT$, the thermal energy of the background field particles). In this Appendix we derive these timescales from Spitzer's (1962) treatment for a beam (test) particle being acted on by field particles which have Maxwellian distributions of temperature T .

In Spitzer's notation, the timescale for the change of a scalar function ϕ of the test particle vector velocity v is found from

$$t = \phi(v) / \langle \Delta\phi(v) \rangle \quad (\text{A.1})$$

where $\langle \Delta\phi \rangle$ denotes the collisional rate of change of $\phi(v)$ for the test particle averaged over species of field particle.

The four time-scales that are used in this thesis are:

$$\text{The slowing down timescale } t_S = v / \langle \Delta v_{\parallel} \rangle ; \quad (\text{A.2})$$

$$\text{The deflection timescale } t_D = v^2 / \langle \Delta v_{\perp}^2 \rangle ; \quad (\text{A.3})$$

$$\text{The energy exchange timescale } t_E = E^2 / \langle \Delta E^2 \rangle ; \quad (\text{A.4})$$

(which are defined in Spitzer, 1962) and

$$\text{The energy loss timescale } t_{EL} = E / \langle \Delta E \rangle$$

i.e.

$$t_{EL} = |v^2 / [-2v \langle \Delta v_{\parallel} \rangle + \langle \Delta v_{\parallel}^2 \rangle + \langle \Delta v_{\perp}^2 \rangle]| \quad (A.5)$$

Physically, t_s and t_{EL} are linear timescales, representing the time for a beam (test) particle's velocity along its original direction of motion, and the beam particle's energy to be reduced to zero. t_D and t_E , on the other hand, represent dispersion time-scales and measure the rate at which the perpendicular velocity and energy distributions spread.

In order to determine these four time-scales we require to evaluate three parameters

$$\langle \Delta v_{\parallel} \rangle = -A_D l_f (1 + m/m_f) G(l_f v) \quad (A.6a)$$

$$\langle (\Delta v_{\parallel})^2 \rangle = (-A_D/v) G(l_f v) \quad (A.6b)$$

$$\langle (\Delta v_{\perp})^2 \rangle = -(A_D/v) (\phi(l_f v) - G(l_f v)) \quad (A.6c)$$

where

$$A_D = \frac{8\pi e^4 n_f Z^2 Z_f^2 \ln \Lambda}{[4\pi\epsilon_0]^2 m^2} \quad (A.7)$$

$$l_f = 1/v_f = \left(\frac{2kT}{m_f} \right)^{-\frac{1}{2}} \quad (A.8)$$

$$\phi = \frac{2}{\pi^{\frac{1}{2}}} \int_0^x e^{-y^2} dy \quad (A.9)$$

$$G(x) = \frac{\phi(x) - x\phi'(x)}{2x^2} \quad (A.10)$$

and where m and Z are respectively the mass and ionic charge of the test particle, and where m_f , n_f , and Z_f are respectively the mass, number density and ionic charge of the field particles.

In practice we are only interested in the values of the time-scales in the limits of $v \gg v_f$ or, in the particular case of t_{EL} , $v \ll v_f$. We, therefore, only require to evaluate $\phi(x)$ and $G(x)$ in the limits $x \rightarrow \infty$ and $x \rightarrow 0$.

As $x \rightarrow \infty$

$$\phi(x) \rightarrow \frac{2}{\pi^{1/2}} \int_0^{\infty} e^{-y^2} dy = 1 \quad (\text{A.11})$$

$$2x^2 G(x) = \phi(x) - \frac{2}{\pi^{1/2}} x e^{-x^2} \rightarrow 1$$

$$\text{i.e. } G(x) \rightarrow 1/(2x^2) \quad (\text{A.12})$$

As $x \rightarrow 0$

$$\phi(x) \rightarrow \frac{2}{\pi^{1/2}} \int_0^x (1 - x^2 \dots) dx \approx \frac{2}{\pi^{1/2}} \left(x - \frac{x^3}{3} \right) \quad (\text{A.13})$$

$$2x^2 G(x) \rightarrow \frac{2}{\pi^{1/2}} x \left(1 - \frac{x^2}{3} - 1 + x^2 \right)$$

$$\text{i.e. } G(x) \rightarrow \frac{2}{3\pi^{1/2}} x \quad (\text{A.14})$$

Therefore, for $v \gg v_f$, i.e. $1_f v \gg 1$

$$t_s = \frac{2 v^3}{A_D (1+(m/m_f))} = \frac{m^2 v^3 [4\pi\epsilon_0]^2}{4\pi e^4 n_f \ln\Lambda (1+(m/m_f))} \quad (\text{A.15})$$

$$t_D = \frac{v^3}{A_D} = \frac{m^2 v^3 [4\pi\epsilon_0]^2}{8\pi e^4 n_f \ln\Lambda} \quad (\text{A.16})$$

$$t_E = \frac{1_f^2 v^5}{2A_D} = \frac{m^2 v^5 [4\pi\epsilon_0]^2}{16\pi e^4 n_f \ln\Lambda v_f^2} \quad (\text{A.17})$$

$$t_{EL} = \frac{v^3 m_f}{A_D m} = \frac{m^2 v^3 [4\pi\epsilon_0]^2 m_f}{8\pi e^4 n_f \ln\Lambda m} \quad (\text{A.18})$$

and for $v \ll v_f$, i.e. $1_f v \ll 1$ and $E/kT \gg 1$

$$t_{EL} = \frac{3\pi^{\frac{1}{2}}}{4 l_f^3 A_D} \frac{m_f}{m} = \frac{3\pi^{\frac{1}{2}} m^2 v_f^3 [4\pi\epsilon_0]^2 m_f}{32\pi e^4 n_f \ln\Lambda m} \quad (\text{A.19})$$

Thus, summing over proton and electron field particles for suprathermal electron test particles (i.e. $v \gg v_e$ the electron thermal velocity)

$$t_s = \frac{m_e^2 v^3 [4\pi\epsilon_0]^2}{12\pi e^4 n \ln\Lambda} \quad (\text{A.20})$$

$$t_D = \frac{m_e^2 v^3 [4\pi\epsilon_0]^2}{8\pi e^4 n \ln\Lambda} \quad (\text{A.21})$$

$$t_E = \frac{m_e^2 v^3 [4\pi\epsilon_0]^2}{16\pi e^4 n \ln\Lambda} \left(\frac{v}{v_e} \right)^2 \quad (\text{A.22})$$

$$t_{EL} = \frac{m_e^2 v^3 [4\pi\epsilon_0]^2}{8\pi e^4 n \ln\Lambda} \quad (\text{A.23})$$

For suprathermal protons (i.e. $E \gg kT$, the thermal energy

of the target particles) colliding with electrons

$$t_{EL}^{pe} = \begin{cases} \frac{m_p^2 v^3 [4\pi\epsilon_0]^2}{8\pi e^4 n \ln \Lambda} \left(\frac{m_e}{m_p}\right) & v_e \ll v \\ \frac{3\pi^{\frac{1}{2}} m_p^2 v_e^3 [4\pi\epsilon_0]^2}{32\pi e^4 n \ln \Lambda} \left(\frac{m_e}{m_p}\right) & v_e \gg v \end{cases} \quad (\text{A.24})$$

and for protons colliding with protons.

$$t_{EL}^{pp} = \frac{m_p^2 v^3 [4\pi\epsilon_0]^2}{8\pi e^4 n \ln \Lambda} \quad (\text{A.25})$$

APPENDIX BCOLLISIONAL BROADENING OF CYCLOTRON LINES

Classically, an electron moving in a magnetic field with a component of velocity perpendicular to the field, if undisturbed, emits a series of infinitely narrow cyclotron lines (i.e. the electron emits a set of infinitely long, sinusoidal, electromagnetic waves) with frequencies that are an integral multiple of the electrons relativistic gyro-frequency. In time, of course, the electron loses energy, and the amplitude of the electromagnetic wave decays. This process, however, takes a time very much longer than the Larmor period and for all practical purposes we can consider an undisturbed electron as moving with a constant velocity for all time.

If an electron moving in a magnetic field collides with another particle, the change in the motion of the electron will result in a change in the phase and/or amplitude of the electromagnetic wave that it is emitting. In a plasma, an electron will be continually undergoing such collisions. The majority of these will be distant encounters and will have only a negligible effect on the phase and amplitude of the electron's radiation. The few close encounters that occur will, however, have a substantial effect on the phase and the amplitude of the radiation, causing a disruption of the electromagnetic wave. Thus, we can consider the electron as emitting a set of continuous sinusoidal waves between such close encounters, and during these encounters we can regard one wave as being terminated and a new, independent, wave begun.

Such an interpretation leads to a Lorentz profile for the cyclotron lines of the form

$$V(\omega) \propto \frac{1}{\pi} \frac{v_c}{(\omega - \omega_0)^2 + v_c^2} \quad (\text{B.1})$$

where ω is the angular frequency, ω_0 is the angular frequency of the radiation of the unperturbed electron, and v_c is the frequency with which close encounters occur (Bekefi, 1966; c.f. Oster, 1960).

In order to determine the collision frequency we must first decide how close an encounter is necessary to disrupt the emitted electromagnetic wave. We adopt as the definition of a close encounter the conditions that either the phase of the wave is altered by 1 radian (the Weiskopf criterion, c.f. Mihalas, 1970), or that the amplitude of the first harmonic changes by a substantial fraction of the pre-collision amplitude. We will show that, for a non-relativistic plasma (i.e. $kT \ll m_e c^2$), collisions in which electrons are deflected through an angle $\theta \ll 1/n$ (where n is the harmonic number) are not close encounters (i.e. have little effect on the phase and amplitude of the e.m. wave in a given harmonic) and use this to derive an expression for the collision frequency.

Firstly, we consider the energy exchange in a collision between a test electron of mass m and velocity $\underline{v} = v_0(1,0)$ and a stationary target particle of mass M . In the centre of mass frame the velocities of the test and target particles before the collision are given, respectively, by

$$\underline{v}_{CM} = \frac{M}{m+M} v_0(1,0) \quad (B.2)$$

$$\underline{V}_{CM} = \frac{m}{m+M} v_0(-1,0) \quad (B.3)$$

and after the collision by

$$\underline{v}'_{CM} = \frac{M}{m+M} v_0(\cos\theta, \sin\theta) \quad (B.4)$$

$$\underline{V}'_{CM} = \frac{m}{m+M} v_0(-\cos\theta, -\sin\theta) \quad (B.5)$$

where θ is the angle through which the particle is deflected in the centre of mass frame.

In the original reference frame (i.e. the frame in which the target particle was originally stationary) the electron's final velocity is

$$\underline{v}' = \underline{v}'_{CM} - \underline{V}_{CM} \quad (B.6)$$

and the change in the electron's energy during the collision is given by,

$$\frac{1}{2}m [v^2 - v'^2] = \frac{1}{2}mv_0^2 \left[\frac{2mM}{(m+M)^2} \sin^2(\theta/2) \right] \quad (B.7)$$

so that the fraction of the energy lost is,

$$1 - \frac{v'^2}{v^2} = \frac{2mM}{(m+M)^2} \sin^2(\theta/2) \quad (B.8)$$

Consequently, if $\theta \ll 1$, the fraction of the energy lost will be small compared to its total energy. We can, therefore,

neglect the energy loss in collisions in which the angle of deflection $\theta \ll 1$. In addition, as can be verified a posteriori, the actual time for a collision to take place will be small compared to an electron's Larmor period and we can treat any collision with $\theta \ll 1$ simply as an instantaneous change in the electron's direction of motion.

Classically, the phase and amplitude of an electromagnetic wave is just the phase and amplitude of the time varying component of its electric field. Thus, the effect of an instantaneous change in direction on the electron's electric field, which for a distant observer is proportional to the change in the retarded potential is,

$$E(\omega) \propto \exp\left\{-i\omega \left(t - \frac{\hat{q} \cdot \underline{\rho}}{c}\right)\right\} \quad (\text{B.9})$$

(correct to order $|\underline{\rho}|/D$)

where $E(\omega)$ is the fourier component of the electric field with frequency ω , $\underline{\rho}(t)$ is the position vector of the electron from some arbitrary point close to the electron, \hat{q} is the direction vector to the observer, and D is the distance to the observer.

We consider, therefore, an electron which undergoes a deflection through an angle θ at $t = 0$ and position $\underline{\rho} = (0,0,0)$, so that its velocity immediately prior to the collision is $\underline{v}_1 = v_0(\cos\phi \sin\chi, \sin\phi \sin\chi, \cos\chi)$, and immediately after the collision is $\underline{v}_2 = v_0(\cos\phi' \sin\chi', \sin\phi' \sin\chi', \cos\chi')$. Thus, for all time, the electron's velocity is given by

$$\mathbf{v} = v_0(\sin\chi\cos(\omega_0 t + \phi), \sin\chi\sin(\omega_0 t + \phi), \cos\chi) \quad t < 0 \quad (\text{B.10})$$

$$\mathbf{v} = v_0(\sin\chi'\cos(\omega_0 t + \phi'), \sin\chi'\sin(\omega_0 t + \phi'), \cos\chi') \quad t > 0$$

and the displacement from the point of collision is

$$\rho = \frac{v_0}{\omega_0} [\sin\chi\{\sin(\omega_0 t + \phi) - \sin\phi\}, \sin\chi\{\cos\phi - \cos(\omega_0 t + \phi)\}], \quad t < 0 \quad (\text{B.11})$$

$$\rho = \frac{v_0}{\omega_0} [\sin\chi'\{\sin(\omega_0 t + \phi') - \sin\phi'\}, \sin\chi'\{\cos\phi' - \cos(\omega_0 t + \phi')\}], \quad t > 0$$

Without loss of generality we can consider an observer in the x-z plane with position vector $\hat{q} = (\sin\theta, 0, \cos\theta)$. Thus the time variation of the electric field, given by Equation (B.9), is

$$\begin{aligned} E_{\perp}(\omega) &\propto \exp \left\{ i \left(\frac{\omega}{\omega_0} \frac{v_0}{c} [\sin\theta \sin\chi \{\sin(\omega_0 t + \phi) - \sin\phi\}] + t \left[\omega_0 \frac{v_0}{c} \cos\chi - \omega \right] \right) \right\} \\ &= \sum_{-\infty}^{\infty} J_n \left[\frac{\omega}{\omega_0} \frac{v_0}{c} \sin\chi \sin\theta \right] \exp(i t [n\omega_0 \sin\chi \sin\theta \\ &\quad + \omega \frac{v_0}{c} \cos\chi \cos\theta - \omega] - i[n\phi - \sin\phi] \sin\theta) \end{aligned} \quad (\text{B.12})$$

before the collision, and after the collision by

$$E(\omega) \propto \sum_{-\infty}^{\infty} J_n \left[\frac{\omega}{\omega_0} - \frac{v_0}{c} \sin\chi' \sin\theta \right] \exp(it[n\omega_0 \sin\chi' \sin\theta + \omega_0 \frac{v_0}{c} \cos\chi' \cos\theta - \omega] - i[n\phi' - \sin\phi'] \sin\theta) \quad (\text{B.13})$$

Therefore, at $t = 0$, the ratio of the amplitude of the n^{th} harmonic after the collision to the amplitude before the collision is

$$\frac{J_n \left(\frac{\omega}{\omega_0} - \frac{v_0}{c} \sin\chi' \sin\theta \right)}{J_n \left(\frac{\omega}{\omega_0} - \frac{v_0}{c} \sin\chi \sin\theta \right)} \leq 1 + n\theta \cot\chi \quad (\text{B.14})$$

(for small angles of deflection i.e. $n\theta \ll \tan\chi$)

Clearly, for a large ensemble of electrons, only a small fraction will have a value of $\chi \ll 1$ and these will in any case only contribute a small fraction of the energy in a line. We can, therefore, say that for $n\theta \ll 1$ no disruption of the e.m. wave will occur due to a change in its amplitude.

Similarly, if we compare the change in phase of the electromagnetic wave

$$\Delta_{\text{phase}} = n\phi - n\phi' + [\sin\phi' - \sin\phi] \sin\theta \leq n\theta \quad (\text{B.15})$$

then if $n\theta \ll 1$ the Weiskopf criterion is not met and no disruption of the wave will occur due to a change in phase.

Thus, for a given harmonic n , collisions will only disrupt

the electromagnetic wave if during the collision the electron is deflected through an angle $\theta \sim 1/n$. The collision frequency ν_c , for that line, is the number of times per second a thermal electron undergoes a collision. This is given by

$$\nu_c = \bar{n} b_0^2 n_s v_e \quad (\text{B.16})$$

where n_s is the number density of scattering centres, v_e is the electron thermal velocity, and b_0 is the maximum impact parameter (i.e. perpendicular distance of the test electrons approach) for which a disruption of the e.m. wave occurs.

The impact parameter in a collision is related to the angle of deflection θ of the test particle by (e.g. Bohr, 1915)

$$b = \frac{Z z e^2}{[4\pi\epsilon_0] m_0 v^2} \frac{1}{\tan(\theta/2)} \quad (\text{B.17})$$

where $m_0 = \frac{m M}{(m+M)}$ the reduced mass of the system and where Z and z are, respectively, the ionic charges of the test and target particles, M and m are, respectively, the masses of the test and target particles, and v is the collision velocity. Therefore,

$$b_0 \sim \frac{e^2}{[4\pi\epsilon_0] m_e v_e^2} \frac{1}{\tan(1/(2n))} \quad (\text{B.18})$$

where n is the harmonic number. i.e.

$$b_0 \sim \frac{e^2}{[4\pi\epsilon_0] m_e v_e^2} \cdot 2n \quad (\text{B.19})$$

so that

$$\nu_c \sim \frac{4\pi e^4}{[4\pi\epsilon_0]^2} \frac{n_s n^2}{(m_e v_e^2)^2} v_e \quad (\text{B.20})$$

which for a white dwarf accretion column gives

$$\nu_c \sim 3 \cdot 10^6 n^2 \dot{M}_{13} / f_{-2} M_1^{4/3} T_7^{5/2} \text{ Hz} \quad (\text{B.21})$$

where \dot{M}_{13} is the accretion rate measured in units of 10^{13} Kgs^{-1} , f_{-2} is the fractional area over which the white dwarf is accreting measured in units of 10^{-2} , M_1 is the white dwarf mass in solar masses, and T_7 is the column temperature measured in units of 10^7 K .

REFERENCES

- Aizu K.: 1973, Prog. Theor. Phys. 49, No. 4, 1184.
- Allen C.W.: 1973, Astrophysical Quantities (Third Edition), Athlone Press.
- Allen D.A., Cherepaschuck A.M.: 1982, Mon. Not. R. astr. Soc. 201, 521.
- Arons J., Lea S.M.: 1976, Astrophys. J. 207, 914.
- Barrett P.E., Chanmugam G.: 1984, Astrophys. J. 278, 298.
- Barrett P.E., Chanmugam G.: 1985, Astrophys. J. 298, 743.
- Bates D.R., Dalgarno A.: 1953, Proc. Phys. Soc. A66, 972.
- Bates D.R., Griffing G.W.: 1953, Proc. Phys. Soc. A66, 961.
- Bates D.R., Griffing G.W.: 1954, Proc. Phys. Soc. A67, 663.
- Bates D.R., Griffing G.W.: 1955, Proc. Phys. Soc. A68, 90.
- Bekefi G.: 1966, Radiative Processes in plasmas, Wylie, New York, Chapter 6.
- Boldt E., Serlemitsos P.: 1969, Astrophys. J. 157, 1157.
- Bohr N.: 1915, Phil. Mag. 30, 581.
- Brown J.C.: 1972, Solar Phys. 26, 441.
- Brown J.C.: 1973, Solar Phys. 31, 143.
- Brown J.C., Craig I.J.D.: 1984, Astron. Astrophys. (Letters) 130, L5.
- Canfield R.C., Chang C.R.: 1985, Astrophys. J. 295, 275.
- Campbell G.C.: 1983, Mon. Not. R. astr. Soc. 205, 1031.
- Cawthorne, T.V.: 1986, (private communication).
- Chanmugam G.: 1980, Astrophys. J. 278, 1122.
- Chanmugam G., Dulk G.A.: 1981, Astrophys. J. 244, 569.
- Cox D.P., Tucker W.H.: 1969, Astrophys. J. 157, 1157.

- Elsner R.F., Lamb F.K.: 1977, *Astrophys. J.* 215, 897.
- Emslie A.G.: 1978, *Astrophys. J.* 224, 241.
- Emslie A.G., Brown J.C.: 1985, *Astrophys. J.* 295, 648.
- Fabianno G., Hartmann L., Raymond J., Steiner J.,
Braudaudi-Raymont G.: 1981, *Astrophys. J.* 243, 911.
- Fabian A.C., Pringle J.E., Rees M.J.: 1976, *Mon. Not. R. astr. Soc.* 175, 43.
- Fite W.L., Brackmann R.T.: 1958, *Phys. Rev.* 113, 1141.
- Fite W.L., Brackmann R.T.: 1958, *Phys. Rev.* 113, 1151.
- Frank J., King A.R.: 1984, *Astron. Astrophys.* 134, 328.
- Frank J., King, A.R., Lasota J.P.: 1983, *Mon. Not. R. astr. Soc.* 202, 183.
- Hearn D.R., Richardson J.A.: 1977, *Astrophys. J. (Letters)* 213, L115.
- Heise J.: 1982, Thesis of the University of Utrecht.
- Heise J., Brinkman A.C., Gronenschild E., Watson M., King A.R.,
Stella L., Kieboom K.: 1985, *Astron. Astrophys. (Letters)* 148, L14.
- Heise J., Kruzewski A., Mewe R., Kahn S., Chlebowski T.,
Seward F.D.: 1986 *Astron. Astrophys.* (submitted).
- Heitler W.: 1954, *The Quantum Theory of Radiation*, Oxford University Press.
- Hoshi R.: 1973, *Prog. Theor. Phys.* 49, 776.
- Hudson H.: 1973, *High Energy Phenomenon on the Sun*, G.S.F.C. document X693-73-193 (ed. Ramaty R., Stone R.G.).
- King A.R.: 1985, (private communication).
- King A.R., Lasota J.P.: 1979, *Mon. Not. R. astr. Soc.* 188, 653.
- King A.R., Lasota J.P.: 1980, *Mon. Not. R. astr. Soc.* 191, 721.

- King A.R., Williams G.A.: 1985, Mon. Not. R. astr. Soc. 215, 1P.
- Kuijpers J., Pringle J.E.: 1982, Astron. Astrophys. 114, L4.
- Lamb D.Q., Masters A.R.: Astrophys. J. (Letters) 234, L117.
- Liebert J., Stockman H.S.: 1979, Astrophys. J. 229, 652.
- Liebert J., Stockman H.S.: 1985, Cataclysmic Variables and Low Mass X-ray Binaries., (ed. Paterrson J., Lamb D.Q.) D. Reidel.
- Liebert J., Stockman H.S., Angel J.R.P., Woolf N.J., Hege K.: 1978, Astrophys. J. 225, 201.
- Liebert J., Tapia S., Bond H.E., Grauer A.D.: 1982 Astrophys. J. 254, 232.
- Masters A.R., Pringle J.E., Fabian A.C., Rees M.J.: 1977, Mon. Not. R. astr. Soc. 178, 501.
- Meggitt S.M.A., Wickramasinghe D.T.: 1982, Mon. Not. R. astr. Soc. 198, 71.
- Meggitt S.M.A., Wickramasinghe D.T.: 1984, Mon. Not. R. astr. Soc. 207, 1.
- Mihalas D.: 1970, Stellar Atmospheres, W.H. Freeman and Company.
- Orall F.Q., Zirker J.B.: 1976, Astrophys. J. 208, 618.
- Oster L.: 1960, Phys. Rev. 119, 144.
- Papaloizou J.C.B., Pringle J.E., MacDonald J.: 1982, Mon. Not. R. astr. Soc. 198, 215.
- Patterson J., Beuerman K., Lamb D.Q., Fabianno G., Raymond J.C., Swank J., White N.E.: 1984, Astrophys. J. 279, 785.
- Raymond J.C., Cox D.P., Smith B.W.: 1976, Astrophys. J. 204, 290.
- Raymond J.C., Doyle J.G.: 1981, Astrophys. J. 245, 1141.
- Raymond J.C., Black J.H., Davis R.J., Dupree A.K., Gursky H., Hartmann L.: 1979, Astrophys. J. (Letters) 230, L95.

- Rothschild R.E., Gruber D.E., Knight F.K., Matteson J.L.,
 Nolan P.L., Swank J.H., Holt S.S., Serlemistos P.J., Mason K.O.,
 Touhy I.R.: 1981, *Astrophys. J.* 250, 723.
- Sakashita S.: 1968, *Prog Theor. Phys.* 39, 235.
- Schmidt G.D., Stockman H.S., Margon B.: 1981, *Astrophys. J.*
 (Letters) 243, L157.
- Shoub E.C.: 1983, *Astrophys. J.* 226, 339.
- Spitzer L.: 1962, *Physics of Fully Ionized Gases*, Interscience.
- Starrfield S., Truran J.W., Sparks W.H.: 1981, *Astrophys. J.*
 (Letters) 243, L27.
- Steir P.M., Barnett C.F.: 1965, *Phys. Rev.* 103, 896.
- Stockman H.S., Folts C.B., Schmidt G.D., Tapia S.: 1983,
Astrophys. J. 271, 725.
- Stockman H.S., Schmidt G.D., Angel J.R.P., Liebert J., Tapia s.,
 Beaver E.A.: 1977, *Astrophys. J.* 217, 815.
- Summers H.P.: 1985, (private communication).
- Summers H.P., McWhirter R.W.P.: 1979, *J. Phys B. Molec. Phys.*
12, No14., 2387.
- Swank J., Lampton M., Boldt E., Holt S., Serlemistos P.: 1977,
Astrophys. J. (letters) 216, L71.
- Szkody P., Capps R.W.: 1980, *Astrophys. J.* 85, 875.
- Tapia S.: 1977 *Astrophys. J.* (Letters) 212, L125.
- Thompson A.M., Brown J.C., Kuijpers J.: 1985, *Astron. Astrophys.*
159, 202.
- Thompson A.M., Cawthorne T.V.: 1986, *Mon. Not. R. astr. Soc.* (in
 press).
- Touhy I.R., Lamb F.K., Garmie G.P., Mason K.O.: 1978, *Astrophys.*
J. (Letters) 226, L17.

- Truran J.W., Starrfield S., Strittmatter P.A., Wyatt S.P.,
Sparks W.M.: 1977, *Astrophys. J.* 211, 539.
- Visvinath N., Wickramasinghe D.T.: 1979, *Nature* 281, 47.
- Weast G.J., Durisen R.H., Imamura J.N., Kylafis N.D., Lamb D.Q.:
1979, *White Dwarfs and Variable Stars (I.A.U. Colloquium No53)*
p140.
- Wesmael F., Henry R.B.C., Shipman H.L.: 1984, *Astrophys. J.* 287,
868.
- Wickramasinghe D.T., Meggitt S.M.A.: 1982, *Mon. Not. R. astr.
Soc.* 198, 975.
- Wild J.P., Hill E.R.: 1971, *Australian J. Phys.* 24, 43.
- Williams G., Johns M., Price C., Hiltner A., Boley F., Maker S.,
Mook D.: 1979, *Nature* 281, 48.
- Young P., Schneider D.P.: 1979, *Astrophys. J.* 230, 502.
- Young P., Schneider D.P., Sackett S.A.: 1981, *Astrophys. J.*
245, 1035.
- Zeldovitch Y.B., Raizer Y.F.: 1967, *Physics of Shock Waves and
High Temperature Hydrodynamic Phenomena*, New York: Academic
Press.

